Ph135 Introduction to Condensed Matter Physics

Linda Ye

Academic Year 2023-2024

Contents

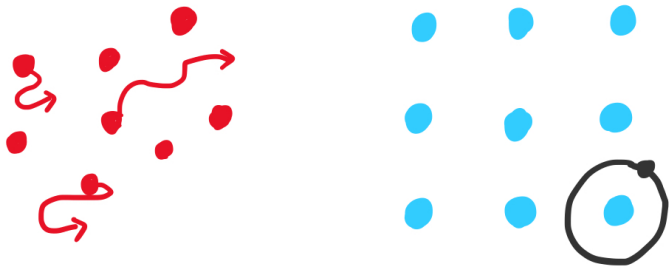

Figure 1: Sketch of particles in the liquid phase (left) and solid phase (right)

1 What does condensed matter physics study and why studying it?

"Condensed" implies that the individual particles that constitute the system are close to each other and one cannot ignore the interaction between the particles in describing these systems. Among the most commonly occuring phases of matter–gas, liquid and solid–the latter two belong to the realm of "condensed matter" (sketches of these two phases see Fig.1).

In this class we will almost exclusively focus on the solid state of matter. Not only because its regular spatial structure makes a systematic description of the system more tractable (therefore more 'elegant'), but also because of the rich physics so far discovered in solid state systems. We will go through some of the important phases in this course.

If we recall that the atom sitting on each site of the solid in Fig.1 is composed of a heavy nucleus, and a much lighter electron moving around the nucleus, it becomes clear that the following two will be the most important questions in understanding the physics of the solids: (1) what happens to these electrons as the atoms are put into the array? (2) what can we say about the heavier part that defines the lattice and sits more or less still? To spoil it a bit, electrons will form energy bands, and lattice will give rise to phonons (which is a term you can think of in analogy to photons, whereas photons carries light, and phonons carries sound in solids). Electrons and phonons are the key concepts we would like to touch on in this class.

So why would one want to study condensed matter physics? (also see Simon, Oxford Solid State Basics, Chapter 0)

- Conecptually, the problems in condensed matter physics are of many-body nature. It is not uncommon for the solid state system we are interested in to have more than the order of 10^{20} particles. In this case, we are not interested in the individual behaviors of each particles (nor is that knowledge very useful), but rather we'd like to study the so-called overall collective behavior of the group of particles (examples of collective behavior include how does the solid conduct electricity, why do water crystallize into ice). This would require new frameworks to think about these so-called emergent behaviors. See Anderson's "More is different", who first advocated for the field of condensed matter as a deep subject of itself. Many of the tools and concepts used in understanding such emergent behavior also have close and deep connections with other field of physics, one of the most profound being symmetry breaking (which unfortunately we won't be covering much, advanced condensed matter physics will look into these in more depth), which is closely related to Higgs mechanism (or Higgs-Anderson mechanism) of mass generation in fundamental particles.

- Since the key subject of study of condensed matter is the solids, which basically form the everyday materials we can get our hands on. Condensed matter is going to be a useful subject to help one understands the properties of everyday matter, for instance, what are the fundamental differences between metals and insulators, semiconductors. If you happen to be an experimentalist, condensed matter would be a fun subject to study regardless of whether your field of study is condensed matter itself–most real-life experimental setups have components that belongs to the realm of condensed matter! Detectors, optical devices and lasers can be made out of semiconductors; giant magnets in the accelerators and quantum computing devices can be made out of superconductors. Not to mention the wide use of solid state devices in our computers and cell phones. Hopefully studying the subject can help one connect to these contemporary technology a bit better. All the

above are talked about more or less from a physics context, but if you are from an engineering background, the same applies.

- Last thing I'll say here is more from a learning perspective, that condensed matter is also a perfect playground for one to apply what one learned in quantum mechanics and statistical mechanics in "real life" settings. If you've enjoyed these subjects you might have fun playing with them in the solid state context. Put it in another way, quantum mechanics and statistical mechanics are what we'll be building on a lot in this course and if you've forgotten about them, you might want to refresh yourself a bit.

The flow of the class will start from the behaviors of the lattice (or phonons) and electrons before having to formally invoke the microscopic periodic structure of the solids. This is also more or less following the chronological order of the understanding of solids. In this part you will learn about the understanding of solids even before the Schrodinger equation or the uncertainty principle has been proposed. Nevertheless at this early stage it is already realized that quantum mechanics is an essential part of the physics of solids. After the first part we will formally introduce the periodic structure and microscopic origins of phonons and electronic bands and Fermi surfaces. We will spend some time on the reciprocal lattice which is a very powerful framework to describe solids. The latter half of the course will be focusing on the electrons in solids. Metals, insulators, semiconductors, electrons in electric and magnetic fields, and hopefully nearing the end we will be able to cover graphene and topological insulators which have been widely studied in the condensed matter community in the past 20 years.

2 Thermal properties of solids

2.1 Heat capacity and Dulong-Petit law

In this section we will discuss a very important chapter in the early understanding of the solid state, namely, the thermal properties of the solids. The discussions I'm going to introduce here are largely motivated by various experimental observations in the physical quantity heat capacity. It is a measurement that we still use today in our lab to characterize solid state materials. As we will see, around the beginning of the 20th century, it has played a key role in driving forward the understanding of solids particularly invoking the necessity to include quantum mechanics into the picture.

Let's recall the definition of heat capacity, which is the energy one needs to absorb to increase the temperature of the system by one degree. You might recall from thermodynamics that heat capacity can be defined in both constant pressure and constant volume conditions as C_p and C_v:

$$C_p = \left(\frac{\partial U}{\partial T}\right)_p, C_v = \left(\frac{\partial U}{\partial T}\right)_v \tag{1}$$

Strictly speaking, these two differ from each other:

$$C_p - C_v = \frac{VT\alpha^2}{\beta_T} \tag{2}$$

(α is thermal expansion and β_T compressibility). For solids, α is typically on the order 10^{-3}, leading to a negligible difference in C_p and C_v in most solid materials. From now on we will assume $C_p \simeq C_v$, and we will use C for convenience. Experimentally it is much easier to measure C_p at ambient pressure than setting up sophisticated instrumentation to keep the volume of a solid constant over a broad range of temperatures.

The heat capacity curves shown in Fig. 2 will guide what we are going to look at in this and the following class, and we will introduce a few models that provides a progressively better understanding of these $C(T)$ curves. Qualitatively speaking, these curves all start from zero at zero temperature, as expected from third law of thermodynamics. As we increase the temperature, C grows and then saturates at the high temperature. The temperature scale at which the saturation takes place is quite different for different materials, which we will come back to below. Nevertheless, the high temperature saturation value is quite similar, taking the value around $3R$. R is the gas constant 8.31 J/mol. If we convert it to a more microscopic unit we have heat capacity $3k_B$ per atom. This is the so-called Dulong-Petit law first discussed in 1819 (!). This can be contrasted with the value for ideal, monoatomic gas, which has heat capacity $\frac{3}{2}k_B$ that is half of the solid-state value.

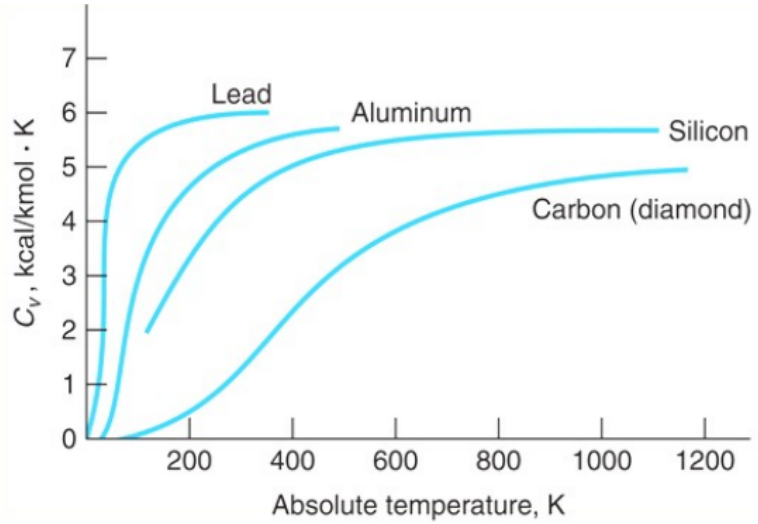

Figure 2: Heat capacity of four elemental solids as a function of temperature

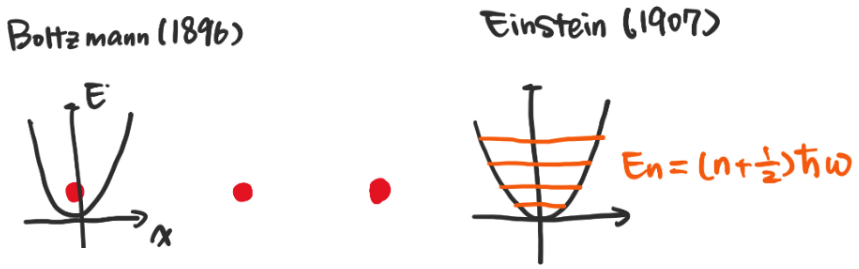

Figure 3: Left: Boltzmann's harmonic oscillator model of atoms; right: Einstein's quantized harmonic oscillator model

2.2 Boltzmann's (classical) harmonic oscillator model

Boltzmann was the first to give a picture of this contrast. If we recall the picture we drew earlier of solids being a regular array of atoms with them not being able to move freely in space. We can approximate the potential experienced by the atoms by a harmonic well and the energy of the atoms can be described by

$$H = \frac{1}{2}m\boldsymbol{v}^2 + \frac{1}{2}k\boldsymbol{x}^2 \tag{3}$$

Note that ideal gas is the only subject to the kinetic energy tem. As temperature is increased, the atoms can thermally fluctuate around the equilibrium position and the very fluctuations are the origin of the heat capacity. Each degree of freedom would give rise to $\frac{1}{2}k_BT$ to the total energy according to the equipartition theorem, contributing $\frac{1}{2}k_B$ to the heat capacity. The total degrees of freedom for the harmonic oscillator is 6, resulting in a temperature-independent heat capacity $3k_B$ (in contrast to ideal gas heat capacity $\frac{3}{2}k_B$.

This classical picture by Boltzmann dating back to 1896 nicely captures the high temperature limit of the heat capacity behavior in solids and provides a basis of modeling the bound atoms in solids as harmonic oscillators–which we will see throughout the class.

2.3 Einstein's treatment: quantized harmonic oscillators

Boltzmann's picture provides a temperature-independent heat capacity value well explaining the Dulong-Petit law; the next question follows is why the observed heat capacity falls below that with lowering temperature. Here is where Einstein comes in (Fig. 3), where he took the notion of harmonic well further and introduced quantized levels of the harmonic oscillators to account for the heat capacity in solids.

We'll start from a one-dimensional harmonic oscillator along, say the x-direction. The energy of the quantized harmonic oscillator takes the following form:

$$E_n = (n + \frac{1}{2})\hbar\omega \tag{4}$$

with equally spaced levels with the lowest energy state $\frac{1}{2}\hbar\omega$ capturing the zero point energy of the harmonic oscillator. To do this we'll recall the partition function Z from stat mech:

$$Z = \sum_n e^{-\beta E_n}, \beta = \frac{1}{k_B T} \tag{5}$$

from which one may calculate the energy and heat capacity of the system via

$$\langle E \rangle = -\frac{1}{Z}\frac{\partial Z}{\partial \beta}, C = \frac{\partial \langle E \rangle}{\partial T} \tag{6}$$

. Put Eq. (4) into (5) and (6) yields:

$$Z = \sum_n e^{-\beta(n+\frac{1}{2})\hbar\omega} = \frac{1}{2\sinh(\frac{\beta\hbar\omega}{2})} \tag{7}$$

and

$$\langle E \rangle = \frac{\hbar\omega}{2}\frac{\cosh(\frac{\beta\hbar\omega}{2})}{\sinh(\frac{\beta\hbar\omega}{2})} = \frac{\hbar\omega}{2} + \frac{\hbar\omega}{e^{\beta\hbar\omega} - 1} \tag{8}$$

It is convenient to view the temperature-dependent part (second term in (8)) of $\langle E \rangle$ as a product of $\hbar\omega$ and its corresponding Bose factor $\frac{1}{e^{\beta\hbar\omega} - 1}$. In other words, this describes a bosonic excitation in the system with energy $\hbar\omega$ (one can check the bosonic nature of the harmononic oscillator model from e.g. the commutation relation of the raising and lowering operators). We will be using the bosonic nature of lattice vibration throughout the course.

This will give us the following form of heat capacity:

$$C = \frac{e^{\beta\hbar\omega}}{(e^{\beta\hbar\omega} - 1)^2}\frac{(\hbar\omega)^2}{k_B T^2} \tag{9}$$

It is not difficult to expand the above calculation to the 3D case where

$$E(n_x, n_y, n_z) = [(n_x + \frac{1}{2}) + (n_y + \frac{1}{2}) + (n_z + \frac{1}{2})]\hbar\omega \tag{10}$$

and the partition function

$$Z_{3D} = (Z_{1D})^3 \tag{11}$$

Giving rise to a heat capacity three times of that in the 1D case:

$$C_{3D} = \frac{3e^{\beta\hbar\omega}}{(e^{\beta\hbar\omega} - 1)^2}\frac{(\hbar\omega)^2}{k_B T^2} \tag{12}$$

It is a quite complex functional form that can be plotted numerically in Fig. 4. The 3D counterpart gives three times that the 1D case and the high temperature end recovers the Dulong-Petit limit we've just looked at. At lower temperature, especially when the temperature become comparable with the level spacing $\hbar\omega$, C is reduced from $3k_B$. This is also clear from the temperature evolution of the Bose factor (see right panel of Fig. 4): the number of excited state at high T appears linear in T, corresponding to the saturation of C, and at low T it gets more and more difficult to excite the states. This results in the "frozen out" of heat capacity at low temperature. To summarize here, thanks to the quantized nature, Einstein's picture reasonably explains why heat capacity falls short of the expectation from the classical Dulong Petit limit by introducing the quantized nature of the harmonic oscillators. Looking at the experimental curves, one can get a sense that this quantized level has an energy scale ranging from 50 K ish for lead, and 200 K or 300 K for aluminum. So one doesn't have to go super low temperture for the quantum mechanical effects to become important.

A comment I'd like to make here is that the horizontal axis of this model is determined by $\hbar\omega$, where $\omega = \sqrt{k/m}$. The higher the spring constant, the lower the atomic mass, the higher ω. With this in mind we can revisit the collection of the curves in Fig. 2, where we can find that the element whose heat capacity saturates at a higher temperature is the lighter (and harder) carbon, while that with the lowest temperature scale is the heavier (and softer)

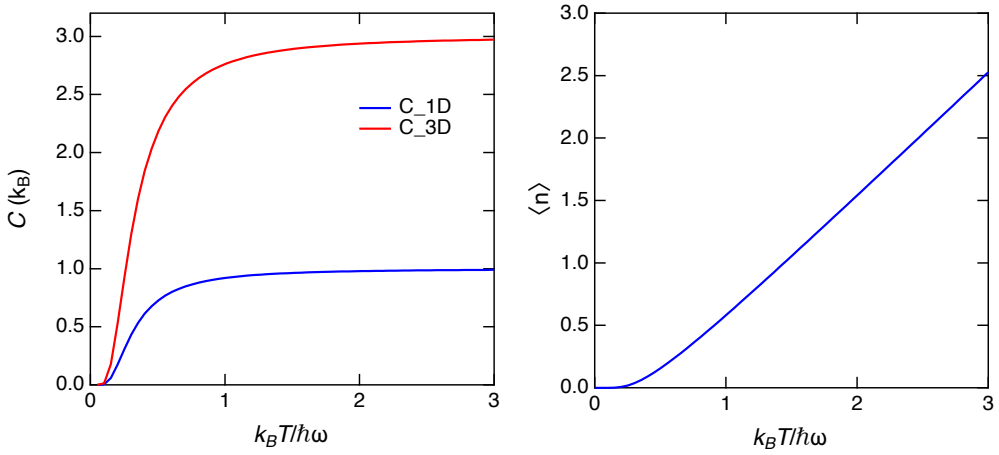

Figure 4: Heat capacity and the Bose factor as a function of temperature normalized by $\hbar\omega$

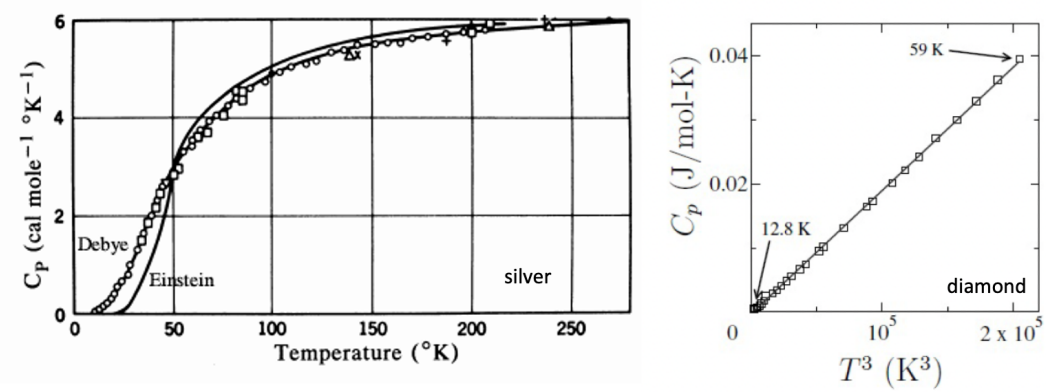

Figure 5: Left: C_p of silver compared with Einstein and Debye theories, respectively. Right: C_p of diamond plotted against T^3.

lead, consistent with the harmonic oscillator picture. As an aside, along the same line, one would expect a solid made of hydrogen to have very large energy scale associated with lattice vibrations–this is behind the anticipation that solid hydrogen can potentially support room temperature superconductivity. To cap here, Einstein's model of the lattice specific suggests that the "freeze out" of heat capacity at low temperature is due to the quantum mechanical nature of the lattice vibrations and has played a quite important role in the early development of understanding of the lattice.

2.4 The Debye model: quantized "phonon" modes

One would see that the Einstein model is not perfect especially at the low temperature end in for instance the left panel of Fig. 5, where it heavily underestimates the growth of C_p near low temperature in silver.

Focusing on the low temperature limit $\beta\hbar\omega \gg 1$, it is not hard to see that the Einstein model gives us an exponential behavior, as in this limit we may approximate $(e^{\beta\hbar\omega}-1)^2$ in the denominator as $(e^{\beta\hbar\omega})^2$, and

$$C \approx 3k_B e^{-\beta\hbar\omega}\hbar\omega\beta^2 \tag{13}$$

($e^{-\beta\hbar\omega}$ will dominate over β^2). Experimentally, it is known that the heat capacity of a lot of materials follow T^3 if it is an insulator (see Fig. 5 right panel for that of diamond), and follows $\gamma T + AT^3$ if it is a metal. This suggests that perhaps the Einstein model might not the whole picture in understanding the thermal properties of the solid.

Debye has realized in 1912, not very long after the Einstein model was proposed, that the vibrations discussed in the harmonic oscillator model of solids is basically sound. Sound propagates in solids and is therefore a wave, and as a result it is important to treat the sound wave in analogy with how Planck in earlier years had treated the light.

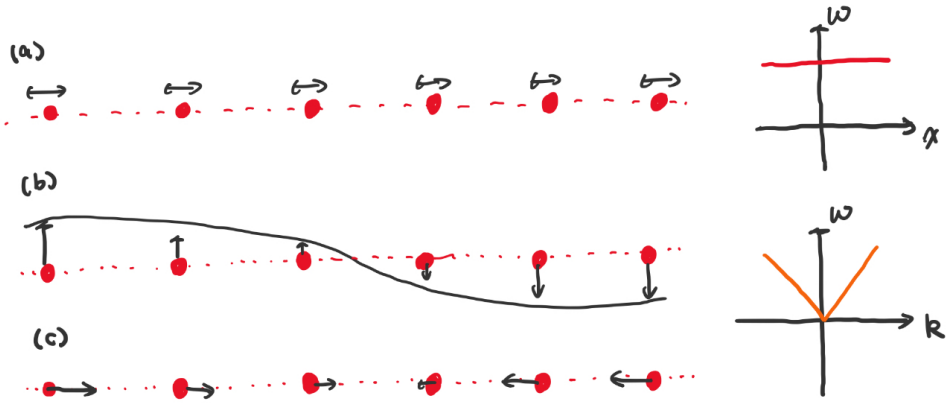

Figure 6: (a) Schematic of the independent harmonic oscillators in the Einstein model. (b,c) Schematic of the lattice vibrations in the Debye model.

As a wave, there's a dispersion relation $\omega = c|\boldsymbol{k}|$ where c is the sound velocity. In light the quanta of light is called photon, the quanta of the sound is called "phonon".

Let's contrast Einstein and Debye's pictures in Fig. 6. The motions of Einstein's harmonic oscillators are independent on each site (Fig. 6a), while in the Debye model, the sound wave requires collective atomic vibration across the lattice (Fig. 6b,c), where the displacement can be described by

$$\boldsymbol{u}(x) = \hat{A}e^{i(kx-\omega t)} \tag{14}$$

In contrast to photons, which only has transverse modes, there can be both transverse (Fig. 6b) and longitudinal waves for phonons (Fig. 6c). Energetically, there is an important difference between the Einstein model and the Debye model shown on the right hand side of Fig. 6: in the Einstein model all the vibration modes have the same energy while the Debye model allows low energy excitations when k is small (also called long wave length excitations). Intuitively, the Debye model makes it easier to excite lattice vibrations, especially at low temperature. This hopefully can rememdy the underestimation of heat capacity in the Einstein model, as we will show in the following.

The rest of Debye's treatment of the lattice vibrations is similar with Einstein. For each collective vibration mode, we have a characteristic energy quanta $\hbar\omega(\boldsymbol{k})$ from the dispersion relation $\omega = c|\boldsymbol{k}|$, and its thermal excitation will be treated identical to that of a boson. Since this is the first time we are encountering the momentum $\boldsymbol{k}$ space, it is worthwhile doing some preparations.

2.4.1 Periodic boundary condition and state counting

In the Einstein model, counting the number of vibration modes is easy–it will be $3N$ with N as the number of atoms in the system. The momentum space can be viewed as a Fourier transform of the real space, while we would like to keep a proper count of the number of total vibrational states. The trick we are going to use here is the periodic boundary condition (Born–von Karman boundary condition), where we artificially connect the beginning and the end of our sample (Fig. 7). This in principle should not affect the physics of the interior if the sample is of a sufficiently large size. Imagine this for an atomic chain of the length L, for any well-defined wave with wave vector k, the boundary condition will require

$$e^{ikL} = 1 \tag{15}$$

As a result, the only allowed k will be

$$k = n\frac{2\pi}{L}, n = 0, \pm 1, \pm 2... \tag{16}$$

Extending this to 3D give the allowed $\boldsymbol{k}$

$$(k_x, k_y, k_z) = (n_x\frac{2\pi}{L_x}, n_y\frac{2\pi}{L_y}, n_z\frac{2\pi}{L_z}) \tag{17}$$

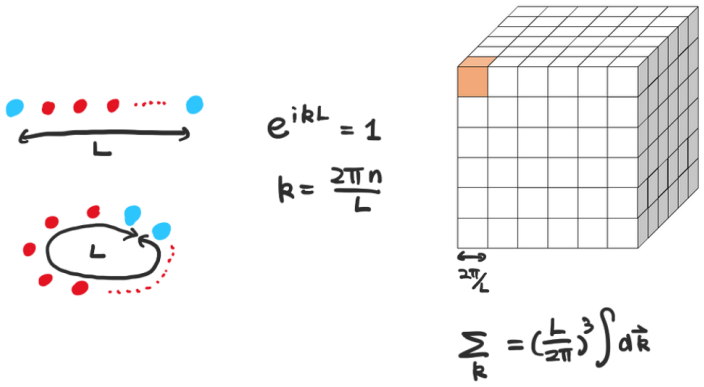

Figure 7: Sketch of the periodic boundary condition and the resulting discrete k-space grid.

which forms a grid in the 3D $\boldsymbol{k}$-space as shown in Fig. 7. The discrete nature of allowed $\boldsymbol{k}$ transforms the summation of different $\boldsymbol{k}$ states to the following integral

$$\sum_{\boldsymbol{k}} = \frac{V}{(2\pi)^3} \int d\boldsymbol{k} \tag{18}$$

It should be noted that the sum scales with the size of the system V, therefore N as well.

2.4.2 Heat capacity of the Debye model

With the above preparation, we are ready to calculate the heat capacity from the Debye model (we use n_B to denote the Bose factor):

$$\langle E \rangle = 3 \sum_{\boldsymbol{k}} \hbar\omega(\boldsymbol{k})[n_B(\hbar\omega(\boldsymbol{k})) + \frac{1}{2}] \tag{19}$$

The factor of 3 is introduced here to account for the one longitudinal and two transverse vibration modes with respect to each wave vector $\boldsymbol{k}$. Here we make the assumption that all these modes have the same sound velocity v. Using $\omega(\boldsymbol{k}) = vk$ (v being the sound velocity, and k the magnitude of $\boldsymbol{k}$), we obtain

$$\langle E \rangle = 3 \sum_{\boldsymbol{k}} \hbar vk[n_B(\hbar vk) + \frac{1}{2}] = 3 \frac{V}{(2\pi)^3} \int d\boldsymbol{k} \hbar vk[n_B(\hbar vk) + \frac{1}{2}] = 3 \frac{V}{(2\pi)^3} \int_0^\infty 4\pi k^2 dk \hbar vk[n_B(\hbar vk) + \frac{1}{2}] \tag{20}$$

Here we define a quantity called density of state $g(\epsilon)$ characterizing the number of states per unit energy ϵ (it is a convenient quantity because ϵ is eventually what comes in the statistical Bose factor). Noting $\epsilon = \hbar vk = \hbar\omega$, we can rewrite $\langle E \rangle$ as follows

$$\langle E \rangle = \int_0^\infty d\epsilon \epsilon g(\epsilon)[n_B(\epsilon) + \frac{1}{2}] \tag{21}$$

with

$$g(\epsilon) = \frac{3V\epsilon^2}{2\pi^2\hbar^3 v^3} \tag{22}$$

You may see g defined with respect to ω in some textbooks, but the essence is the same.

The temperature dependent part in $\langle E \rangle$, $\langle E' \rangle$ is

$$\langle E' \rangle = \int_0^\infty d\epsilon \epsilon g(\epsilon) n_B(\epsilon) = \int_0^\infty d\epsilon \epsilon g(\epsilon) \frac{1}{e^{\beta\epsilon} - 1} = \frac{3V}{2\pi^2\hbar^3 v^3} \int_0^\infty d\epsilon \frac{\epsilon^3}{e^{\beta\epsilon} - 1} \tag{23}$$

Redefine $\beta\epsilon = x$,

$$\langle E' \rangle = \frac{3V}{2\pi^2\hbar^3 v^3 \beta^4} \int_0^\infty dx \frac{x^3}{e^x - 1} = \frac{3Vk_B^4 T^4}{2\pi^2\hbar^3 v^3} \int_0^\infty dx \frac{x^3}{e^x - 1} = \frac{V\pi^2 k_B^4 T^4}{10\hbar^3 v^3} \tag{24}$$

(the integral yields $\pi^4/15$). The resulting heat capacity is

$$C = \frac{\partial \langle E' \rangle}{\partial T} = \frac{2V\pi^2 k_B^4 T^3}{5\hbar^3 v^3} \tag{25}$$

which correctly captures the T^3 behavior in the heat capacity of solids (strictly speaking, insulating solids).

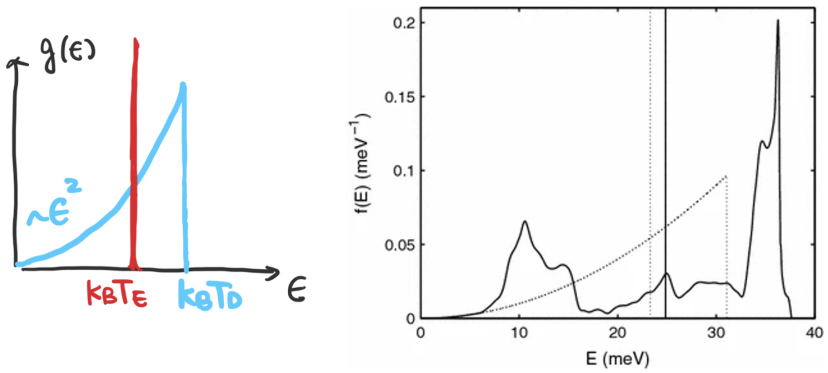

Figure 8: Left: density of states for the Debye and Einstein models, respectively. Right: calculated phonon density of states in Germanium. Taken from J.F.R. Archilla et al., Springer Series in Materials Science, vol 221, pp 343-362 (2015)

2.4.3 Debye temperature

You may have noticed that in the previous section we did not set an upper bound for the integration in the $\boldsymbol{k}$ space. This seems to suggest an infinite number of vibrational modes. While intuition may tell you that the total number of vibrational modes may not exceed $3N$ in the Einstein picture. This is reconciled in the Debye model by introducing a cutoff frequency ω_D and corresponding Debye temprature T_D via $\hbar\omega_D = k_B T_D$, where

$$3N = \int_0^{\hbar\omega_D} d\epsilon g(\epsilon) \tag{26}$$

This dictates

$$6\pi^2 v^3 n = \omega_D^3 \tag{27}$$

where $n = N/V$, and the cutoff Debye frequency $\omega_D = (6\pi^2 v^3 n)^{1/3}$. We should note that at low T the cutoff should affect very little the results in the previous section, as $1/(e^{\beta\epsilon} - 1)$ falls near zero if ϵ is sufficiently large.

With the cutoff defined one may calculate the Debye heat capacity across the entire temperature regime. See Fig. 5 for that calculated for silver with $T_D = 215$ K. As a consistency check, we may also estimate the high temperature limit of the Debye theory. In this case we take the approximation that $e^{\beta\epsilon} \approx 1 + \beta\epsilon$:

$$\langle E' \rangle \approx 3 \int_0^{\hbar\omega_D} d\epsilon \frac{g(\epsilon)}{\beta} = 3k_B \int_0^{\hbar\omega_D} d\epsilon g(\epsilon) = 3Nk_B \tag{28}$$

This recovers the Dulong-Petit limit.

2.5 Summary of the chapter

Here we've looked at two early models to account for the thermal properties of solids. Even without taking into account the microscopics (which we will cover in later classes), we see the usefulness of harmonic oscillator model, the necessity to take into account quantum mechanics, and also the wave nature of phonons. The term phonon actually won't be coined until 1930s. Pretty remarkable how all these aspects are figured out before systematic treatment of the periodic structure of the lattice itself is established.

At the very end of the section, let's revisit the comparison between the Einstein and Debye model in terms of the phonon density of state (summarized in Fig. 8). One can see that Einstein model gives rise to a delta function at the characteristic oscillator frequency and Debye model more or less a gradual increase with a sharp cut off. A real life density of state profile of phonons is shown in Fig. 8: at lower energies, how the phonon density of states approaches zero is much better captured by the Debye model (Fig. 8 right panel), and this is reflected in the better description of the low temperature heat capacity by the Debye model. The Einstein model can phenomenologically capture the sharp peaks in the phonon density of states at higher energies.

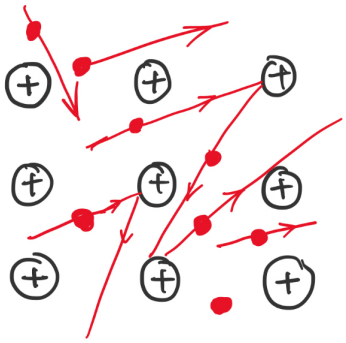

Figure 9: Schematic of the electrons under consideration in the Drude model

3 Electrons in metals

In the previous lectures we've seen that some essential properties of the lattice in the early understanding of the solids, here we'd like to move to the electrons in metallic systems. A lot of the developments we will discuss in the following classes took place around the same time with what we've seen in the last classes–this is a period that precedes the full development of the theory of solids, and around the same time when important aspects of quantum mechanics were bit by bit revealed. You'll hopefully see how a very similar line of stories play out here.

In this chapter, aside from heat capacity we've touched on in last chapter, we'll be focusing on a set of transport phenomena associated with electrons in metals (thanks to their mobile nature!). Experimentally, the most important transport coefficients are electrical transport (this is essentially the Ohm's law $V = IR$)

$$j = \sigma E \tag{29}$$

thermal transport that can be defined in an analogous manner

$$j_Q = \kappa(-\nabla T) \tag{30}$$

The two channels may even crosstalk, generating the so-called thermoelectric transport. The thermoelectric effect has a few different forms, the simplest one being the so-called Seebeck coefficient S

$$S = -\frac{\Delta V}{\Delta T} \tag{31}$$

(the Seebeck effect is behind how thermocouple works)

Electrical transport thanks to its compact implementation is often among the few accessible experimental tools for condensed matter physicists at extremely high pressure, high magnetic field, and in samples with limited sizes.

3.1 Drude model: resistivity and Hall effect

The problem we'd like to describe is the transport of electrons in metals. Instead of individual electrons, we are interested in the 'mean' movement of a group of electrons. We may define the mean velocity and momentum of the groups as

$$\boldsymbol{v}_D = \frac{1}{N}\sum_i \boldsymbol{v}_i \tag{32}$$

$\boldsymbol{v}_D$ often called the drift velocity and we denote the corresponding 'mean' momentum as $\boldsymbol{p}$. A sketch of the free-to-move electrons under consideration is shown in Fig. 9, where the positively charged ions remain immobile.

The Drude theory uses a relxation time τ to account for the loss of momentum of electrons to obstacles they encounter, such as the lattice. At a given time interval dt, the probability of each electron experiencing a scattering event is dt/τ. A simplification in the theory is that the electrons will lose their momentum after each collision, therefore the momentum lost by collision can be written as $dt/\tau * \boldsymbol{p}$. Therefore we get the following time evolution of $\boldsymbol{p}$:

$$\frac{d\boldsymbol{p}}{dt} = \boldsymbol{F} - \frac{\boldsymbol{p}}{\tau} \tag{33}$$

Here $\boldsymbol{F}$ represents the external forces applied on the electrons, including the electrical or magnetic fields:

$$\boldsymbol{F} = -e(\boldsymbol{E} + \boldsymbol{v} \times \boldsymbol{B}) \tag{34}$$

We note that we adopt a notation such that e is the magnitude of the electron charge. One may view the $\boldsymbol{p}/\tau$ term in Eq. (2) as a drag force, or friction to the group of electrons. Without external fields, Eq. (2) describes a decay of momentum from its initial value to zero:

$$\boldsymbol{p}(t) = \boldsymbol{p}_0 e^{-t/\tau} \tag{35}$$

3.1.1 Electric field only

In the presence of only electric field,

$$\frac{d\boldsymbol{p}}{dt} = -e\boldsymbol{E} - \frac{\boldsymbol{p}}{\tau} \tag{36}$$

In the steady state $d\boldsymbol{p}/dt = 0$ giving

$$\boldsymbol{p} = -e\boldsymbol{E}\tau \tag{37}$$

The steady stream of movement of electrons gives rise electrical current. The current density $\boldsymbol{j}$ will therefore be:

$$\boldsymbol{j} = -en\boldsymbol{v} = \frac{ne^2\tau}{m_e}\boldsymbol{E} \tag{38}$$

3.1.2 Conductivity and resistivity tensors

Here we define two physical quantities, the conductivity σ and resistivity ρ. The former describing $\boldsymbol{j}$ induced by $\boldsymbol{E}$, and the latter $\boldsymbol{E}$ induced by $\boldsymbol{j}$. Since both $\boldsymbol{j}$ and $\boldsymbol{E}$ are vectors, strictly speaking both σ and ρ should be second rank tensors with

$$j_i = \sigma_{ij}E_j, E_k = \rho_{kl}j_l \tag{39}$$

It is not difficult to get

$$\sigma_{ij}\rho_{jk} = I \tag{40}$$

For Eq. (7), in the case where both $\boldsymbol{E}$ and $\boldsymbol{j}$ are along x (the direction of E and j should align in the absence of magnetic field and also spatial anisotropy):

$$\sigma_{xx} = \frac{ne^2\tau}{m_e}, \rho_{xx} = \frac{m_e}{ne^2\tau} \tag{41}$$

The definition of both quantities may seem redundant at first sight, and they are convenient at different occassions. Experimentally, most of the time it is practically easier to supply a constant current to the sample and measure voltage (therefore electric field), and you may see most experimental reports shown in ρ_{ij}. Theoretically, it can be more handy to use σ_{ij} as it can be expressed as the correlation function of current density.

Additionally, it is convenient to define the so-called mobility μ of the electrons:

$$|\boldsymbol{v}| = \mu|\boldsymbol{E}| \tag{42}$$

And one can figure out that

$$\mu = \frac{e\tau}{m}, \sigma_{xx} = ne\mu \tag{43}$$

This quantity is often used to indicate the cleaness of materials. Typical metals on the order of 1000 cm^2/Vs, and the highest go above 10^7 cm^2/Vs (see Fig. 10).

3.1.3 In the presence of both electric and magnetic fields

Here we introduce magnetic field into Eq. (5):

$$\frac{d\boldsymbol{p}}{dt} = -e(\boldsymbol{E} + \boldsymbol{v} \times \boldsymbol{B}) - \frac{\boldsymbol{p}}{\tau} \tag{44}$$

The steady state solution is

$$m\boldsymbol{v} = -e\boldsymbol{E}\tau - e\boldsymbol{v} \times \boldsymbol{B}\tau \tag{45}$$

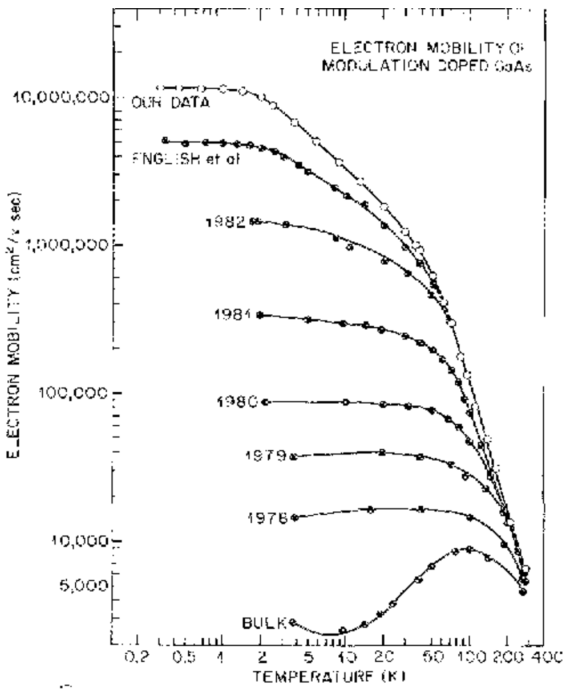

Figure 10: Progressive improvement of electronic mobility in GaAs quantum wells. Reference: Appl. Phys. Lett. 55, 1888–1890 (1989)

Let's replace $\boldsymbol{v}$ with $-\boldsymbol{j}/ne$:

$$m\frac{\boldsymbol{j}}{ne} + \frac{\boldsymbol{j}\times\boldsymbol{B}\tau}{n} = e\boldsymbol{E}\tau \tag{46}$$

For simplicity, let's assume $\boldsymbol{B}$ is along the z axis, E and j in the ab plane. The above can be rewritten as:

$$\begin{aligned}\frac{m}{ne^2\tau}j_x + \frac{B}{ne}j_y &= E_x\\ \frac{m}{ne^2\tau}j_y - \frac{B}{ne}j_x &= E_y\end{aligned} \tag{47}$$

Giving us the resisivity tensor within the xy plane

$$\rho_{ij} = \begin{pmatrix}\frac{m}{ne^2\tau} & \frac{B}{ne}\\ -\frac{B}{ne} & \frac{m}{ne^2\tau}\end{pmatrix} \tag{48}$$

The diagonal term is field-independent and is the same with our derivation above for the case without magnetic field. The off-diagonal term is the Hall effect. It is linear in magnetic field and inversely proportional to the carrier density of the system. The most common way to measure the Hall effect is to use a slab geometry and measure the voltage perpendicular to the current (see Fig. 11), and that the accumulation of electrons at the ends of the sample provides an electric field that counter-balances the Lorentz force. Another fun geometry to think about is the Corbino geometry composed of concentric circles (see right panel of Fig. 11). There the Hall currents don't show up in the voltage, but instead show up as a current surrounding the loop and therefore generates a magnetization proportional to σ_{xy}. This geometry is itself often experimentally used to eliminate Hall effect in the the transport response (since it turns Hall effect to magnetization, which is generally more difficult to measure), but theoretically used as gedanken experiments to understand the quantization in the quantum Hall effect (see Laughlin's charge pump).

Hall effect is a widely used method to extract carrier densities of different materials (see homework). Conversely, if the carrier density is know, one can use the Hall effect to measure magnetic fields–this is how Hall sensors work.

For completeness, we also write out the conductivity tensor in the xy plane under magnetic field here:

$$\sigma_{ij} = \begin{pmatrix}\frac{ne\mu}{1+(\mu B)^2} & -\frac{ne\mu^2 B}{1+(\mu B)^2}\\ \frac{ne\mu^2 B}{1+(\mu B)^2} & \frac{ne\mu}{1+(\mu B)^2}\end{pmatrix} \tag{49}$$

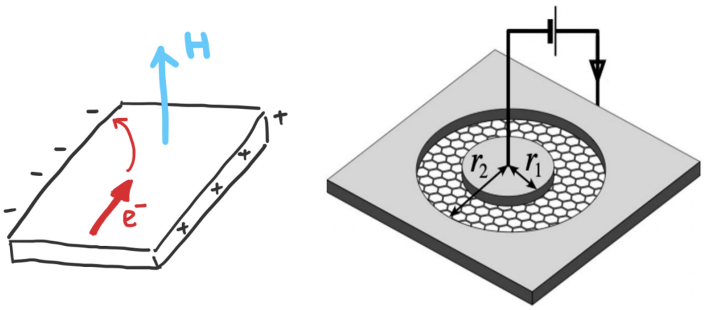

Figure 11: Schematic of the Hall effect in a slab geometry (left) and schematic of the corbino geometry (right)

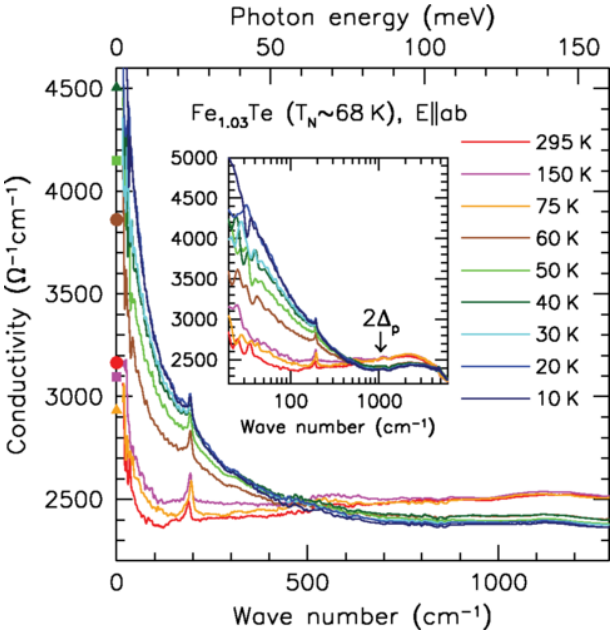

Figure 12: Optical conductivity of FeTe. Reference: Phys. Rev. B 90, 121114(R) (2014).

$\rho_{yx}/\rho_{xx} = \sigma_{xy}/\sigma_{xx} = \mu B \equiv \tan(\Theta_H)$, and Θ_H is often called the Hall angle, which gives the relative orientation between the electric field vector $\boldsymbol{E}$ and electric current vector $\boldsymbol{J}$.

3.2 AC Drude model: plasma frequency of metals

Having looked at the electron transport under the magnetic field, we turn to another aspect of electrons in metals that can be captured by the Drude model: the optical properties of metals.

To do this we start from Eq. (5) and let the electric field to be of AC nature $\boldsymbol{E} = \boldsymbol{E_0} e^{i\omega t}$. We attempt to solve Eq. (5) with an oscillating current with a potential phase shift from the applied field:

$$\boldsymbol{p} = \boldsymbol{p}_0 e^{i(\omega t + \phi)} \tag{50}$$

This gives rise to

$$i\omega\tau \boldsymbol{p}_0 e^{i\phi} = -e\tau \boldsymbol{E}_0 - \boldsymbol{p_0} e^{i\phi} \tag{51}$$

where

$$\boldsymbol{p}_0 e^{i\phi} = \frac{-e\boldsymbol{E}_0\tau}{1 + i\omega\tau} \tag{52}$$

and

$$\boldsymbol{j}_0 e^{i\phi} = \frac{ne^2\boldsymbol{E}_0\tau}{m(1 + i\omega\tau)} \tag{53}$$

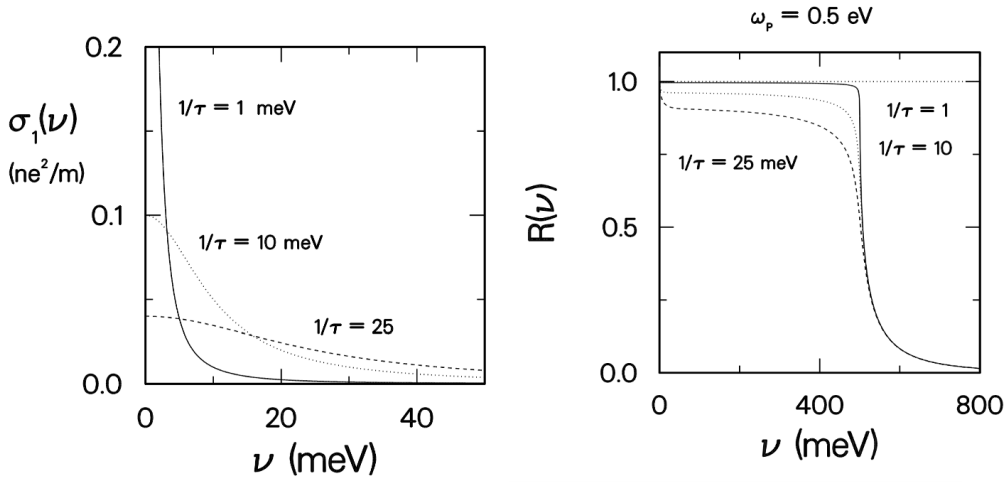

Figure 13: Real part of optical conductivity (left) and reflectance (right) of the Drude model as a function of frequency.

We can obtain a complex conductivity $\sigma(\omega)$

$$\sigma(\omega) = \frac{ne^2\tau}{m}\frac{1-i\omega\tau}{1+(\omega\tau)^2} \tag{54}$$

This is the optical conductivity–measuring the full frequency dependence of optical conductivity is a way to extract τ and the carrier density n.

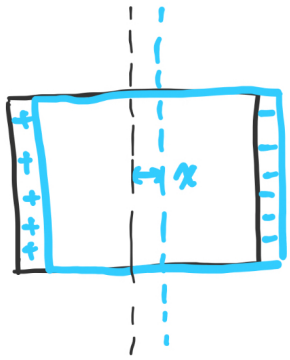

Figure 14: Schematic of the collective plasma oscillation

The AC Drude model also allows one to analyze the reflection and refraction of metals. We will not focus on derivation here but refer one to e.g. Chapter 2 of Dresselhaus Solid State Physics Lecture Notes[1]. The key result is that the Drude model gives reflectance near 1 for metals at frequencies below a so-called plasma frequency ω_p

$$\omega_p^2 = \frac{ne^2}{\epsilon_0 m} \tag{55}$$

ω_p corresponds to a collective oscillation of the electrons on top of the positively charged ionic background. Consider a finite size sample with electron density n and the uniform charge displaces from its original location by x (here σ indicates the surface charge density, not to be confused with conductivity defined above):

$$E = \frac{\sigma}{\epsilon_0} = -\frac{nex}{\epsilon_0} \tag{56}$$

The motion of these electrons becomes

$$m\ddot{x} = -\frac{ne^2}{\epsilon_0}x \tag{57}$$

[1] https://web.mit.edu/6.732/www/opt.pdf

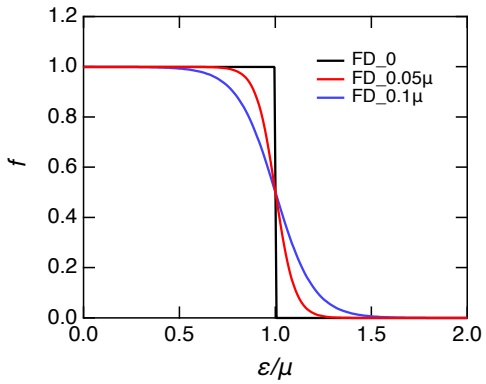

Figure 15: Fermi-Dirac distribution

Giving the characteristic frequency of this collective motion of electrons driven by external electric field. For regular metals, this frequency falls into the range of ultraviolet. Above this frequency metals are expected to be transparent.

3.3 The fermionic nature of electrons

The above discussion are all semiclassical but captures some essential properties of metals–including electrical conduction and its interaction with light. In the following we will start introducing the quantum mechanical nature of the electrons.

3.3.1 Fermi Dirac distribution

Recall the Fermi-Dirac distribution

$$f_{FD} = \frac{1}{e^{(\epsilon-\mu)/k_BT}+1} \tag{58}$$

Here μ indicates the chemical potential. A simple picture of the chemical potential is that at $T = 0$, $f_{FD} = 0$ if $\epsilon > \mu$ and $f_{FD} = 1$ if $\epsilon < \mu$. At finite temperature, this sharp step function is smeared out with its width is around k_BT.

We start with "free" electrons whose wave function are plane waves in space $e^{i(\boldsymbol{k}\cdot\boldsymbol{x}-\epsilon t/\hbar)}$ and energy

$$\epsilon(\boldsymbol{k}) = \frac{\hbar^2\boldsymbol{k}^2}{2m} \tag{59}$$

We will use the periodic boundary condition introduced above, which only allows the following $\boldsymbol{k}$ values:

$$(k_x, k_y, k_z) = n_x\frac{2\pi}{L_x}, n_y\frac{2\pi}{L_y}, n_z\frac{2\pi}{L_z} \tag{60}$$

The total number of electrons N should be (the factor of 2 comes from the spin degeneracy of electrons as they are $S = 1/2$ particles)

$$N = 2\sum_{\boldsymbol{k}} f_{FD} = 2\frac{V}{(2\pi)^3}\int d\boldsymbol{k}\frac{1}{e^{(\epsilon(\boldsymbol{k})-\mu)/k_BT}+1} \tag{61}$$

3.3.2 Zero temperature properties: Fermi energy, Fermi surface

Let's now focus on the zero temperature limit of the Fermi-Dirac distribution, and define the zero temperature chemical potential μ as the Fermi energy E_F; the corresponding wave vector is the Fermi wave vector k_F. The significance of these quantities is that if $\epsilon < E_F(k < k_F)$, the electronic state is (singly) occupied; if $\epsilon > E_F(k > k_F)$ the state is not occupied.

In this case,

$$N = 2\frac{V}{(2\pi)^3}\int^{|\boldsymbol{k}|<k_F} d\boldsymbol{k} = \frac{2V}{(2\pi)^3}(\frac{4\pi}{3}k_F^3) \tag{62}$$

where k_F is defined as the largest wave vector that is occupied:

$$k_F = (3\pi^2 n)^{1/3} \tag{63}$$

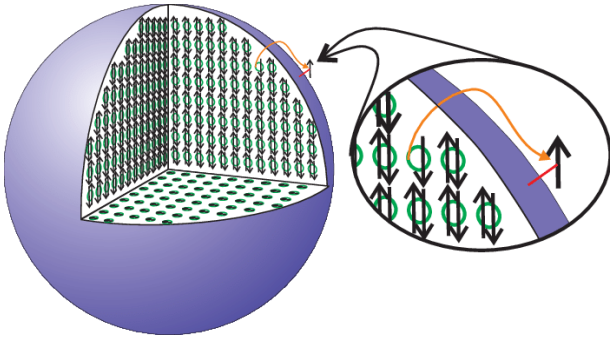

Figure 16: Schematic of the Fermi sea. Taken from Contemporary Physics 40(2):95 (1999)

We can also get the corresponding Fermi energy E_F:

$$E_F = \frac{\hbar^2(3\pi^2 n)^{2/3}}{2m} \tag{64}$$

The occupied states form a spherical region in the k-space as shown in Fig. 16. The surface of the sphere is the so-called Fermi surface that separates regions in the k-space that is occupied and unoccupied.

In the simple picture of one free electron per atom, we may estimate the Fermi energy to be on the order of 7 eV, corresponding to a temperature scale (we will call this the Fermi temperature T_F) on the order of 10^5 K. This is a very high energy scale and solid metals easily melt before one reaches that temperature. In other words, the electrons in metals form a very deep ocean, and our working temperatures basically just scratches the surface. A side note is that the above discussion only uses the fermionic nature of the electrons and one should be able to use a similar framework to describe the degenerate neutron stars.

3.3.3 Zero temperature properties: density of states and Pauli paramagnetism

Recalling the density of state we've introduced above for lattice vibrations, here we can similarly introduce a density of states for the electrons $g(\epsilon)$ here ($g(\epsilon)$ is defined per unit volume):

$$N = V\int_0^\infty d\epsilon g(\epsilon) f_{FD}(\epsilon) \tag{65}$$

In the context of the free electron model we've been working with

$$g(\epsilon)d\epsilon = \frac{2}{(2\pi)^3}4\pi k^2 dk \tag{66}$$

With $d\epsilon/dk = \hbar^2 k/m$,

$$g(\epsilon)d\epsilon = \frac{2}{(2\pi)^3}4\pi k^2 \frac{m}{\hbar^2 k}d\epsilon = \frac{m\sqrt{2m\epsilon}}{\pi^2\hbar^3}d\epsilon \tag{67}$$

We find $g(\epsilon) \sim \epsilon^{1/2}$. Note that this only holds for the three dimensional case (in the homework you will be asked to work out the 1D and 2D cases). One can write $g(\epsilon)$ in a slightly simpler form

$$g(\epsilon) = \frac{3n}{2E_F}(\frac{\epsilon}{E_F})^{1/2} \tag{68}$$

As a direct application of the notion of density of states, we can calculate the magnetic susceptibility of a metal. We introduce an additional Zeeman term to the Hamiltonian of electrons:

$$\mathscr{H} = \frac{\hbar \boldsymbol{k}^2}{2m} + g\mu_B \boldsymbol{B}\cdot\boldsymbol{\sigma} \tag{69}$$

$g = 2$ for electron spin, and σ is the spin of the electron, which can take values of $\pm 1/2$. The resulting energies for spin up and spin down electrons are

$$\begin{aligned}\epsilon(\boldsymbol{k},\uparrow) &= \frac{\hbar^2\boldsymbol{k}^2}{2m} + \mu_B B \\ \epsilon(\boldsymbol{k},\downarrow) &= \frac{\hbar^2\boldsymbol{k}^2}{2m} - \mu_B B\end{aligned} \tag{70}$$

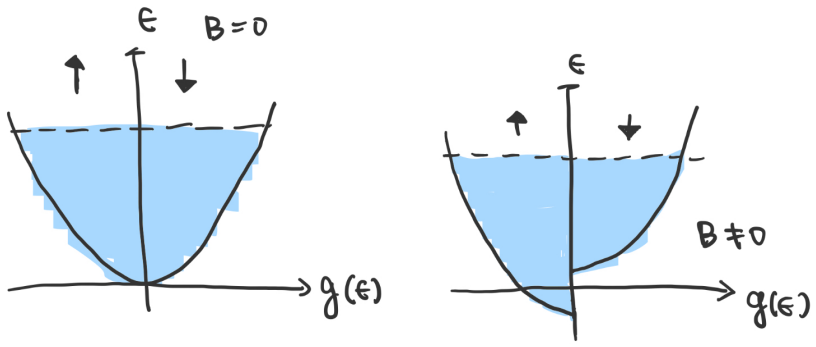

Figure 17: Caption

In the density of state picture the magnetic field causes an energetical shift between the up and down spins. The total magnetization (at zero temperature) will be a difference between the up and down spins. Note that for each spin spicies, the density of states is $g(E_F)/2$, giving us

$$M = (g(E_F)/2 * \mu_B B * 2) * \mu_B = g(E_F)\mu_B^2 B \tag{71}$$

As a result the magnetic susceptibility $\chi \equiv M/H = \mu_0 M/H$ is

$$\chi = \mu_0 \mu_B^2 g(E_F) \tag{72}$$

This predicts a temperature-independent paramagnetic susceptibility of metals that originates from the Pauli exclusion principle of the electrons, therefore termed Pauli paramagnetism.

As an side, when the density of states gets very large, one needs to start thinking about the interactions between the electrons, and this can drive a ferromagnetic order splitting the bands away from the Fermi level. This is what happens in Fe, Co, Ni where they are near their density of states peaks.

3.3.4 Finite temperature effects: Sommerfeld expansion and heat capacity of metals

In the previous section we have seen a few important concepts that arise from the Fermi Dirac distribution of the electrons in metals, including Fermi surface, Fermi energy, density of states, and magnetic susceptibility of metals. In the following we'd like to take into account finite temperature effects.

Sommerfeld expansion (1928) is a framework for calculating properties related to the Fermi-Dirac distribution at low temperatures. It can be often found in one of the two following forms: here $H(\epsilon)$ is an energy-dependent function that smoothly varies with μ (from now on we use f to denote the Fermi-Dirac distribution f_{FD}.)

$$\int_{-\infty}^{+\infty} H(\epsilon) f(\epsilon) d\epsilon = \int_{-\infty}^{\mu} H(\epsilon) d\epsilon + \frac{\pi^2}{6}(k_B T)^2 H'(\mu) + \frac{7\pi^4}{360}(k_B T)^4 H'''(\mu) + O(\frac{k_B T}{\mu})^6 \tag{73}$$

or alternatively

$$\int_{-\infty}^{+\infty} H(\epsilon) \frac{\partial f}{\partial \epsilon} d\epsilon = H(\mu) + \frac{\pi^2}{6}(k_B T)^2 H''(\mu) + \frac{7\pi^4}{360}(k_B T)^4 H''''(\mu) + O(\frac{k_B T}{\mu})^6 \tag{74}$$

These two forms are related, and see a discussion connecting these notions from the corresponding chapter in Grosso Solid State Physics (uploaded to canvas). The main idea is that if $H(\epsilon)$ itself is a smooth function with ϵ, we can Taylor expand $H(\epsilon)$ around μ and convert the integrations in Eq. 73 and 74 involving $f(\frac{\partial f}{\partial \epsilon})$ to $\int (\epsilon - \mu)^n f d\epsilon$ ($\int d\epsilon (\epsilon - \mu)^n (\frac{\partial f}{\partial \epsilon})$).

We will see the usefulness of Eq. 74 in a few sections. In this section we will focus on Eq. 73 and apply it to calculating the internal energy of the Fermi sea. What Eq. 73 does may be viewed as separating f into a step function (its zero temeprature value) and a deviation from it (see Fig. 18). The deviation itself is odd around μ. Let's first apply this to the total number of electrons in our system: if we take $H(\epsilon) = g(\epsilon)$, we obtain the total number of electrons per volume

$$n = \int_{-\infty}^{+\infty} g(\epsilon) f(\epsilon) d\epsilon = \int_{-\infty}^{\mu} g(\epsilon) d\epsilon + \frac{\pi^2}{6}(k_B T)^2 g'(\mu) + O(T^4) \tag{75}$$

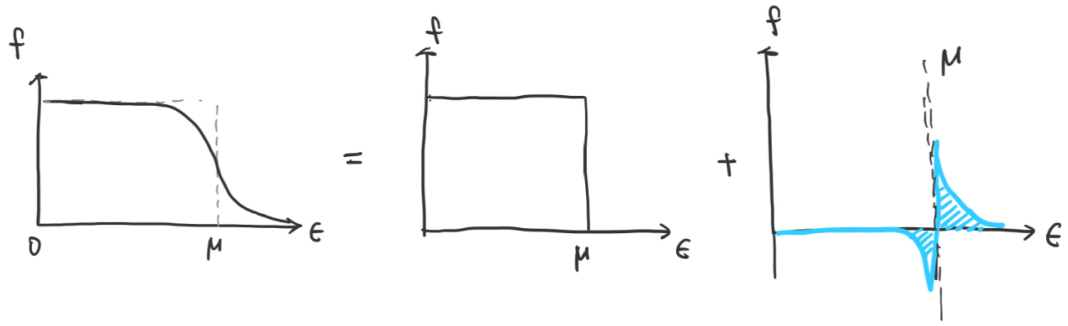

Figure 18: A simplified sketch of the Sommerfeld expansion. The upper and lower row depicts the Fermi-Dirac distribution decomposed into its step function and its deviation.

Which has to equal that at zero temperature:

$$n = \int_{-\infty}^{\mu} g(\epsilon)d\epsilon + \frac{\pi^2}{6}(k_B T)^2 g'(\mu) = \int_{-\infty}^{E_F} g(\epsilon)d\epsilon \tag{76}$$

This can be rewritten as (to the lowest order)

$$g(E_F)(E_F - \mu) = \frac{\pi^2}{6}(k_B T)^2 g'(E_F) \tag{77}$$

suggesting that the chemical potential can depend on energy

$$\mu = E_F - \frac{\pi^2}{6}(k_B T)^2 \frac{g'(E_F)}{g(E_F)} \tag{78}$$

We note that since $g'(E_F)/g(E_F) = 1/(2E_F)$, the temperature-dependence of μ is therefore to the first order of $\frac{k_B T}{E_F}$, and is not significant until $k_B T$ approaches T_F. This is related to thermoelectricity.

If we take $H(\epsilon) = \epsilon g(\epsilon)$, we can calculate the internal energy

$$U = \int_{-\infty}^{+\infty} \epsilon g(\epsilon) f(\epsilon) d\epsilon = \int_{-\infty}^{\mu} \epsilon g(\epsilon) d\epsilon + \frac{\pi^2}{6}(k_B T)^2 [g(\mu) + \mu g'(\mu)] + O(T^4) \tag{79}$$

The first term in the integral can be approximated as

$$\int_{-\infty}^{\mu} \epsilon g(\epsilon) d\epsilon = \int_{-\infty}^{E_F} \epsilon g(\epsilon) d\epsilon + (\mu - E_F) E_F g(E_F) \tag{80}$$

Combining Eq. (77) and (80) yields

$$U = \int_{-\infty}^{E_F} \epsilon g(\epsilon) d\epsilon + \frac{\pi^2}{6}(k_B T)^2 g(E_F) \tag{81}$$

The first term being the ground state energy and the second term gives the leading temperature dependence of U. As a result, the heat capacity of these electrons will be

$$C = (\frac{\partial U}{\partial T}) = \frac{\pi^2}{3} k_B^2 T g(E_F) \tag{82}$$

This accounts for the T-linear heat capacity observed in metals $AT^3 + \gamma T$. The coefficient of the T-linear heat capacity is often denoted as γ and is called the Sommerfeld coefficient. For normal metals, the absolute value is far from k_B per electron, consistent with the "condensed" nature of the Fermi surface. In certain materials termed heavy fermions, the electronic heat capacity can get much larger, which comes from these conduction electrons abosrbing entropy of other localized spins in the system (each localized spin has entropy $k_B \ln 2$).

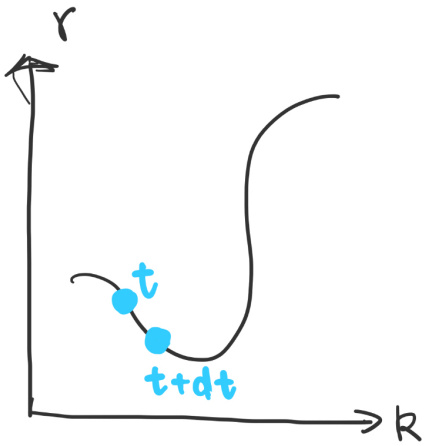

Figure 19: Caption

3.3.5 Revisit transport with Fermi-Dirac distribution: Boltzmann transport

One of the most widely used framework to model transport of particles with a distribution function is the Boltzmann transport equation (1872). The equation itself was put forward to describe classical fluid, but can be readily applied to incorporate the Fermi-Dirac distribution into the transport of electrons in solids. An expanded version of the discussions here can be found in Girvin and Yang, Modern Condensed Matter Physics.

The distribution function f is allowed to be dependent on momentum, position and time $f(\boldsymbol{k}, \boldsymbol{r}, t)$; without collisions, the probability of an electron taking a particular point in the phase space should not change, given we properly trace where the particle came from in the previous instance of time (Fig. 19):

$$f(\boldsymbol{k}, \boldsymbol{r}, t)d\boldsymbol{k}(t)d\boldsymbol{r}(t) = f(\boldsymbol{k} - \frac{F}{\hbar}dt, \boldsymbol{r} - \boldsymbol{v}dt, t - dt)d\boldsymbol{k}(t - dt)d\boldsymbol{r}(t - dt) \tag{83}$$

and $d\boldsymbol{k}(t)d\boldsymbol{r}(t) = d\boldsymbol{k}(t - dt)d\boldsymbol{r}(t - dt)$ (the latter is the conservation of phase space, i.e. Liouville's theorem). Thus

$$\frac{df}{dt} = \frac{\partial f}{\partial t} + \frac{\partial \boldsymbol{r}}{\partial t} \cdot \nabla_{\boldsymbol{r}} f + \frac{\partial \boldsymbol{k}}{\partial t} \cdot \nabla_{\boldsymbol{k}} f = \frac{\partial f}{\partial t} + \boldsymbol{v} \cdot \nabla_{\boldsymbol{r}} f + \frac{\boldsymbol{F}}{\hbar} \cdot \nabla_{\boldsymbol{k}} f = 0 \tag{84}$$

When collisions between the particles are considered, the Boltzmann equation can be written as

$$\frac{\partial f}{\partial t} + \boldsymbol{v} \cdot \nabla_{\boldsymbol{r}} f + \frac{\boldsymbol{F}}{\hbar} \cdot \nabla_{\boldsymbol{k}} f = (\frac{\partial f}{\partial t})_{coll} \tag{85}$$

where all the collision processes are incorporated in the right hand side term. Note that the Boltzmann formulation is semiclassical in the sense that here the momentum and position of a given particle can be determined simultaneously.

We start with a steady state ($\partial f/\partial t = 0$) in the presence of an electric field. Furthermore, $\nabla_{\boldsymbol{r}} f = 0$ given we have a uniform sample. We are left with

$$-\frac{e\boldsymbol{E}}{\hbar} \cdot \nabla_{\boldsymbol{k}} f = (\frac{\partial f}{\partial t})_{coll} \tag{86}$$

Here we assume the external fields introduce a small perturbation to f such that $f = f_0 + f_1$, where f_0 is the equilibrium Fermi-Dirac distribution. Additionally, we work with the following relaxation time approximation:

$$(\frac{\partial f}{\partial t})_{coll} = -\frac{1}{\tau}(f - f_0) = -\frac{f_1}{\tau} \tag{87}$$

Only keeping terms linear with the electric field,

$$-\frac{e\boldsymbol{E}}{\hbar} \cdot \nabla_{\boldsymbol{k}} f = -\frac{e\boldsymbol{E}}{\hbar} \cdot \nabla_{\boldsymbol{k}} f_0 = -\frac{f_1}{\tau} \tag{88}$$

Giving

$$f_1 = e\boldsymbol{E} \cdot \boldsymbol{v}\tau(\frac{\partial f_0}{\partial \epsilon}) \tag{89}$$

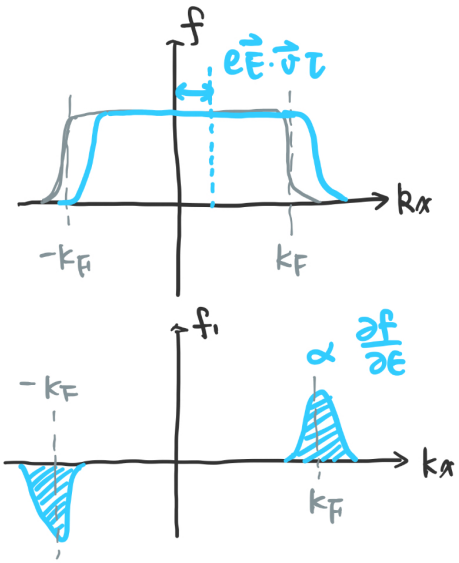

Figure 20: Schematic of electric field-induced deviation of the distribution function from the Fermi sea

Alternatively, since

$$f_1 = \frac{e\boldsymbol{E}}{\hbar}\nabla_{\boldsymbol{k}} f_0 \tag{90}$$

We can view the new distribution f as

$$f = f_0 + f_1 \simeq f_0(\boldsymbol{k} + \frac{e\boldsymbol{E}}{\hbar}\tau) \tag{91}$$

with an overall translation of the occupied states in the k-space with the electric field.

The electric field induced deviation of distribution function is illustrated in Fig. 20. One may immediately notice that the deviation from thermal equilibrium only takes place near the Fermi wave vector and therefore the Fermi-Dirac distribution forces that only electrons near the Fermi surface are driven out of the thermal equilibrium and contribute to the scattering processes.

The electrical current through the sample can be calculated through (factor of 2 comes from spin degree of freedom)

$$\boldsymbol{j} = -\frac{2e}{(2\pi)^3}\int d\boldsymbol{k}\boldsymbol{v} f_1 = -\frac{2e^2}{(2\pi)^3}\int d\boldsymbol{k}\boldsymbol{v}(\boldsymbol{E}\cdot\boldsymbol{v})\tau(\frac{\partial f_0}{\partial \epsilon}) \tag{92}$$

Taking $\boldsymbol{j} \parallel \boldsymbol{E} \parallel x$:

$$j_x = -\frac{2e^2}{(2\pi)^3}\int d\boldsymbol{k}(E_x v_x^2)\tau(\frac{\partial f_0}{\partial \epsilon}) \tag{93}$$

This can be written in terms of density of states $g(\epsilon)$ via $\frac{2}{(2\pi)^3}\int d\boldsymbol{k} = \int d\epsilon g(\epsilon)$

$$\sigma_{xx} = -e^2\int d\epsilon g(\epsilon) v_x^2(\frac{\partial f_0}{\partial \epsilon})\tau \tag{94}$$

Here we use the following approximation $(-\frac{\partial f_0}{\partial \epsilon}) \simeq \delta(\epsilon - E_F)$

$$\sigma_{xx} = \frac{e^2 g(E_F) v_F^2}{3}\tau = \frac{ne^2\tau}{m} \tag{95}$$

This recovers what we have obtained from the Drude model above. Simon's book has a section devoted to discussing why Drude model works so well given its simple form. The main idea is that the Drude model can be viewed as describing the motion of the center of the mass of the Fermi sea.

3.3.6 Thermal and thermoelectric transport

The Boltzmann formulism also allows us to model the thermal and thermoelectric transport phenomena in metals. This part is largely taken from Girvin and Yang. Here we consider a weak gradient of chemical potential and temperature, aside from the applied external electric field. The "gradient" forces us to take into account the $\boldsymbol{v} \cdot \nabla_{\boldsymbol{r}} f$ term in the Boltzmann equation:

$$\nabla_{\boldsymbol{r}} f = (\frac{\partial f_0}{\partial T})\nabla T + (\frac{\partial f_0}{\partial \mu})\nabla \mu \tag{96}$$

From the form of the Fermi-Dirac distribution itself

$$\frac{\partial f_0}{\partial \mu} = -\frac{\partial f_0}{\partial \epsilon}, \frac{\partial f_0}{\partial T} = \frac{\epsilon(\boldsymbol{k}) - \mu}{T}(-\frac{\partial f_0}{\partial \epsilon}) \tag{97}$$

Eq. 96 becomes

$$\nabla_{\boldsymbol{r}} f = (-\frac{\partial f_0}{\partial \epsilon})[\frac{\epsilon(\boldsymbol{k}) - \mu}{T}\nabla T + \nabla \mu] \tag{98}$$

Along with the electric field term $\frac{\boldsymbol{F}}{\hbar} \cdot \boldsymbol{\nabla}_{\boldsymbol{k}} F = -e\boldsymbol{E} \cdot \boldsymbol{v}/\hbar(\partial f_0/\partial \epsilon)$ the total deviation from f_0 is

$$f_1 = \tau(\frac{\partial f_0}{\partial \epsilon})[\frac{\epsilon(\boldsymbol{k}) - \mu}{T}\nabla T + \nabla \mu + e\boldsymbol{E}] \cdot \boldsymbol{v} \tag{99}$$

The first term describes the heat flow in the system driven by temperature gradient. $\nabla\mu$ is the chemical potential gradient that can drive particle flow, but it differs from the electric field as a "statistical force". One may think about it as describing a diffusion of particles from a high density location to a lower density location. We can define an electrochemical potential $\tilde{\mu} = \mu - e\Phi$ (Φ being the electric potential) and associated effective electric field $\boldsymbol{\Sigma} \equiv \nabla\mu/e + \boldsymbol{E}$. An important note is that the voltage probed by external electrodes is the electrochemical potential.

Electric and heat currents are defined respectively as follows

$$\begin{aligned} \boldsymbol{j} &= -2e \int \frac{d\boldsymbol{k}}{(2\pi)^3} \boldsymbol{v} f_1 \\ \boldsymbol{j}_Q &= 2 \int \frac{d\boldsymbol{k}}{(2\pi)^3} \boldsymbol{v}[\epsilon(\boldsymbol{k}) - \mu] f_1 \end{aligned} \tag{100}$$

and we can define the following transport equations

$$\begin{aligned} \boldsymbol{j} &= L^{11}\boldsymbol{\Sigma} + L^{12}(-\nabla T) \\ \boldsymbol{j}_Q &= L^{21}\boldsymbol{\Sigma} + L^{22}(-\nabla T) \end{aligned} \tag{101}$$

Where [2]

$$\begin{aligned} L^{11} &= \sigma \\ L^{21} &= TL^{12} = -\frac{\pi^2}{3e}(k_B T)^2(\frac{\partial \sigma}{\partial \epsilon}) \\ L^{22} &= \frac{\pi^2}{3}\frac{k_B^2 T}{e^2}\sigma \end{aligned} \tag{104}$$

Below we consider a measurement condition without electrical current flow, where $\boldsymbol{j} = 0$. It directly follows from $\boldsymbol{j} = 0$:

$$\frac{\boldsymbol{\Sigma}}{\nabla T} = \frac{L^{12}}{L^{11}} \tag{105}$$

[2] Eq. 104 can be obtained from the Sommerfeld expansion listed in Eq. 74 and by defining

$$\sigma(\epsilon) = 2e^2\tau(\epsilon) \int \frac{d\boldsymbol{k}^3}{(2\pi)^3} \frac{v_x^2}{3} \delta(\epsilon(\boldsymbol{k}) - \epsilon) \tag{102}$$

and

$$\mathscr{L}^{(\alpha)} = \int d\epsilon(-\frac{\partial f^0}{\partial \epsilon})(\epsilon - \mu)^\alpha \sigma(\epsilon) \tag{103}$$

Furthermore, $L^{11} = \mathscr{L}^{(0)}$, $L^{12} = \frac{1}{-eT}\mathscr{L}^{(1)}$, $L^{22} = \frac{1}{e^2 T}\mathscr{L}^{(2)}$.

This gives the Seebeck coefficient $S \equiv -\dfrac{\boldsymbol{\Sigma}}{\boldsymbol{\nabla} T}$ through the following Mott formula:

$$S = -\frac{\pi^2}{3}(\frac{k_B}{e})k_B T(\frac{1}{\sigma}\frac{\partial \sigma}{\partial \epsilon}) \tag{106}$$

suggesting that S will be a physical quantity that is sensitive to fine features of the electronic states near the Fermi level.

In the free electron model

$$S \propto -(\frac{k_B}{e})\frac{k_B T}{E_F} \tag{107}$$

indicating that S is also a physical quantity sensitive to the "depth" of the Fermi sea. This is consistent with metals generally have a small Seebeck coefficients, while it can become really large in semiconducting materials.

Thermal conductivity can be obtained in a similar configuration ($\boldsymbol{j} = 0$):

$$\kappa = L^{22} - \frac{L^{21}L^{12}}{L^{11}} \tag{108}$$

The second term is very small and the thermal conductivity is found to be related to the electrical conductivity via

$$\frac{\kappa}{\sigma T} = \frac{\pi^2}{3}(\frac{k_B}{e})^2 \tag{109}$$

This is the so-called Wiedemann-Franz law.

3.4 Summary: transport and thermodynamic properties of metals

In this chapter we have looked at selected physical properties of electrons in metals. We first examined the semiclassical Drude model, which led us through

- Conductivity
- Hall effect
- Optical properties of metals

Introducing the fermionic nature of electrons we went through

- Fermi energy (level), Fermi wave vector
- Pauli paramagnetism
- Sommerfeld expansion and heat capacity of the electrons in metals

At the last section, revisting the transport phenomena pictured in the Drude model with the Fermi-Dirac distribution (via Boltzmann transport formulism) brings us to

- conduction and scattering of electron mostly take place around the Fermi level
- thermoelectricity and Widemann-Franz law in metals

For the electrical conductivity, Drude model more or less gives a reasonable discription, while one may see that the classical Drude model gives wrong predictions for the thermoelectricity and thermal conductivity (see Simon Oxford Solid State Basics for a short discussion), and only properly taking into account the Fermi-Dirac statistics can these quantities be correctly treated.

4 The building blocks of solids: the periodic table

In this chapter in order to prepare for diving into an in-depth study of phonons and electrons in the presence of real-life periodic structure of solids, let's take a step back and take a look at the fundamental building blocks of solids. This will involve a bit chemistry (we will try to include the bare minimum from a physicist's perspective), but in the end you will find a lot of discussions based on quantum mechanics and electrostatics. In particular, the covalent bonding lays the basis of later discussions on band formation.

4.1 Quantum number and orbitals

The periodic table is a systematic way of categorizing the different chemical elements based on their electronic states. We can start from reviewing the solution to the hydrogen and hydrogen-like atoms (Schrodinger equation in a spherical potential), can be labeled by the following four quantum numbers n, l, m, m_s. The wave function is often of the form

$$\phi_{nlm} = R_{nl}(r)Y_m^l(\theta,\phi)|\uparrow,\downarrow\rangle \tag{110}$$

Where the radial function R is determined by n and l and the angular evolution Y characterized by l and m.

- n is the principal quantum number, roughly speaking, corresponds to the number of nodes in the radial direction of the wave functions (this applies strictly speaking only the $l = 0$ case), can take integers (1,2,3,...)
- $l = 0, 1, ..., n-1$, is the angular momentum, which together with m determine the angular distribution of the wave function. $l = 0, 1, 2, 3, 4$ are callled s, p, d, f, g orbitals, respectively. The shape of the orbitals is one of the most important features characterizing the electronic states with realistic details. We will also call the group of states with the same n and l a shell as n, l together determine the energy of the states in an atom.
- $m(l_z) = -l, ...l$ ($2l+1$ degeneracies for each l). The angular distribution of a (l, m) state can be described by the spherical harmonics Y_l^m. Y_l^m itself is a complex function, and sometimes it is convenient to make linear combinations of these states to make real space representations. The new linear combinations are termed cubic (or kubic) harmonics. Here we take the example of the p electronic state:

$$\begin{aligned}
|p_z\rangle &= |1,0\rangle = Y_1^0 \\
|p_x\rangle &= \frac{1}{\sqrt{2}}(|1,-1\rangle - |1,1\rangle) = \frac{1}{\sqrt{2}}(Y_1^{-1} - Y_1^1) \\
|p_y\rangle &= \frac{i}{\sqrt{2}}(|1,-1\rangle + |1,1\rangle) = \frac{i}{\sqrt{2}}(Y_1^{-1} + Y_1^1)
\end{aligned} \tag{111}$$

  and d electronic state:

$$\begin{aligned}
|d_{z^2}\rangle &= Y_2^0 \\
|d_{xz}\rangle &= \frac{1}{\sqrt{2}}(Y_2^{-1} - Y_2^1) \\
|d_{yz}\rangle &= \frac{i}{\sqrt{2}}(Y_2^{-1} + Y_2^1) \\
|d_{xy}\rangle &= \frac{i}{\sqrt{2}}(Y_2^{-2} - Y_2^2) \\
|d_{x^2-y^2}\rangle &= \frac{1}{\sqrt{2}}(Y_2^{-2} + Y_2^2)
\end{aligned} \tag{112}$$

  The real representation of the electronic states can be quite convenient in thinking about the microscopic environment the electrons are put in. The subscripts are used to capture the sign variation of the wave function in different quadrants of x, y, z. For f electrons the different orbitals are labeled as $z^3, xz^2, yz^2, xyz, z(x^2 - y^2), x(x^2 - 3y^2)$ and $y(3x^2 - y^2)$.
- $m_z = \pm 1/2$, at last, m_s the spin degree of freedom. This can enter the energetics once the effect of spin-orbit coupling is taken into account (relevant for heavier elements where the relativistic spin-orbit coupling begins to be important, and especially important for describing magnetism in rare earth elements).

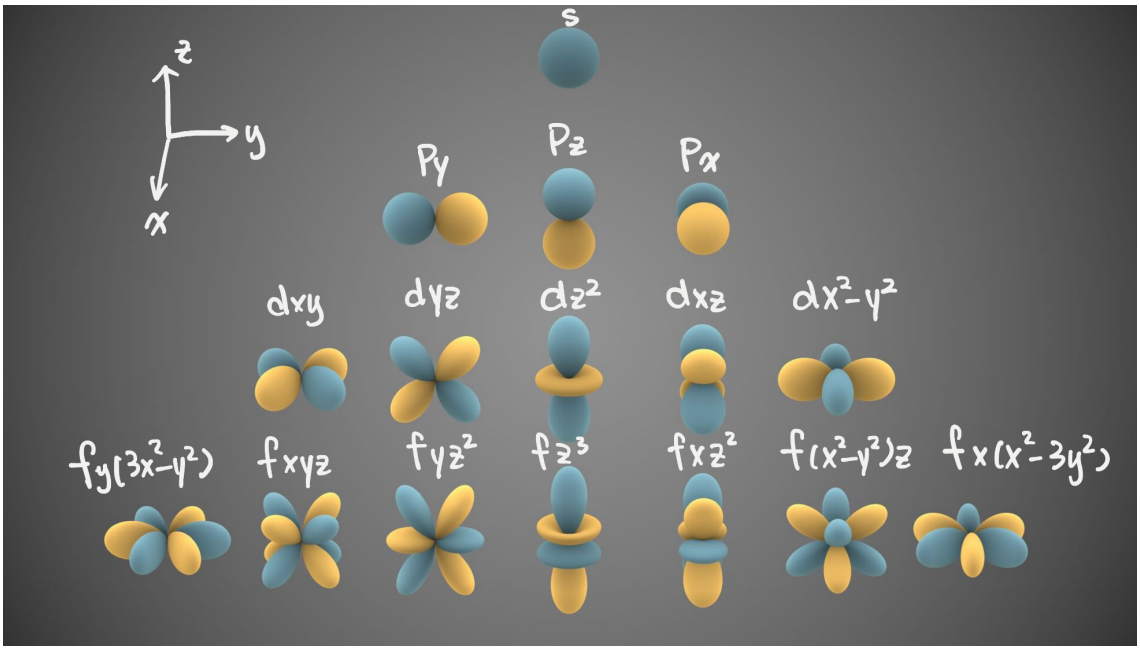

Figure 21: Schematic of the cubic spherical harmonics and the corresponding orbital states (adapted from wikipedia)

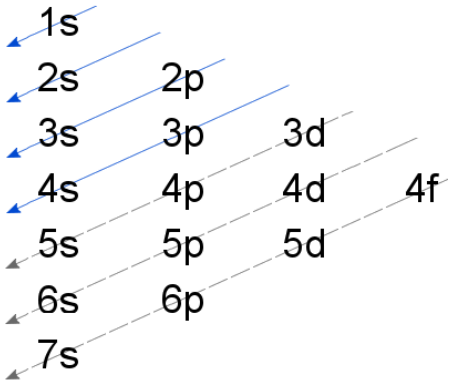

Figure 22: Madelung's rule of energetic order of the different (n, l) atomic shells

4.2 Filling of the electronic states and valence electrons

Considering multiple electrons in a single atom, there are a number of empirical rules that summarizes how these electrons are accomodated in the atomic levels we looked at above:

- Madelung's rule: the energy of the orbitals has an order $n + l$; when two shells have the same $n + l$, the shell with smaller n has lower energy.
- Aufbau principle: an entire shell should be filled before a new one can be started.
- Hund's rule: if multiple orbitals are available, fill different orbitals with parallel spins. Start filling with the opposite spin once all slots are already singly occupied.

The shell-filling sequence determines the overall structure of periodic table with each block representing the "filling" process of the particular orbital. The electrons in the outermost shell of a given element are called the valence electrons. In most cases, the inner shell electrons are pretty much inert, and can be viewed as an entity with the atomic core, and we will be concerned with the effective charge of the nucleus–which is a positive charge identical to the number of valence electrons.

The number of valence electrons determines the chemical property and the periodic table is structured by the valence electrons such that elements with similar chemical properties are put in the same column (inert gas at the

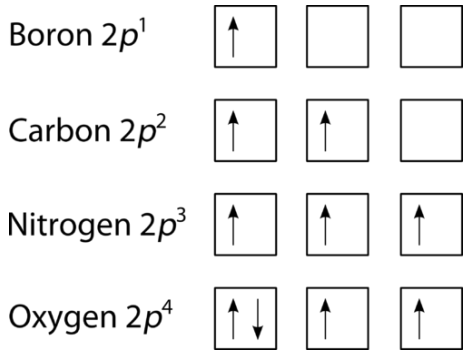

Figure 23: Hund's rule of electron filling applied to $2p$ elements

rightmost column, akali metal first column). The valence electrons are not only key for chemical activity, but also for band formation in compounds.

The periodic table also captures many systematic trends in both physical and chemical properties of atoms, and therefore often used as a road map when considering questions like "can element A and B form a stable compound?" and "how would the structure and lattice constant change if A element is substituted by C?"

Below we give three different examples of trends across the periodic table.

- Atomic radius

  See Fig. 24. The left side of the periodic table always comes with a larger atomic size, and roughly speaking this comes from a stronger attraction when the numbers of both positive charge in the atomic core and the electrons increase going from left to right. Atoms tend to grow larger as one goes down the periodic table, but this trend is not as strong as the decrease of atomic size from left to right. The alkali and alkali earth elements in general have the largest size among all. These elements (Na, K, Sr, Ba) sometimes act to effectively separate the electrons in three dimensional solids into relatively isolated two-dimensional layers (KFe2As2, CsV3Sb5).

- Ioinization, affinity and electronegativity

  The following will be concerning the ability of a given atom to lose or gain electrons. We define three closely related quantities: ionization energy, electron affinity and (Mulliken) electronegativity:

  - (first) ionization energy = (lowest) energy required to remove an electron from an atom to form an cation
  - electron affinity = energy gain for creating a negative ion by attaching an extra electron to an atom to form an anion
  - electronegativity = 0.5(electron affinity+ionization energy)

  The respective trends of the three are summarized in Fig. 25. They more or less show a similar qualitative trend: it is easy to lose electrons and form cations on the left side of the periodic table, and easy to gain electrons and form anions on the right. The alkali metal and halogen columns are the best examples at the two ends of the periodic table (here we ignore the chemically inert noble gas on the far right). This is driven by a more generic trend that **a fully filled shell is energetically favorable**.

5 The forces that hold solids together: chemical bonding in solids

In this chapter we'd like to go over a few different types of solids and the underlying force that holds these solids together. The content in this chapter belongs both to solid state physics and solid state chemistry. Again, the aim of this chapter is (1) to review the necessary chemistry to get familiar with the different types of solid state materials, (2) the description of covalent bonding bears the essential spirit of formation of electronic bands, which we will come back to in later chapters.

Ionic bonding, covalent bonding, metallic bonding and van der Waals bonding are the most important types of chemical bonding that play a role in supporting the solid state crystal structures. It can happen that more than one mechanism of bonding is at play for the same material. The strength of the underlying chemical bonding roughly speaking, correspond to the melting point of materials. Aside from these hydrogen bond is also sometimes

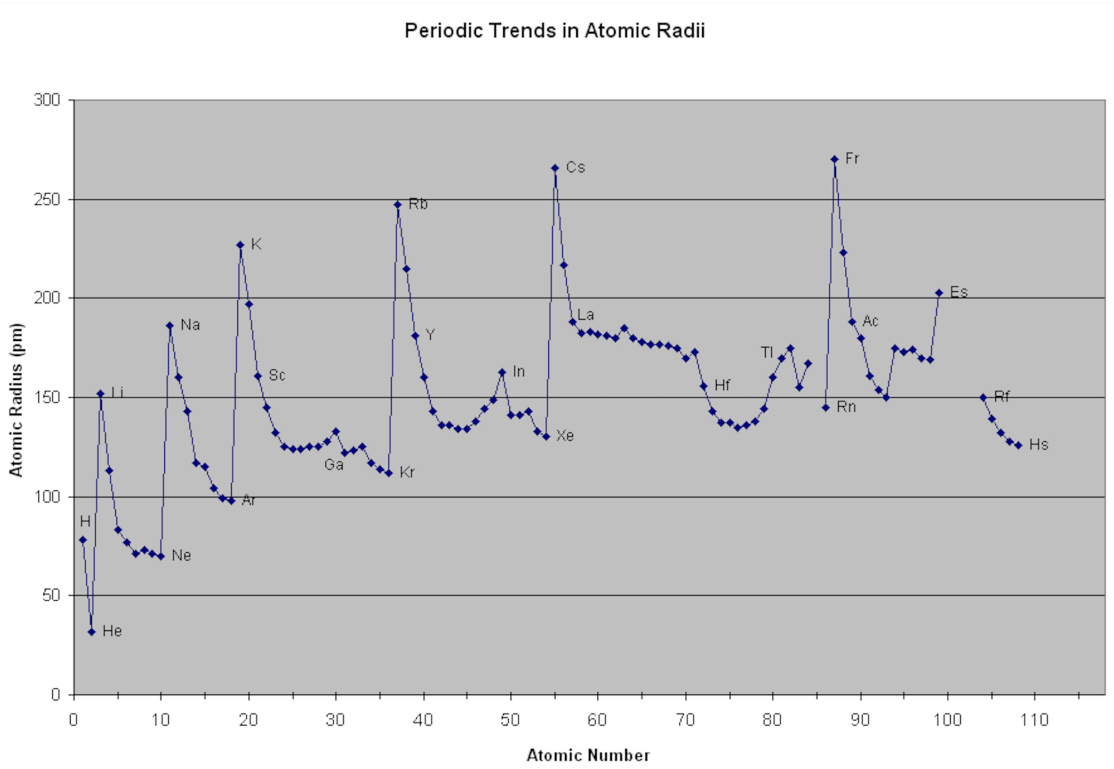

Figure 24: Evolution of atomic radius with atomic number (image credit: Angelo State University)

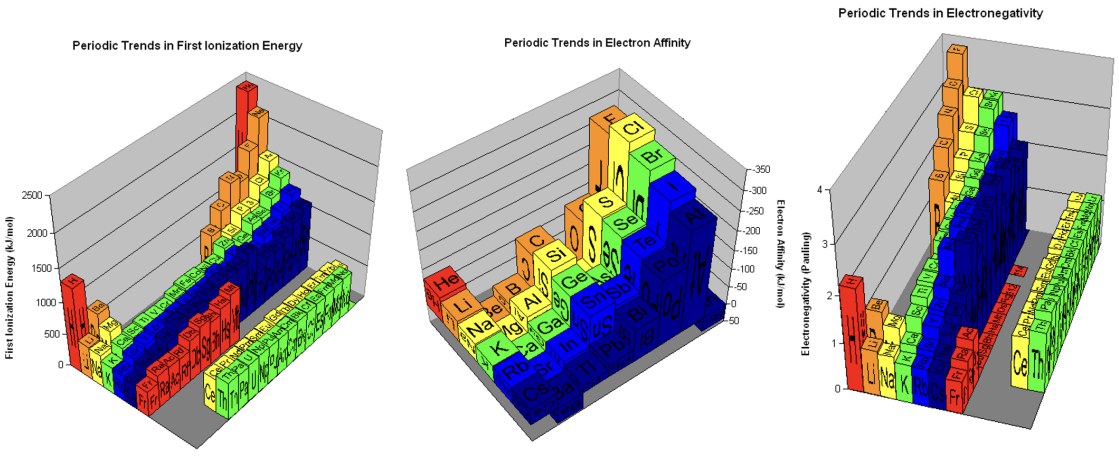

Figure 25: Left to right: trends of first ionization energy, electron affinity and electronegativity across the periodic table

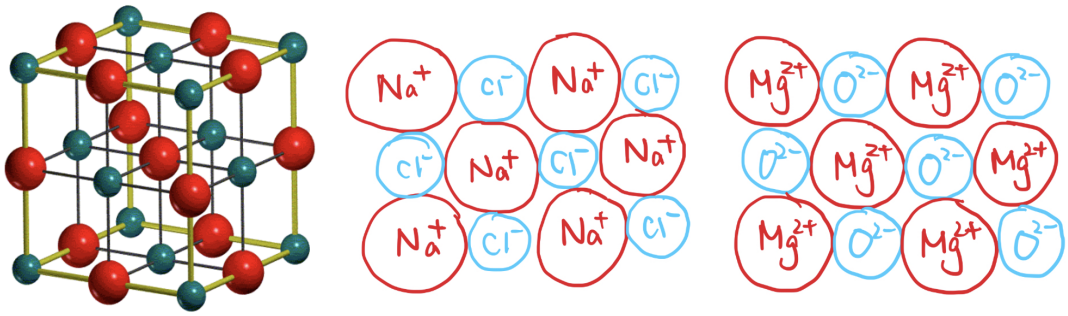

Figure 26: Left to right: the common crystal structure of NaCl and MgO, and the respective ionic distribution

encountered, while it is much more important in the structure of water ice, and a broader class of organic and biological materials.

5.1 Ionic Bonding

Ionic bonding mostly occurs when a solid is composed of elements with very different electronegativity. The most classical example of ionic solids is NaCl, and the constituent elements are coming from the two ends. The cohesion energy comes from the Coulomb interaction between the ions, and ionic solids typically have relatively high melting point (a proxy for the strength of bonding in a given material). The crystal can be thought about as a close packing of the charged cations and anions (see Fig. 26).

MgO has the identical crystal structure with NaCl and is also a classic example of ionic solids (Fig. 26). The melting point of MgO (2852 degC) is higher than NaCl (801 degC)–recall that Coulomb force scales with Q^2.

5.2 Covalent Bonding

Covalent bonding takes place when the electronegativity of the atoms forming the bond is comparable, especially when they are the same element. An electrostatic picture as we laid out in the ionic crystals doesn't apply anymore. Nevertheless it is known that many covalently bonded crystals such as diamond and graphite are structurally extremely robust and their melting temperatures are also exceptionally high (diamond, graphite, 3600 degC), suggesting a very different mechanism (not surprisingly, involving quantum mechanics) at play.

To illustrate the origin of covalent bonding, we will go over the formation of hydrogen molecule from two individual hydrogen atoms. We will first use a model based on localized orbitals, and then provide an alternative picture using a toy model of electrons confined in boxes. Our discussion here will capture the spirit of band formation we'll cover in later chapters.

5.2.1 Formation of hydrogen molecules

Let's start from two hydrogen atoms and consider the resulting electronic states when we put them close to each other. We will assume the position of the nuclei is fixed while finding out the electronic states. This is termed "Born-Oppenheimer" approximation–that atomic cores move much more slower than the electrons and as far as we are concerned with the electron states, the ions can be viewed as fixed. For two identical nuclei, we have the following Hamiltonian

$$H = K + V_1 + V_2 \tag{113}$$

where

$$K = \frac{\boldsymbol{p}^2}{2m} \tag{114}$$

and V_i indicates the Coulomb potential energy around nuclei i

$$V_i = \frac{e^2}{4\pi\epsilon_0 |\boldsymbol{r} - \boldsymbol{R}_i|} \tag{115}$$

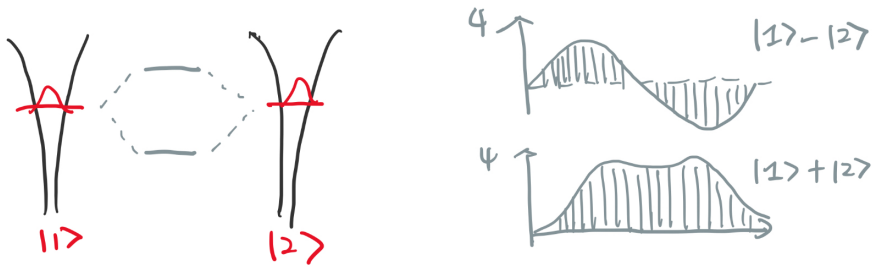

Figure 27: Sketches of the formation of bonding and antibonding states

Instead of solving this numerically, we attempt a variational approach as follows

$$|\psi\rangle = \phi_1|1\rangle + \phi_2|2\rangle \tag{116}$$

where $|i\rangle$ is an atomic orbital around atom i (or alternatively a "tight-binding" orbital). Eq. 116 is often known as LCAO (linear combination of atomic orbitals), which comes from

$$(K + V_i)|i\rangle = \epsilon_0|i\rangle \tag{117}$$

where ϵ_0 is the eigenstate in the presence of only one atom. In other words, our starting point is that the new eigen wave function will be a linear superposition of the solution to the individual Schrodinger equations. We will take an approximation that

$$\langle i|j\rangle = \delta_{ij} \tag{118}$$

This is a simlification and won't affect our main discussions (see homework for a more comprehensive version of the theory where we don't assume the orthorgonality).

The energy of the trial wave function is

$$E = \frac{\langle\psi|H|\psi\rangle}{\langle\psi|\psi\rangle} \tag{119}$$

and for the ground state $\delta E = 0$ it holds that

$$\frac{\partial E}{\partial \phi_i} = \frac{\partial E}{\partial \phi_i^*} = 0 \tag{120}$$

We can spell out

$$\begin{aligned} \langle\psi|\psi\rangle &= \phi_1^*\phi_1 + \phi_2^*\phi_2 \\ \langle\psi|H|\psi\rangle &= H_{11}\phi_1^*\phi_1 + H_{12}\phi_1^*\phi_2 + H_{21}\phi_2^*\phi_1 + H_{22}\phi_2^*\phi_2 \end{aligned} \tag{121}$$

where

$$\begin{aligned} H_{11} &= \epsilon_0 + \langle 1|V_2|1\rangle \\ H_{12} &= \langle 1|V_1|2\rangle \\ H_{21} &= \langle 2|V_2|1\rangle \\ H_{22} &= \epsilon_0 + \langle 2|V_1|2\rangle \end{aligned} \tag{122}$$

Eq. 119 becomes

$$E(\phi_1^*\phi_1 + \phi_2^*\phi_2) = H_{11}\phi_1^*\phi_1 + H_{12}\phi_1^*\phi_2 + H_{21}\phi_2^*\phi_1 + H_{22}\phi_2^*\phi_2 \tag{123}$$

Taking a partial derivative against ϕ_1^* and ϕ_2^* and use Eq. 120 we obtain

$$\begin{aligned} E\phi_1 &= H_{11}\phi_1 + H_{12}\phi_2 \\ E\phi_2 &= H_{21}\phi_1 + H_{22}\phi_2 \end{aligned} \tag{124}$$

Suggesting that (ϕ_1, ϕ_2) can be viewed as the eigenvector of the following matrix and E the eigenvalue [3]

$$\begin{pmatrix} H_{11} & H_{12} \\ H_{21} & H_{22} \end{pmatrix} \tag{125}$$

[3]Strictly speaking the variational principle only applies to the ground state. Here since we have a 2D space spanned by $|1\rangle$ and $|2\rangle$, the state orthorgonal to the ground state is automatically the excited state in the problem

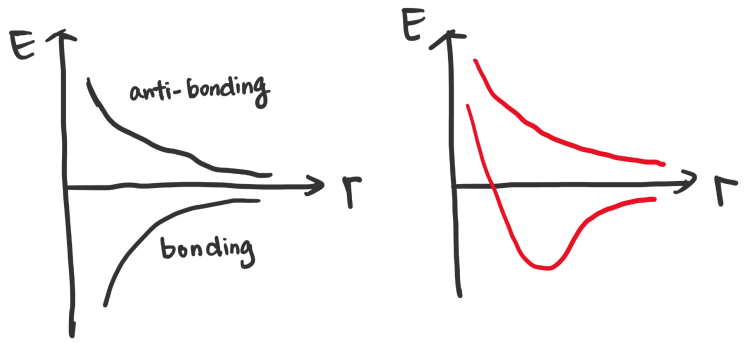

Figure 28: Schematic of evolution of bonding and anti-bonding states with inter-atomic distance. The left panel only considers the r-dependence of t while the right panel illustrates a more realistic scenario taking into account the Coulomb repulsion between the nucleus.

If 1 and 2 are identical atoms, we know that $\langle 1|V_2|1\rangle = \langle 2|V_1|2\rangle \equiv V_0$ and $\langle 1|V_1|2\rangle = \langle 2|V_1|1\rangle \equiv t$ (here we assume $t < 0$, so that there is an energy gain by allowing the wave function centered in atom 1 to experience the Coulomb attraction of atom 2). The latter, t, is termed as the hopping integral. The matrix is now

$$\begin{pmatrix} \epsilon_0 + V_0 & t \\ t & \epsilon_0 + V_0 \end{pmatrix} \tag{126}$$

Whose eigen states are

$$\begin{aligned} |\psi_b\rangle &= \frac{1}{\sqrt{2}}(|1\rangle + |2\rangle) \\ |\psi_a\rangle &= \frac{1}{\sqrt{2}}(|1\rangle - |2\rangle) \end{aligned} \tag{127}$$

$|\psi_b\rangle$ ($|\psi_a\rangle$) is the bonding (anti-bonding) state with eigen energy $\epsilon_0 + V_0 \mp t$, respectively. The wave function of the two states are schematically depicted in Fig. 27. The hopping integral t gives rise to an energy gain of the electronic states by allowing the wave function originally located at different sites to hybridize with each other. Conceptually, the bonding and anti-bonding states energies evolve with the inter-atomic distance r as illustrated in the left panel of Fig. 28. A more realistic scenario is illustrated in the right panel, where the low-r rise of both energies is included to account for that it is energetically unfavorable to put two hydrogen atoms too close with each other, where the Coulomb repulsion between the nucleus will start to kick in.

5.2.2 Particle-in-a-box picture of covalent bonding

The above section provides a molecular picture of covalent bond formation and can be complemented by a particle-in-a-box picture we introduce below. As illustrated in Fig. 29, the ground state energy of two isolated square wells are

$$E_0 = \frac{\hbar^2}{2m}(\frac{\pi}{L})^2 \tag{128}$$

By brute force combining the two wells to form a well with width $2L$, the ground state energy becomes

$$E_0' = \frac{\hbar^2}{2m}(\frac{\pi}{2L})^2 \tag{129}$$

and the first excited state being

$$E_1' = \frac{\hbar^2}{2m}(\frac{2\pi}{2L})^2 \tag{130}$$

The kinetic energy gain will be

$$\Delta E_0 = \frac{\hbar^2}{2m}(\frac{3\pi^2}{4L^2}) \tag{131}$$

This is a very simple model but qualitatively illustrates a kinetic energy gain by allowing an electron to move in a more spatially expanded potential well. The ground state wave function resembles the bonding state in the previous

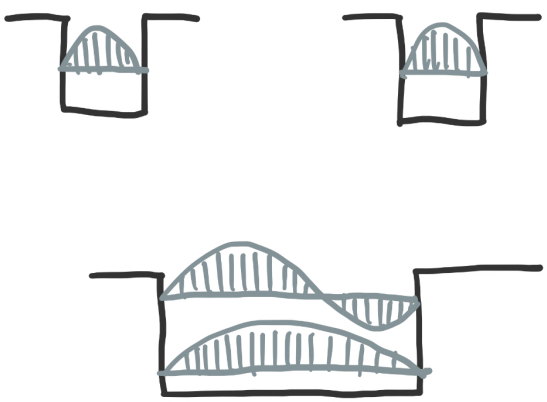

Figure 29: Illustration of the covalent bond formation by a toy particle-in-a-box model

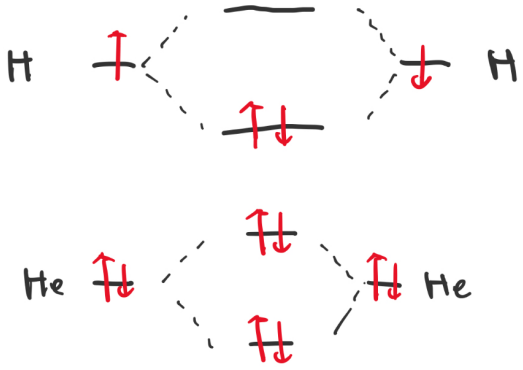

Figure 30: Comparing the filling of the bonding and antibonding states in H and He

section in that both are the most slowly-varying wave function in space in the respective circumstances. The common spirit is that by sharing the electronic states there is a quantum mechanical kinetic energy gain. Note that this notion will also be at play when we introduce metallic bonding below–it can also be loosely compared with the notion of "sharing economy" in social science.

5.2.3 Remarks on covalent bonding

With the covalent picture, we may compare why hydrogen atoms form molecules H2 but He atoms do not. The two scenarios are contrasted in Fig. 30: when we hypothetically form bonding and antibonding states via covalent bonding, we can visualize the filling of the newly formed molecular states. Each of the new levels can accomondate two electrons (one for each spin due to Pauli exclusion principle). For H (He), each atom provides 1 (2) electrons, filling only the bonding state (both the bonding and antibonding states) and the total energy gain is $2t$ (0) after filling the molecular levels. Thus the formation of H2 can fully benefit from the covalent bonding but not the formation of He2.

An alternative, often chemist's view is that by sharing one electron each, now effectively each hydrogen atom has two electrons, and a fully filled s shell is always favored. In this picture, for a given atom, there are only a limited number of covalent bonds one can form before the system becomes saturated, and this number is essentially related to the number of valence electrons one has.

The above picture is for s-orbitals whose hopping is described by a single, isotropic number, regardless of the orientation of the bond itself. Since t contains the wave function overlap with the atomic potentials, orbitals with more complex angular evolution such as the p, d, f orbitals can host a few different bonds depending on the orientation

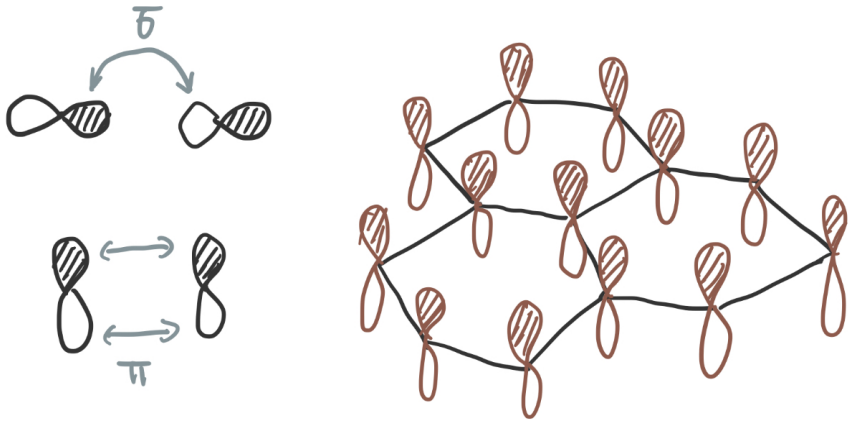

Figure 31: Left: σ and π bondings of the p orbitals. Right: p_z orbitals in graphene

of the orbitals.

In the case of p atomic orbitals, the first two kinds of bonds are σ and π bonds as illustrated in Fig. 31. The indices used to label different types of bonds $(\sigma, \pi, \delta, \phi)$ are the corresponding Greek letters of s, p, d, f used to describe atomic orbitals themselves. The labels are determined by the rotation symmetry of the orbitals participating the bonding around an axis connecting the two atoms [4]. The electronic states near the Fermi level of graphene for instance, originates from the π bonds of $2p_z$ orbitals of carbon (Fig. 31).

5.3 Metallic Bonding

Similar to ionic crystals, in metals there are both positively and negatively charged components of the solids: electrons are itinerant and free to move around, while the positively charged ionic cores stay in their places (recall the picture we discussed in the Drude model). Electrostatic attraction between the cations and the delocalized electrons provide the bonding force.

Additionally, the electrons in metals also enjoy a kinetic energy gain by being able to move around the entire crystal rather than being confined around a single atom, akin to the covalent bonding process.

Metallic bonds are in general less directional than covalent bonds–as a result, a lot of metals are malleable and are often the best materials for machining.

5.4 van der Waals bonding

When atoms can neither transfer electrons (as in ionic bonds) or share electrons (as in covalent and metallic bonds), van der Waals bonding can be the last resort. It takes between atoms without static charge or static electric dipole. The electric field generated by an instantaneous dipole (note that the dipole is fluctuating) of atom 1 at atom 2 can induce an electric dipole $\boldsymbol{p}_2$ at atom 2:

$$\boldsymbol{p}_2 = \chi \boldsymbol{E}_1, E_1 = \frac{p_1}{4\pi\epsilon_0 r^3} \tag{132}$$

with χ the polarizibility. The resulting potential energy is given below

$$U(r) = -\boldsymbol{p}_2 \cdot \boldsymbol{E_1} = \frac{-|p_1||p_2|\chi}{(4\pi\epsilon_0 r^3)^2} \tag{133}$$

This is a higher order process than direct electrostatic interaction between objects possessing net electric charges or net electric dipoles. The van der Waals force is the main bonding force in noble gas–the weak strength of van der Waals force is related to the low melting point of noble gases (that they remain in the gaseous phase at room temperature already tells the weak bonding)–He (-), Ne (25 K), Ar (83.81 K), Kr (115.78 K), Xe (161.40 K).

Van der Waals bonding also takes place in very anisotropic materials–where covalent bonding is saturated in a certain direction or within a certain plane. The weak van der Waals force allows one to use a relatively weak mechanical force to break the van der Waals 'bonds' by using, for instance, scotch tape (a lot of tapes work via the van der Waals force as well). This is essentially how one makes isolated, few-layer and even monolayer devices of van der Waals crystals such as graphene and transition metal dichalcogenides (these are also often called 2D materials).

[4] In other words, the "angular momentum" of the participating orbitals around the axis

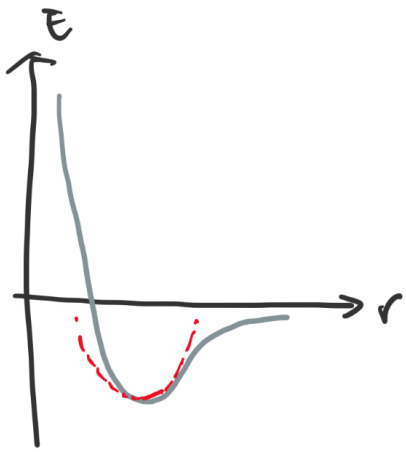

Figure 32: Schematic of internal energy of solids with the interatomic distance r

As an aside, we introduce the Lennard-Jones potential often used to describe of the energy of moleduclar crystals as a function of interatomic distance:

$$V(r) = \frac{A}{r^{12}} - \frac{B}{r^6} \tag{134}$$

the B term describes the van der Waals energy gain while A/r^{12} term is introduced to more or less model a hard sphere at low r. This gives a potential qualitatively similar to $E(r)$ sketched above for covalent bonding.

5.5 Thermal expansion and anharmonicity

In this section we've reviewed a few mechanisms of solid bonding, and you've seen qualitatively an inter-atomic potential like that shown in Fig. 32. The minimal corresponds to the equilibrium inter-atomic distance x_{eq}. One can always do a Taylor expansion around the minimum ($\kappa_2, \kappa_3 > 0$, the latter reflecting the steeper slope at the lower r side)

$$V(x) = U(x_{eq}) + \kappa_2(x - x_{eq})^2 - \kappa_3(x - x_{eq})^3 + ... \tag{135}$$

The harmonic ponential is related to our harmonic oscillator modeling of the atomic vibrations in the previous section. The anharmonicity (κ_3 term) also plays a role, and its most well known manifestation is in the thermal expansion of materials. We may calculate the average displacement $\langle x \rangle$ using the Boltzmann distribution of V:

$$\langle x \rangle = \frac{\int_{-\infty}^{\infty} x e^{-\beta V(x)} dx}{\int_{-\infty}^{\infty} e^{-\beta V(x)} dx} \tag{136}$$

where

$$\begin{aligned} \int_{-\infty}^{\infty} x e^{-\beta V(x)} dx = \int_{-\infty}^{\infty} x e^{-\beta\kappa_2 x^2} (e^{\beta\kappa_3 x^3}) dx &\simeq \int_{-\infty}^{\infty} x e^{-\beta\kappa_2 x^2} (1 + \beta\kappa_3 x^3) dx \\ &= \int_{-\infty}^{\infty} e^{-\beta\kappa_2 x^2} \beta\kappa_3 x^4 dx \end{aligned} \tag{137}$$

and

$$\int_{-\infty}^{\infty} e^{-\beta V(x)} dx \simeq \int_{-\infty}^{\infty} e^{-\beta\kappa_2 x^2} dx \tag{138}$$

Redefining $\beta\kappa_2 x^2 \equiv y^2$ and using the following results

$$\int_{-\infty}^{\infty} x^4 e^{-x^2} dx = \frac{3}{4}\sqrt{\pi}, \int_{-\infty}^{\infty} e^{-x^2} dx = \sqrt{\pi} \tag{139}$$

We can obtain

$$\langle x \rangle = \frac{3\kappa_3 k_B T}{4\kappa_2^2} \tag{140}$$

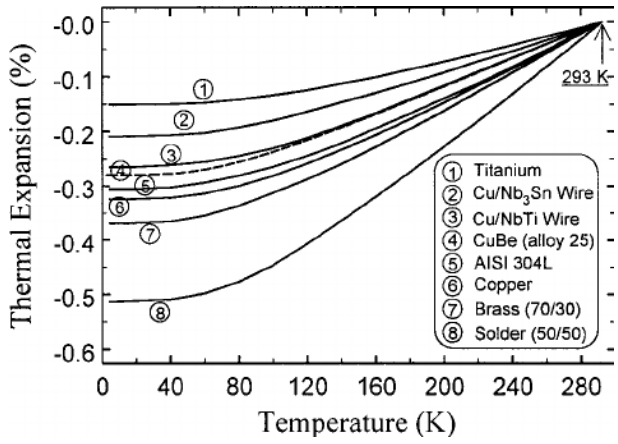

Figure 33: Thermal expansion as a function of temperature for selected materials

This gives rise to a linear thermal expansion proportional to the anharmonicity κ_3. The classical model accounts for the high temperature linear behavior of thermal expansion; at low T quantum mechanical effects sets in and the thermal expansion coefficient $\alpha \equiv dL/dT$ will become lower and saturates at the low temperature end.

5.6 Summary

One of the best manifestations of the difference among the above bonding mechanisms is the charge distribution in the corresponding solid state systems calculated from first principles. We end this section by contrasting the charge distribution of MgO, Be and Si in Fig. 34, which are typical hosts of ionic, metallic and covalent bonds, respectively. For MgO, both positive and negative charges are centered around the cations and anions; for Be, the positive charge are located near the Be sites while the negative charge (electrons) is spread out across the system; for Si, the sharing of electrons between Si atoms and an enhanced electron density between the atoms is apparent (more pronounced in the difference map, where a constant background is substracted).

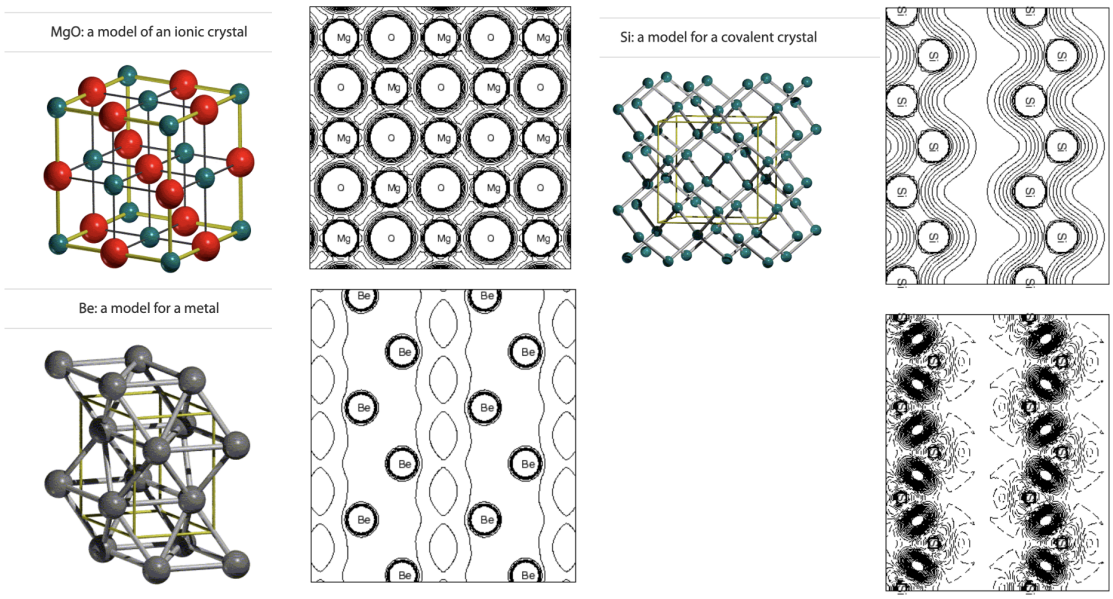

Figure 34: Calculated charge distribution of MgO, Be and Si, respectively. For MgO, Be and Si the total charge density map is shown; for Si we also show the difference charge density map (a uniform background is subtracted). Reference: Crystal Tutorial Project

6 Treating the periodic structure: 1D toy models

In this chapter we start dealing with the vibrations and electronic eigenstates of periodic lattices. For simplicity, we confine ourselves to 1D models (the motion of both atoms and electrons are confined in one dimension x). The goal of this chapter is to obtain the essential features of quantum mechanical eigenstates of periodic systems; we also would like to compare our results with the early understanding of solids without taking into account the microscopic, periodic structure and see what are the successes and limitations.

6.1 Phonons in 1D

6.1.1 Monoatomic solids

Figure 35: Schematic of monoatomic chain

Here we directly follow the harmonic approximation from the previous chapter and consider a chain of atoms connected with its nearest neighbor by springs with constant κ. The distance between the equilibrium positions of neighboring atoms is a (we will call this a lattice constant) and atomic mass m. The equilibrium position of the n^{th} atom $x_n = na$. We consider small deviations δx_n from x_n:

$$x_n = na + \delta x_n \tag{141}$$

In the harmonic approximation

$$V = \sum_i \frac{\kappa}{2}(x_{i+1} - x_i - a)^2 = \sum_i \frac{\kappa}{2}(\delta x_{i+1} - \delta x_i)^2 \tag{142}$$

The restoring force at site n is

$$F_n = -\frac{\partial V}{\partial \delta x_n} = \kappa(\delta x_{n+1} - \delta x_n) + \kappa(\delta x_{n-1} - \delta x_n) \tag{143}$$

Giving rise to the following equation of motion

$$m\ddot{\delta x}_i = \kappa(\delta x_{i-1} + \delta x_{i+1} - 2\delta x_i) \tag{144}$$

We take the following ansatz (which describes a plane wave of coupled harmonic oscillation)

$$\delta x_n = Ae^{i(\omega t - kna)} \tag{145}$$

This plugged in Eq. 144 gives

$$-m\omega^2 Ae^{i(\omega t - kna)} = \kappa Ae^{i(\omega t - kna)}(e^{ika} + e^{-ika} - 2) = \kappa Ae^{i(\omega t - kna)}[2\cos(ka) - 2] \tag{146}$$

$$m\omega^2 = 2\kappa[1 - \cos(ka)] = 4\kappa \sin^2(\frac{ka}{2}) \tag{147}$$

$$\omega = 2\sqrt{\frac{\kappa}{m}}|\sin(\frac{ka}{2})| \tag{148}$$

This is the dispersion relation of phonons in the 1D coupled harmonic oscillator model. One can find this is periodic with the periodicity $ka/2 = \pi$ or $k = 2\pi/a$ (Fig. 36) Near $k = 0$ the low energy part is similar with Debye model where the $\omega \sim k$.

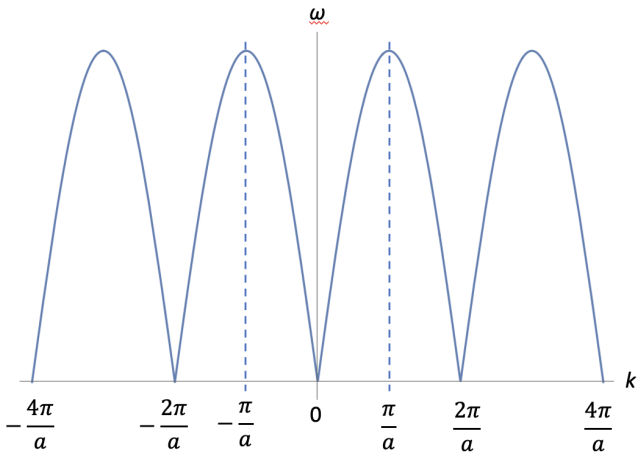

Figure 36: Dispersion relation $\omega(k)$ of 1D monoatomic lattice vibration. The dispersion is periodic with k (periodicity $2\pi/a$) and the two vertical dashed lines indicate the first Brillouin zone.

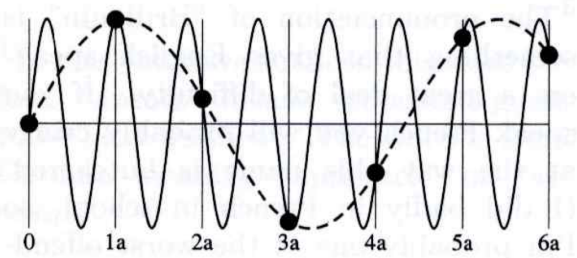

Figure 37: Solid and dashed lines indicate waves with wave vector of k and $k + 2\pi/a$. They correspond to the same pattern of displacement on the atomic chain and are physically identical.

6.1.2 Reciprocal lattice, Brillouin zone

An important principle as we see from this example is that **a system periodic in real space with periodicity a is periodic in the reciprocal k space with periodicity** $2\pi/a$. The periodic unit in the k-space (reciprocal space) is known as the Brillouin zone. The "first Brillouin zone" is centered near $k = 0$ and is bounded by $k = \pm\pi/a$ (Brillouin zone boundary) and in principle contains all the information needed for the periodic system of interest.

We also make the following statement that states labeled by k and $k + 2\pi/a$ are physically the same state. We can take a look at what does it really mean (Fig. 37). For

$$\delta x_n = Ae^{i(\omega t - kna)} \tag{149}$$

substituting k by $k + 2\pi/a$:

$$\delta x_n = Ae^{i(\omega t - kna - 2n\pi)} = Ae^{i(\omega t - kna)} \tag{150}$$

And one way to think about this is that we are only sampling the waves at discrete points in space, therefore k and $k + 2\pi/a$ are indistinguishable!

k thus defined is called the crystal momentum–by definition, k and $k + 2n\pi/a$ is the same state. One can stitch the two ends of the Brillouin zone together and form a loop. This should be contrasted with the infinite k space we were discussing at the very beginning.

Alternatively, if one prefers thinking about an infinite k-space, we can define a reciprocal lattice composed of a set of reciprocal space points physically equivalent to $k = 0$. These lattice points are denoted by G_n–whenever we encounter G_n we are taken back to the origin. In 1D, the reciprocal lattice points G_n are

$$0, \pm\frac{2\pi}{a}, \pm 2\frac{2\pi}{a}, \pm 3\frac{2\pi}{a}, ... \tag{151}$$

For G_n,

$$e^{iG_m x_n} = 1 \tag{152}$$

for all x_n belonging to the real space lattice. The two ways of thinking about the Brillouin zones correspond respectively to the reduced and extended zone schemes which we will come back to.

6.1.3 Velocity, density of states, crystal momentum

In the low wave length limit

$$\omega \simeq ka\sqrt{\frac{\kappa}{m}} \tag{153}$$

thus the sound velocity of the 1D chain is

$$v_s = a\sqrt{\frac{\kappa}{m}} \tag{154}$$

At larger k it may be useful to define a group velocity

$$v_g = \frac{d\omega}{dk} \tag{155}$$

which will be different from the phase velocity v_p

$$v_p = \frac{\omega}{k} \tag{156}$$

The group velocity v_g approaches zero near the Brillouin zone boundary. One way of viewing this is that this is a standing wave with the neighboring atoms oscillating out of phase, and don't propagate; this standing wave can be viewed as a coherent superposition of two waves traveling with wave vectors of $\pm(\pi/a)$.

The low wavelength part recovers the Debye model while the higher energy, short wavelength part is our new result here. Here we check the number of states–recall the Debye model introduces somewhat artificial bounds of ω_D and k_{cutoff}.

Naively the states in the first Brillouin zone $-\pi/a \sim \pi/a$ would be all the states we are interested in. Giving a chain with N atoms with length Na, the periodic boundary condition implies that

$$e^{i\pi Na} = 1 \tag{157}$$

resulting in

$$k = \frac{2\pi p}{L} = \frac{2\pi p}{Na} \tag{158}$$

The number of points within $\pm\pi/a$ is therefore

$$\frac{2\pi/a}{2\pi/Na} = N \tag{159}$$

suggesting that the first Brillouin zone captures the N modes in the system.

6.1.4 Phonons

Here we formally define the quanta of each vibration mode at a given k, called phonons. Here we define a new set of position and momentum variables Q_k and P_k (they are Fourier transforms of x_i and p_i at site i):

$$\begin{aligned} Q_k &= \frac{1}{\sqrt{N}}\sum_l e^{ikal}x_l \\ P_k &= \frac{1}{\sqrt{N}}\sum_l e^{-ikal}p_l \end{aligned} \tag{160}$$

which satisfies the following communtation relations (homework)

$$[Q_k, P_{k'}] = i\hbar\delta_{k,k'}, [Q_k, Q_{k'}] = [P_k, P_{k'}] = 0 \tag{161}$$

The Hamiltonian of the system is

$$H = \frac{1}{2m}\sum_k [P_k^* P_k + m^2\omega_k^2 Q_k^* Q_k] \tag{162}$$

Therefore each mode belonging to individual k can be viewed as an independent, quantum mechanical harmonic oscillator. Phonon number n of a given phonon mode corresponds to the mode having energy of

$$(n + \frac{1}{2})\hbar\omega_k \tag{163}$$

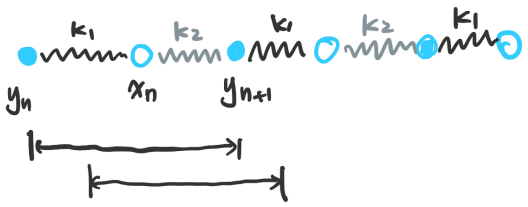

Figure 38: Schematic of the diatoimc chain along with two different ways of defining the unit cell.

6.1.5 Diatomic solids

Now let's move to the diatomic chain. Here we define the unit cell as the minimal unit required to describe the structure. There's no unique way of defining the unit cell while they should all give the same number of atoms within a single unit cell (Fig. 38). The concept 'basis' refers to the internal structure within a unit cell. We sometimes call the group of the equivalent atoms a sublattice of the system.

In the most generic scenario, the diatomic chain would have two atoms with different masses and different spring constants. Here we assume the two masses in the unit cell to be identical, while the two spring constants are different. This simplifies the calculation without losing the essential features we'd like to discuss; this simplification also makes it convenient for us to take the two spring constants back to be identical to compare with the monoatomic case.

Labeling the displacement of the two atoms by x_n, y_n respectively:

$$\begin{aligned} m\ddot{\delta x}_n &= \kappa_1(\delta y_n - \delta x_n) + \kappa_2(\delta y_{n+1} - \delta x_n) \\ m\ddot{\delta y}_n &= \kappa_1(\delta x_n - \delta y_n) + \kappa_2(\delta x_{n-1} - \delta y_n) \end{aligned} \tag{164}$$

Taking a similar ansatz with the previous section (assuming the two atoms vibrate coherently, and the lattice constant is taken as a; the oscillation of the two atoms can have a phase difference, while this is "absorbed" in A_x and A_y themselves):

$$\begin{aligned} \delta x_n &= A_x e^{i(\omega t - kna)} \\ \delta y_n &= A_y e^{i(\omega t - kna)} \end{aligned} \tag{165}$$

This leads to

$$\begin{aligned} -\omega^2 m A_x &= \kappa_2 A_y e^{ika} + \kappa_1 A_y - (\kappa_1 + \kappa_2) A_x \\ -\omega^2 m A_y &= \kappa_1 A_x + \kappa_2 A_x e^{-ika} - (\kappa_1 + \kappa_2) A_y \end{aligned} \tag{166}$$

which further leads to the following matrix

$$m\omega^2 \begin{pmatrix} A_x \\ A_y \end{pmatrix} = \begin{pmatrix} \kappa_1 + \kappa_2 & -\kappa_1 - \kappa_2 e^{ika} \\ -\kappa_1 - \kappa_2 e^{-ika} & \kappa_1 + \kappa_2 \end{pmatrix} \begin{pmatrix} A_x \\ A_y \end{pmatrix} \tag{167}$$

One can find the matrix is unitary, and can solve the eigenvalues:

$$m\omega^2 = (\kappa_1 + \kappa_2) \pm |\kappa_1 + \kappa_2 e^{ika}| = (\kappa_1 + \kappa_2) \pm \sqrt{\kappa_1^2 + \kappa_2^2 + 2\kappa_1\kappa_2 \cos(ka)} \tag{168}$$

The branches can be plotted as in Fig. 39.

A few things to note:

- There are two branches for each given k, identical with the number of atoms within an unit cell; the number of normal modes $2N$ is identical with the number of total atoms (The number of degrees of freedom checks out!).
- At low wavelength, there's a sound-wave like branch of the dispersion, which we call the acoustic mode. The sound velocity is (consider springs connected in series)

$$v_s = a\sqrt{\frac{\kappa_1\kappa_2}{2m(\kappa_1 + \kappa_2)}} \tag{169}$$

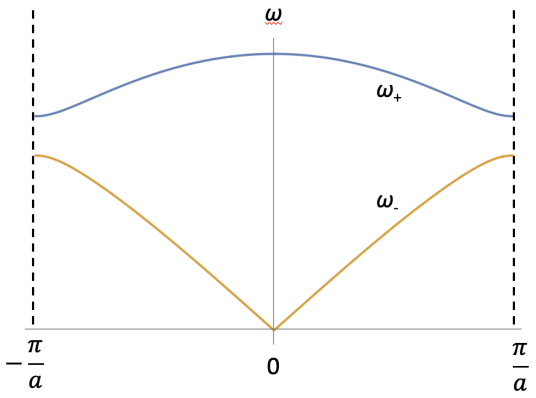

Figure 39: Solution of $\omega(k)$ for the diatomic chain.

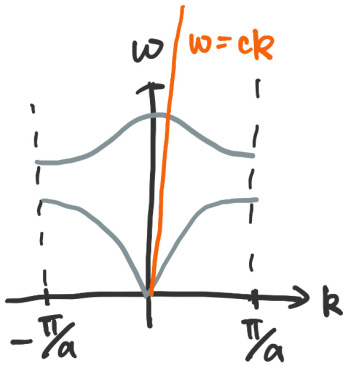

Figure 40: Comparing the diatomic chain phonon dispersion with the photon dispersion $\omega = ck$

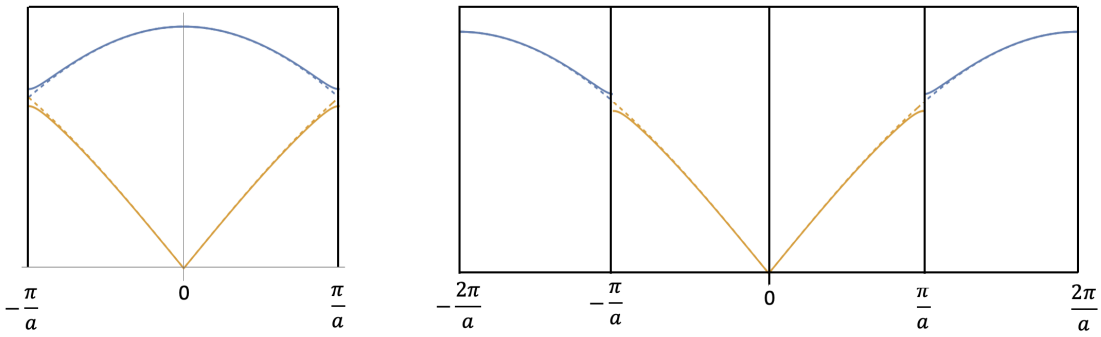

Figure 41: Reduced zone (left panel) and extended zone (right panel) representation of diatomic chain with different spring constants (solid lines), compared with when the two spring constants are set to be identical (dashed lines).

- The wave function of the other mode at the long wavelength limit ($k = 0$) is a standing wave with out-of-phase oscillation between the two atoms. We can check the eigen vectors at $k = 0$:

$$m\omega^2 \begin{pmatrix} A_x \\ A_y \end{pmatrix} = (\kappa_1 + \kappa_2) \begin{pmatrix} 1 & -1 \\ -1 & 1 \end{pmatrix} \begin{pmatrix} A_x \\ A_y \end{pmatrix} \tag{170}$$

  With acoustic mode being

$$\begin{pmatrix} A_x \\ A_y \end{pmatrix} = \begin{pmatrix} 1 \\ 1 \end{pmatrix} \tag{171}$$

  and optical mode being

$$\begin{pmatrix} A_x \\ A_y \end{pmatrix} = \begin{pmatrix} 1 \\ -1 \end{pmatrix} \tag{172}$$

  This is often called the optical mode. The name comes from the fact that if the charge carried by the two atoms are different, there will be a fluctuating electric dipole generated in the solid, which allows this mode to couple to light. As a matter of fact, optical absorption is one of the most common experimental means to determine optical phonon energies. However, it should be noted that using light, only optical modes near the zone center can be accessed–for light to be absorbed to create a phonon, let's say, both momentum and energy of the photon and phonons should be conserved (see Fig. 40). Since light travels much faster than sound, only small momentum optical phonon can cross the photon dispersions in the $k \to 0$ limit.

- More generally, if we have M atoms in a unit cell instead, one would obtain 1 acoustic mode, $M - 1$ optical modes (all these additional modes are associated with inhomogeneous charge fluctuations). In 3D, 3 acoustic modes and $3M - 3$ optical modes.

6.1.6 Comparing diatomic and monoatomic chains

To compare the diatomic and monoatomic scenarios, we introduce two different, complementary schemes to plot the phonon dispersions: reduced zone scheme (everything shown between $\pm\pi/a$) and extended zone scheme (each zone shows one branch). The two schemes are shown respectively in Fig. 41.

Here it is very useful to think in the extended zone scheme, in which we also plot the monoatomic dispersion corresponding to a lattice constant of $a/2$ (dashed dispersion). One may view the relation of the two as gradually turning on the difference between the two springs in a monoatomic chain with lattice constant $a/2$; doing this will change the periodicity of the system from $a/2$ to a and a gap at $\pm\pi/a$ (the new Brillouin zone boundary) can be gradually opened. With the new periodicity, one may "fold" the band dispersion at the new periodicity to get the left panel of Fig. 41. The zone folding is a useful notion to think about turning on weak perturbations such as at the formation of a charge density wave.

6.2 Tight-binding electrons in 1D

We will do an excursion to consider electrons in solids again. The purpose of putting the discussions here is to emphasize the similarity of phonon dispersion relation and electron band formation in the presence of the lattice.

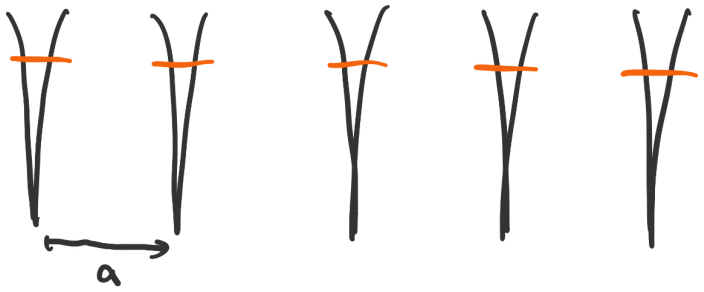

Figure 42: Schematic of a tight-binding chain

We start from the tight-binding model (an extension of the LCAO model) on a 1D chain where each site n has a localized quantum mechanical state $|n\rangle$. The following assumptions are made:

$$\langle n|m\rangle = \delta_{nm} \tag{173}$$

and the eigenwave function $|\Psi\rangle$ is a linear combination of the local states

$$|\Psi\rangle = \sum_i \phi_i |i\rangle \tag{174}$$

ϕ_i are coefficients. The set of coefficients are solved from the following matrix

$$\sum_m H_{nm}\phi_m = E\phi_n \tag{175}$$

with

$$H_{nm} = \langle n|H|m\rangle \tag{176}$$

In the 1D tight-binding model

$$H = K + \sum_j V_j \tag{177}$$

with K the kinetic energy and V_j the atomic potential at site j

$$V_j = V(\boldsymbol{r} - \boldsymbol{R_j}) \tag{178}$$

$$H|m\rangle = (K + V_m)|m\rangle + \sum_{j\neq m} V_j|m\rangle \tag{179}$$

The first part of Eq. 179 is merely the onsite Hamiltonian with

$$(K + V_m)|m\rangle = \epsilon_s|m\rangle \tag{180}$$

The rest of Eq. 179 is the hopping term

$$\langle n|V_j|m\rangle = \begin{cases} V_0, & \text{if } m = n = j \pm 1 \\ -t, & \text{if } m = n \pm 1 \\ 0, & \text{otherwise} \end{cases} \tag{181}$$

This leads to the matrix elements

$$H_{nm} = (\epsilon_0)\delta_{nm} - t(\delta_{n+1,m} + \delta_{n-1,m}) \tag{182}$$

where $\epsilon_0 = \epsilon_s + V_0$.

As with phonons we take the following ansatz for the solution

$$\phi_n = \frac{e^{-ikna}}{\sqrt{N}} \tag{183}$$

leading to

$$\sum_m H_{nm}\phi_m = \epsilon_0 \frac{e^{-ikna}}{\sqrt{N}} - t(\frac{e^{-ik(n+1)a}}{\sqrt{N}} + \frac{e^{-ik(n-1)a}}{\sqrt{N}}) = E\frac{e^{-ikna}}{\sqrt{N}} \tag{184}$$

$$E = \epsilon_0 - t(e^{ika} + e^{-ika}) = \epsilon_0 - 2t\cos(ka) \tag{185}$$

As with phonons we find a dispersion of the electrons periodic in $2\pi/a$ and the dispersion is also flat near the Brillouin zone boundary (Fig. 43). We can apply a very similar standing wave picture at $\pm\pi/a$. Each branch of the dispersion is called a band, and this nomenclature is used to emphasize that this is the allowed range of energies that can be taken by an electron. The bandwidth is defined as $|E_{max} - E_{min}|$, and in the present case is $2t$.

6.2.1 Bloch theorem

Here we formally introduce the Bloch theorem, Which states that the eigenwave function of the periodic Hamiltonian H should take the following form

$$\psi_k(r) = e^{ikr}u_k(r) \tag{186}$$

with $u_k(r)$ a periodic function ($R = na$, defined as an integer multiple of a)

$$u_k(r + R) = u_k(r) \tag{187}$$

To quote Bloch himself, "When I started to think about it, I felt that the main problem was to explain how the electrons could sneak by all the ions in a metal.... By straight Fourier analysis I found to my delight that the wave differed from the plane wave of free electrons only by a periodic modulation" (when we introduce scattering we will introduce this Fourier transform picture.)

The Bloch theorem is sometimes written in the following alternative form

$$\psi_k(r + R) = e^{ikR}\psi_k(r) \tag{188}$$

It is easy to verify that the ansatz we took above in Eq. 183 satisfies this condition:

$$\psi_k(r) = \frac{1}{\sqrt{N}}\sum_{R'} e^{ik\cdot R'}\phi(r - R') \tag{189}$$

$$\psi_k(r + R) = \frac{1}{\sqrt{N}}\sum_{R'} e^{ik\cdot R'}\phi(r - R' + R) \tag{190}$$

By changing variable $R'' \equiv R' - R$ (therefore $R' = R'' + R$ and summation with R' would be the same with that with respect to R''):

$$\psi_k(r + R) = \frac{1}{\sqrt{N}}\sum_{R''} e^{ik\cdot R}e^{ik\cdot R''}\phi(r - R'') = e^{ikR}\psi_k(r) \tag{191}$$

A simple proof of the Bloch theorem comes from considering the translational symmetry of the total Hamiltonian H. Let's say the translational operation by R ($R = na$) is T_R, which commutes with H (in other words, translation is a symmetry of H, and this holds for arbitary R)

$$[T_R, H] = 0 \tag{192}$$

Therefore H and all the translational operations T_R can be simultanously diagonalized. Therefore $\psi(r)$ should be an eigenstate of T_R:

$$T_R\psi(r) = \psi(r + R) = c(R)\psi(r) \tag{193}$$

with $\psi(r + R)$ and ψ differ from each other by a constant. Given that the probability of finding an electron at a given position should not change before and after the translation

$$|\psi(r)|^2 = |\psi(r + R)|^2 \tag{194}$$

which gives

$$|c(R)|^2 = 1 \tag{195}$$

Also it is easy to verify that

$$c(R + R') = c(R)c(R') \tag{196}$$

The form that best satisfying all the above requirements are (k being a real number)

$$c(R) = e^{ikR} \tag{197}$$

One may view k as a "label" for the different one-dimensional representations of the translation symmetry operation. Alternatively, k is the good quantum number of the electron states in the presence of translational symmetry.

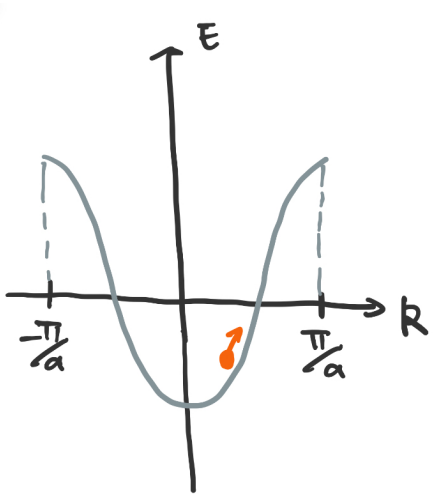

Figure 43: Bloch band of 1D tight-binding model; the orange electron and the arrow associated with it indicate the effect of an applied electric field.

6.2.2 Electron equation of motion

The motion of a Bloch electron state at wave vector k can be treated as if it is the center of a wave packet; the velocity therefore will be the group velocity v_g of the wave packet at k (recall $v_g = d\omega/dk$ and $\omega = E/\hbar$)

$$v = \frac{1}{\hbar}\nabla_k E(\boldsymbol{k}) = \frac{1}{\hbar}\frac{dE}{dk} \tag{198}$$

When an external force is applied to this wave packet (energy change being identical to the work done on the electron)

$$\delta E(k) = Fv\delta t \tag{199}$$

We know that

$$\frac{dE}{dt} = \frac{dE}{dk}\frac{dk}{dt} = \hbar v\frac{dk}{dt} \tag{200}$$

Eq. 199 and 200 gives rise to a Newton second law like relation

$$\hbar\frac{dk}{dt} = F \tag{201}$$

In the presence of electric field

$$\hbar\frac{dk}{dt} = -eE \tag{202}$$

in other words, the main role of the electric field on the band states is to move such states along the crystal momentum axis. The discussions we've went through on Drude and Boltzmann models are still valid, the only difference being that instead of the electron momentum, in solids, the proper "momentum" will need to be taken as the crystal momentum instead.

We can also consider the acceleration of electrons

$$a = \frac{dv}{dt} = \frac{dv}{dk}\frac{dk}{dt} = \frac{1}{\hbar}\frac{d^2E}{dk^2}\frac{dk}{dt} = \frac{1}{\hbar^2}\frac{d^2E}{dk^2}F \tag{203}$$

We may define the band effective mass of the band electrons

$$\frac{1}{m^*} = \frac{1}{\hbar^2}\frac{d^2E}{dk^2} \tag{204}$$

with which the equation of motion can be written as the familiar form $F = m^*a$.

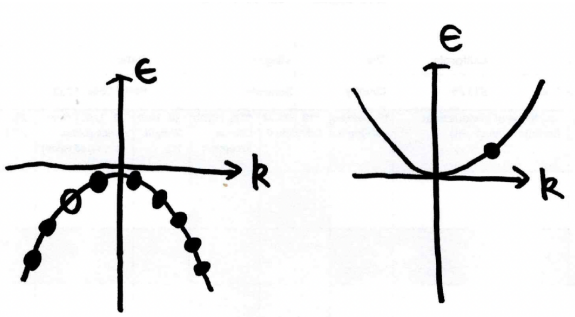

Figure 44: Comparison of equivalent electron (left) and hole (right) pictures

6.2.3 Band filling, electrons and holes

If each atomic site contributes one electron, the Bloch band will be half-filled (here we take into account the spin degrees of freedom). If each atomic site contributes two electrons, the model Bloch band will be fully filled.

Imagine we apply an electric field to a fully filled band. Eq. 202 moves the electronic states in k, while this doesn't change the fact that the band is fully occupied.

$$j = (-e) \sum_{-\pi/a < k \leq \pi/a} v = 0 \tag{205}$$

indicating that a fully filled band cannot conduct electricity. Only partially filled bands do. The former correspond to insulators and the latter metals.

Next we discuss electron conduction near the band edges. Let's start from one electron near the minimum–near $k = 0$ where $E(k)$ is parabolic, and one may figure out that

$$\frac{1}{m^*} = \frac{2ta^2}{\hbar^2} \tag{206}$$

Here the electronic state may be almost viewed as a free electron with a renormalized mass that does not seem to have a direct relation with m_e; the origin of the dispersion is instead the hopping dynamics of electrons across different atomic sites. An immediate consequence of Eq. 204 is that one may obtain an apparent negative mass near $\pm\pi/a$. This leads us to introduce the concept of holes.

Here we consider a scenario where the band is filled aside from one electron labeled with k_0. The current is therefore

$$j = (-e) \sum_{k \neq k_0} v(k) = (+e) v(k_0) \tag{207}$$

(to get the latter half we used Eq. 205), suggesting that it is more convenient to view the missing k_0 state as a hole carrying positive charge. Taking this notion further, under an electric field from Eq. 203 we have

$$a = (-Ee) \frac{1}{m^*(k_0)} \tag{208}$$

Here near the band top, $m^*(k_0) < 0$, therefore it is convenient to define an effective mass for the hole

$$m_h^*(k_0) = -m^*(k_0) = |m^*(k_0)| \tag{209}$$

with which the equation of motion is as if the missing electron is carrying a positive charge:

$$m_h^*(k_0) a = E(+e) \tag{210}$$

6.3 Summary

In this chapter we treated both phonons and electrons in one-dimensional lattices–the solutions can be viewed as "modified" plane waves based on the atoms, or the electronic states sitting at the atoms. Such states can be uniquely defined up to the Brillouin zone boundary. Some of the results here can compare closely with our initial discussions of the Debye/Drude models while new notions emerge, including standing wave-like zone boundary modes, optical phonons and holes. In the following we will visit the 2D and 3D cousins of these states.

7 Describing a periodic structure in 2D and 3D

We've looked at a few essential features of electrons and phonons in a periodic structure in the simplest 1D case. From here on we will add more realistic features in higher dimensions including 2D and 3D. You may find some other solid state and condensed matter textbooks start from contents in this chapter.

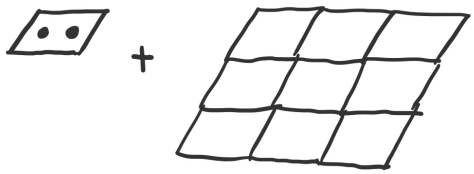

Figure 45: Unit cell and the Bravais lattice

Given a periodic structure, one can figure out that it should be described by (1) the fundamental building block as well as (2) the way it is tiled throughout space (see Fig. 45). The former correspond to the unit cell and the latter the Bravais lattice.

7.1 The Bravais lattice

Lattice system	Point group (Schönflies notation)	5 Bravais lattices	
		Primitive (p)	Centered (c)
Monoclinic (m)	C_2	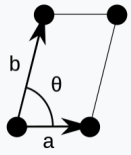 Oblique (mp)	
Orthorhombic (o)	D_2	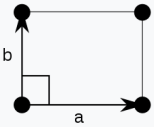 Rectangular (op)	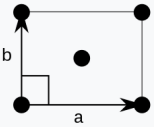 Centered rectangular (oc)
Tetragonal (t)	D_4	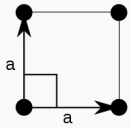 Square (tp)	
Hexagonal (h)	D_6	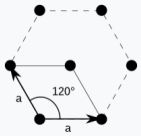 Hexagonal (hp)	

Figure 46: 2D Bravais lattice and point group. You may wonder why the centered rectangular lattice is itself a category–it comes from the point group symmetry slightly different from what one can see from the minimal periodic structure. Each point in the Bravais lattice represent a unit cell.

The Bravais lattice is a concept introduced to understand the different ways periodic units related with each other by translational operation can fill out the entire space. Each point in the Bravais lattice stands for a unit cell of the

periodic structure (internal structure within a unit cell is allowed). Here we define primitive translational vectors $\{\boldsymbol{a}_1, \boldsymbol{a}_2\}$ in 2D and $\{\boldsymbol{a}_1, \boldsymbol{a}_2, \boldsymbol{a}_3\}$ in 3D. A given Bravais lattice point can be expressed by

$$\boldsymbol{R} = n_1\boldsymbol{a}_1 + n_2\boldsymbol{a}_2 \tag{211}$$

for 2D and

$$\boldsymbol{R} = n_1\boldsymbol{a}_1 + n_2\boldsymbol{a}_2 + n_3\boldsymbol{a}_3 \tag{212}$$

for 3D. One can view the primitive translational vectors as the basis of the two and three dimensional peridoic structures. The different Bravais lattices can be categorized by their spatial symmetries.

Let's start from the 2D case (see Fig. 46). The five different types of Bravais lattices are categorized by the symmetry of the resulting lattice; in particular,

- whether $|\boldsymbol{a}_1| = |\boldsymbol{a}_2|$
- the angle between $\boldsymbol{a}_1$ and $\boldsymbol{a}_2$
- rotational symmetry of the Bravais lattice (one may prove that only 2, 3, 4, 6 fold rotation symmetries are possible for Bravais lattices to fill the entire 2D plane)

The 3D Bravais lattices are more complicated (Fig. 47) and there are in total 19 allowed Bravais lattices. For the cubic lattices, there are three variations, simple cubic, body-centered cubic (bcc) and face-centered cubic (fcc). One may sit down and work out why e.g. tetragonal lattices only have simple tetragonal and body-centered tetragonal cases (face-centered tetragonal is identical with the body-centered tetragonal).

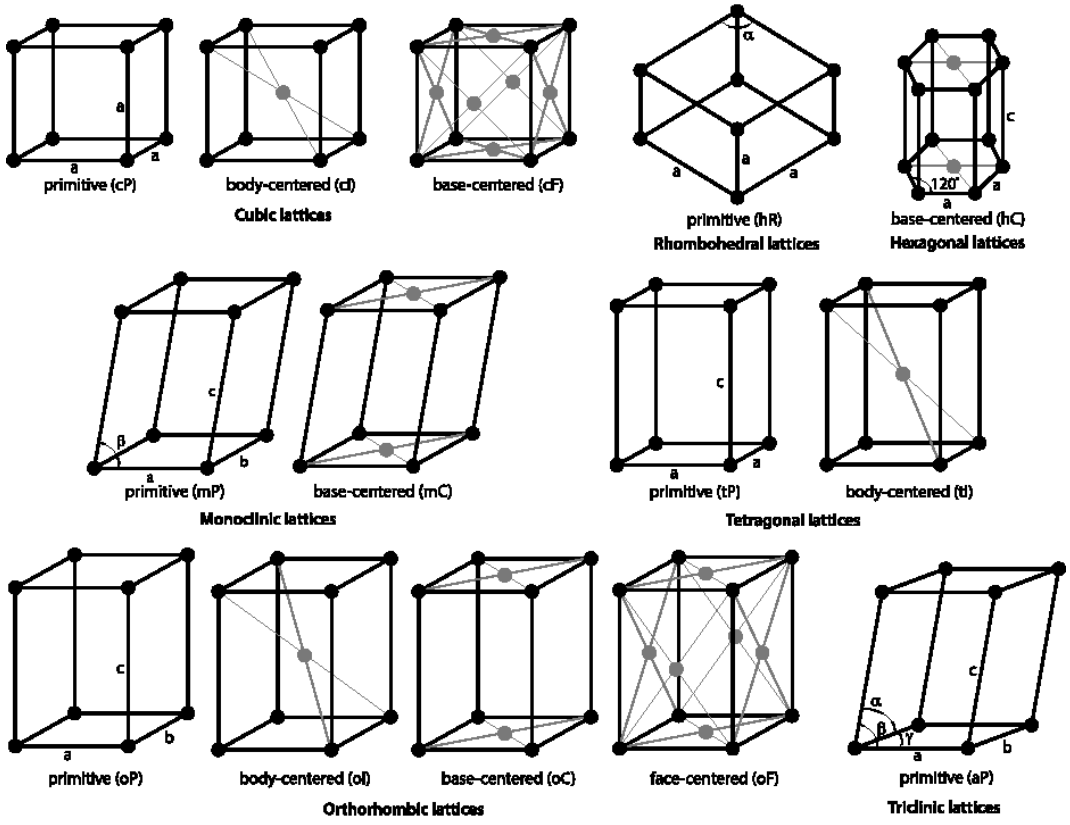

Figure 47: 3D Bravais lattice.

The Bravais lattice governs how lattice motifs are filling the space, and determines the shape of the Brillouin zone and is fundamental to the diffraction experiments as we will focus on below. Note that although here we discuss the Bravais lattices in the context of symmetries, the actual symmetry of a given material cannot be determined by the symmetry of its Bravais lattice alone.

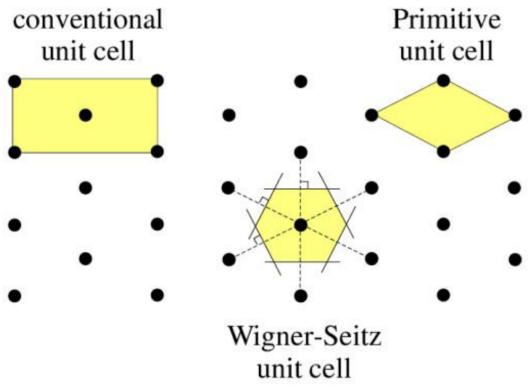

Figure 48: Different ways of taking the unit cell given a hexagonal 2D Bravais lattice

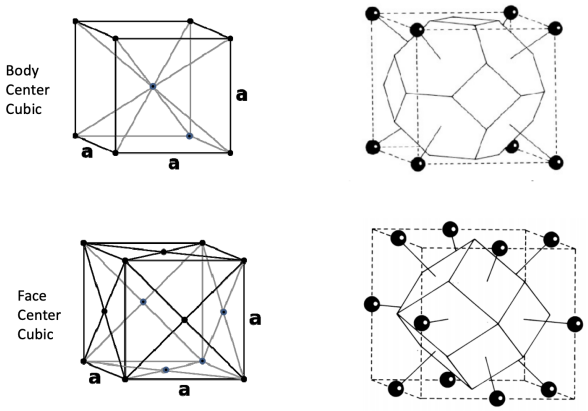

Figure 49: Conventional and Wigner-Setiz cells of the bcc and fcc lattices, respectively.

7.2 Unit cell and basis

A unit cell refers to the minimal pattern that is repeated in the entire structure. The primitive unit cell includes one Bravais lattice point; sometimes for convenience, a unit cell with othorgonal axes will be taken (conventional unit cell) while can contain more than one Bravais lattice points (see Fig. 48).

Another elegant, while not necessarily simple way of defining the unit cell is the so-called Wigner-Seitz cell. It starts from one Bravais lattice point, and make boundaries around the lattice point by planes cutting the connection between it and the adjacent points by half. See fig. 49 for the conventional cells (left column) and Wigner-Seitz cells (right column) of the bcc and fcc lattices, respectively.

Basis refers to the internal structure within a unit cell. We've touched on this when we had two atoms within a unit cell of the one dimensional atomic chain. The Bravais lattice and the basis altogether provides a complete description of a given crystal structure. In Fig. 50 see the example of the honeycomb lattice; there are two atoms within a unit cell.

7.3 Reciporal lattice

Recall that in 1D, we have defined the reciprocal lattice G_n as all the points equivalent with $k = 0$:

$$e^{iG_n a} = 1 \tag{213}$$

with $G_n = 2\pi n/a$. We may directly replicate this definition to 2D and 3D:

$$e^{i\boldsymbol{G}\cdot\boldsymbol{R}} = 1 \tag{214}$$

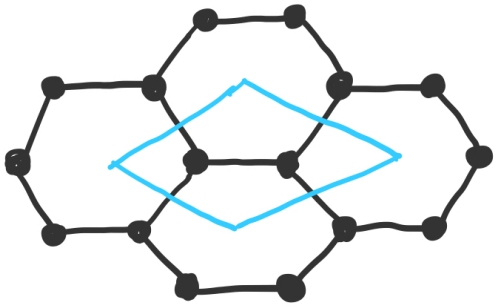

Figure 50: Honeycomb lattice and its unit cell

for all $\boldsymbol{R}$ belonging to the Bravais lattices. Recall that $\boldsymbol{R} = n_1\boldsymbol{a}_1 + n_2\boldsymbol{a}_2 + n_3\boldsymbol{a}_3$, if we choose a set of basis $\boldsymbol{b}_j$ satisfying

$$\boldsymbol{a}_i \cdot \boldsymbol{b}_i = 2\pi\delta_{ij} \tag{215}$$

We will get a complete description of the reciprocal lattice points

$$\boldsymbol{G} = m_1\boldsymbol{b}_1 + m_2\boldsymbol{b}_2 + m_3\boldsymbol{b}_3 \tag{216}$$

where m_1, m_2, m_3 are integers. It is customary to take the following form of reciprocal lattice vectors:

$$\begin{aligned}
\boldsymbol{b_1} &= 2\pi\frac{\boldsymbol{a}_2 \times \boldsymbol{a}_3}{\boldsymbol{a}_1 \cdot (\boldsymbol{a}_2 \times \boldsymbol{a}_3)} \\
\boldsymbol{b_2} &= 2\pi\frac{\boldsymbol{a}_3 \times \boldsymbol{a}_1}{\boldsymbol{a}_2 \cdot (\boldsymbol{a}_3 \times \boldsymbol{a}_1)} \\
\boldsymbol{b_3} &= 2\pi\frac{\boldsymbol{a}_1 \times \boldsymbol{a}_2}{\boldsymbol{a}_3 \cdot (\boldsymbol{a}_1 \times \boldsymbol{a}_2)}
\end{aligned} \tag{217}$$

One may check that this satisfies Eq. 234.

7.4 Brillouin zone

The first Brillouin zone in 3D is defined as the Wigner-Seitz cell of the reciprocal lattice. Brillouin zone is the basis of where band structures/phonon dispersions of solids live.

As an exercise, let's also spend some time thinking about the reciprocal lattice of the bcc and fcc lattices.

Starting with bcc (Fig. 49), the proper primitive unit cell has the following set of translational vectors (here a is the lattice constant for the conventional unit cell)

$$\begin{aligned}
\boldsymbol{a_1} &= (-0.5, 0.5, 0.5)a \\
\boldsymbol{a_2} &= (0.5, -0.5, 0.5)a \\
\boldsymbol{a_3} &= (0.5, 0.5, -0.5)a
\end{aligned} \tag{218}$$

which gives us the following reciprocal space vectors

$$\begin{aligned}
\boldsymbol{b_1} &= \frac{2\pi}{a}(0, 1, 1) \\
\boldsymbol{b_2} &= \frac{2\pi}{a}(1, 0, 1) \\
\boldsymbol{b_3} &= \frac{2\pi}{a}(1, 1, 0)
\end{aligned} \tag{219}$$

For fcc (Fig. 49), the translational vectors will be (here a is again the lattice constant for the conventional unit cell)

$$\begin{aligned}
\boldsymbol{a_1} &= (0, 0.5, 0.5)a \\
\boldsymbol{a_2} &= (0.5, 0, 0.5)a \\
\boldsymbol{a_3} &= (0.5, 0.5, 0)a
\end{aligned} \tag{220}$$

which gives us the following reciprocal space vectors

$$\begin{aligned} \boldsymbol{b_1} &= \frac{2\pi}{a}(-1,1,1) \\ \boldsymbol{b_2} &= \frac{2\pi}{a}(1,-1,1) \\ \boldsymbol{b_3} &= \frac{2\pi}{a}(1,1,-1) \end{aligned} \tag{221}$$

One can see that bcc and fcc Bravais lattices are reciprocal lattices of each other. Therefore the first Brillouin zone for the fcc (bcc) lattice will have the form of the Wigner-Seitz cell of the bcc (fcc) lattice itself. A complete list of the shape of Brillouin zone along with their high symmetry points are included in the attachment.

7.5 Fourier transform picture

The reciprocal lattice may be viewed as a Fourier transform of the real space Bravais lattice. This can be seen most clearly from the 1D case; if we start from a delta function like density of a periodic structure

$$\rho(r) = \sum_n \delta(r - na) \tag{222}$$

The Fourier transform of $\rho(r)$ will be

$$\int dr e^{ikr}\rho(r) = \sum_n \int dr e^{ikr}\delta(r-na) = \sum_n e^{ikna} = \frac{2\pi}{a}\sum_m \delta(k - 2\pi m/a) \tag{223}$$

Resulting in the reciprocal lattice. The δ function we've taken for $\rho(r)$ is clearly an approximation, and if we allow internal structure and let $\rho(r)$ be a periodic function where $\rho(r+R) = \rho(r)$, the Fourier transform becomes (r' defined within a unit cell)

$$\int dr e^{ikr}\rho(r) = \int dr e^{ikR}e^{ikr'}\rho(r'+R) = \sum_R e^{ikR}\int_{u.c.} dr' e^{ikr'}\rho(r') = \frac{2\pi}{a}\sum_R \delta(k-G)\int_{u.c.} dr' e^{ikr'}\rho(r') \tag{224}$$

with the internal structure captured by a so-called structural factor

$$S(k) \equiv \int_{u.c.} dr' e^{ikr'}\rho(r') \tag{225}$$

The above expressed in 3D can be

$$F[\rho(r)] = \sum_{\boldsymbol{R}} e^{i\boldsymbol{k}\cdot\boldsymbol{R}} = \frac{(2\pi)^D}{v}\sum_{\boldsymbol{G}} \delta^D(\boldsymbol{k}-\boldsymbol{G})S(\boldsymbol{k}) \tag{226}$$

And the structural factor (which plays an important role in diffraction experiments)

$$S(\boldsymbol{k}) \equiv \int_{u.c.} d\boldsymbol{r'} e^{i\boldsymbol{k}\cdot\boldsymbol{r'}}\rho(\boldsymbol{r'}) \tag{227}$$

8 Symmetries of solids

Here we'd like to introduce the notion of symmetries to the periodic structures of solids. The most important symmetry elements encountered in solids are

- Translation
- Rotation
- Inversion $(x,y,z) \to (-x,-y,-z)$. Inversion reverses the sign of electric dipole, but preserves the sign of magnetic dipole. If a given system has inversion symmetry, no spontaneous electrical dipole is allowed.

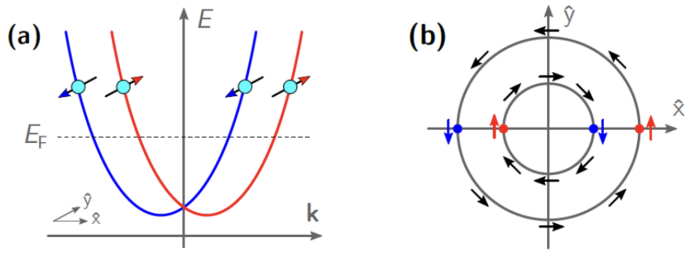

Figure 51: Schematic of Rashba spin splitting commonly found on surface of heavy metals

- Reflection (in other words, mirror symmetry). If the mirror plane is perpendicular to z-axis, the mirror operation can be expressed as $(x, y, z) \to (x, y, -z)$. This is closely related to the inversion symmetry.

  Note that electric dipole and magnetic dipole under reflection are very different (one is a polar vector, the other an axial vector). Using the axial nature of the magnetic dipoles we can make some guesses of the direction of spins for the so-called Rashba surface state

  $$H(\boldsymbol{k}) = \frac{\hbar^2 \boldsymbol{k}^2}{2m} + \lambda(\boldsymbol{\sigma} \times \boldsymbol{k}) \tag{228}$$

  The 2D surface state of spin-orbit coupled metals is often found to have an in-plane spin texture described by the Rashba Hamiltonian (Fig. 51). One may check this out by verifying the spin texture breaks the mirror plane of the surface, while obeys mirror symmetries with mirror planes perpendicular to the surface normal.

  Example two: monolayer transition metal dichacogenides.

- Time reversal symmetry, should be present when one don't have magnetic order (can check that for the above Rashba states). If a system have both inversion and time reversal symmetries, the band structure will be doubly degenerate everywhere in the Brillouin zone.

Neumann's principle states that if a crystal is invariant with respect to certain symmetry operations, any of its physical properties must also be invariant with respect to the same symmetry operations, or otherwise stated, the symmetry operations of any physical property of a crystal must include the symmetry operations of the point group of the crystal.

Point group symmetries are what determines the symmetry of given physical quantities. It includes all the symmetry operations that leaves the points in the lattice unchanged and does not include translation symmetry. Space group adds translational symmetry in addition to the symmetry operations included in point groups. A more complete description of the consequences in the band structure. Space group includes a class of symmetry operations called non-symmorphic symmetries, including screw and glide symmetries (they are found to be important for protecting band degeneracies).

9 Neutron and X-ray diffraction

Diffraction of waves by the lattice has been among the most important tools to study the internal structure of solids. In particular, waves with wavelengths comparable with the lattice constants are the most effective in probing the microscopic structure at sub-nanometer length scales (the wave length of visible light is too long for this purpose). The most commonly used is the X-ray (very short wavelength light) and neutrons.

9.1 Laue and Bragg conditions

9.1.1 Laue condition

Fig. 52 shows the scattering conditions we are interested in. Incident wave vector $\boldsymbol{k}$ and scattered wave vector $\boldsymbol{k}'$. According to Fermi's golden rule (let's now restrict ourselves to elastic scattering processes)

$$\Gamma(\boldsymbol{k}, \boldsymbol{k}') = \frac{2\pi}{\hbar} |\langle \boldsymbol{k}|V|\boldsymbol{k}'\rangle|^2 \delta(E_{\boldsymbol{k}} - E_{\boldsymbol{k}'}) \tag{229}$$

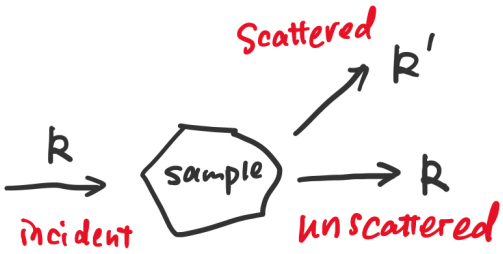

Figure 52: Caption

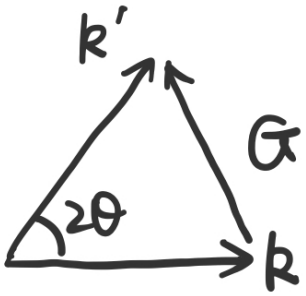

Figure 53: Caption

The matrix element

$$\langle \boldsymbol{k}|V|\boldsymbol{k}'\rangle = \int d\boldsymbol{r}\frac{e^{-\boldsymbol{k}'\cdot\boldsymbol{r}}}{\sqrt{V}}V(\boldsymbol{r})\frac{e^{\boldsymbol{k}\cdot\boldsymbol{r}}}{\sqrt{V}} = \frac{1}{V}\int d\boldsymbol{r}e^{-i(\boldsymbol{k}'-\boldsymbol{k})\cdot\boldsymbol{r}}V(\boldsymbol{r}) \tag{230}$$

This expression is quite generic; in the case where $V(\boldsymbol{r})$ is periodic, this matrix element reduces to zero unless $\boldsymbol{k}-\boldsymbol{k}' = \boldsymbol{G}$, where $\boldsymbol{G}$ is a reciprocal lattice vector. Very similar to how we have performed the Fourier transform above, the matrix element may be written as

$$\langle \boldsymbol{k}|V|\boldsymbol{k}'\rangle = \frac{1}{V}[\sum_{\boldsymbol{R}} e^{-i(\boldsymbol{k}-\boldsymbol{k}')\cdot\boldsymbol{R}}][\int_{uc} d\boldsymbol{r}' e^{-i(\boldsymbol{k}'-\boldsymbol{k})\cdot\boldsymbol{r}'}V(\boldsymbol{r}')] \tag{231}$$

where the first term implies that

$$\boldsymbol{k}'-\boldsymbol{k} = \boldsymbol{G} \tag{232}$$

and this is the so-called Laue condition.

In the elastic scattering scenario

$$|\boldsymbol{k}| = |\boldsymbol{k}'| \tag{233}$$

Giving

$$|\boldsymbol{G}| = 2|\boldsymbol{k}|\sin\theta \tag{234}$$

if $2|\boldsymbol{k}|$ is smaller than the first non-zero reciprocal space vector, Eq. 234 won't be satisfied. Recall $k = 2\pi/\lambda$, the condition that non-zero diffraction can be observed will be

$$\lambda < a/2 \tag{235}$$

The most commonly used wavelength for X-ray diffraction experiments include Cu $K\alpha$ with $\lambda = 1.54$ Åand Mo $K\alpha$ with $\lambda = 0.71$ Å. Both are significantly shorter than typical lattice constants 3-5 (or even more) Å.

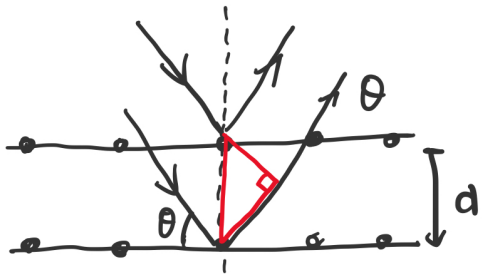

Figure 54: Caption

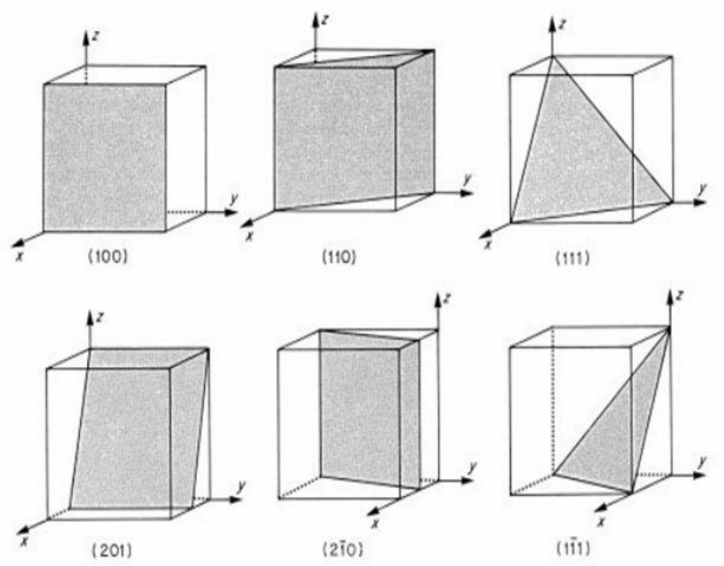

Figure 55: Caption

9.1.2 Bragg condition

A different view of the diffraction described above is to think about the constructive interference of a diffraction grating composed of the lattice planes.

For a scenario illustrated in Fig. x the condition for constructive interference is

$$n\lambda = 2d\sin\theta \tag{236}$$

For the illustrated simple case, we may work out that the Bragg and Laue conditions are equivalent with each other.

9.1.3 Lattice planes and Miller indices

Each reciprocal lattice vector can be expressed as a linear superposition of the basis vectors $\boldsymbol{b}_i$:

$$\boldsymbol{G} = h\boldsymbol{b}_1 + k\boldsymbol{b}_2 + l\boldsymbol{b}_3 \tag{237}$$

and the set of integer numbers (hkl) is called the Miller indices. Each $\boldsymbol{G}$ corresponds to a set of planes that intersects with the real space lattice. A useful shortcut to denote these planes is the following:

$$\frac{1}{x_1} : \frac{1}{x_2} : \frac{1}{x_3} = h : k : l \tag{238}$$

where x_i are the intersection of the lattice planes with the three real space axes. The spacing between the planes will be

$$d_{h,k,l} = \frac{2\pi}{|\boldsymbol{G}|} = \frac{2\pi}{\sqrt{h^2|\boldsymbol{b}_1|^2 + k^2|\boldsymbol{b}_2|^2 + l^2|\boldsymbol{b}_3|^2}} \tag{239}$$

9.2 Scattering amplitudes and exctinction rules

Eq. 231 tells us that the scattering amplitude is largely determined by the so-called structure factor

$$S(\boldsymbol{G}) = \int_{u.c.} d\boldsymbol{r} e^{i\boldsymbol{G}\cdot\boldsymbol{r}} V(\boldsymbol{r}) \tag{240}$$

And frequently it is convenient to note

$$I_{hkl} \propto |S_{hkl}|^2 \tag{241}$$

And it is often a good assumption that the scattering potential $V(x)$ can be viewed as a summation over all the individual atoms (j denotes the j-th atom)

$$V(\boldsymbol{x}) = \sum_j V_j(\boldsymbol{x} - \boldsymbol{x}_j) \tag{242}$$

9.2.1 Neutrons

Neutrons interact with solids through two primary pathways–(a) neutrons get scattered off by nuclei (through some sort of nuclear strong force) and (b) through the magnetic interaction between neutron spin and the magnetic field generated by electron spins. The former is of the following form

$$V(\boldsymbol{x}) = \sum_j f_j \delta(\boldsymbol{x} - \boldsymbol{x}_j) \tag{243}$$

and f_j a number proportional to the nuclear cross section b_j depending on the number of neutrons and protons in a given nuclei (therefore isotope-dependent). Therefore the corresponding structural factor is

$$S(\boldsymbol{G}) \sim \sum_j b_j e^{i\boldsymbol{G}\cdot\boldsymbol{x}_j} \tag{244}$$

The interaction between the magnetic moments of the neutron and the electron is

$$V(\boldsymbol{r}) = -\gamma\mu_N \boldsymbol{\sigma} \cdot \boldsymbol{B}(\boldsymbol{r}) \tag{245}$$

and as a result neutron scattering is an extremely powerful tool to study magnetic order in solids.

9.2.2 X-rays

X-rays on the other hand mainly interact with the electrons in a given system through a Thomson scattering-like process. The interaction between light and these electrons will be proportional to Z_j (atomic number, also the number of electrons)

$$V_j(\boldsymbol{x} - \boldsymbol{x}_j) = Z_j g_j(\boldsymbol{x} - \boldsymbol{x}_j) \tag{246}$$

Note that we don't have a simple delta function here as in neutron scattering cross section, but a more extended function depending on the distribution of the charge cloud around an atom. And the structural factor

$$S(\boldsymbol{G}) = \sum_{u.c} f_j(\boldsymbol{G}) e^{i\boldsymbol{G}\cdot\boldsymbol{x}_j} \tag{247}$$

where f is the form factor determined by the Fourier transform of the electron density around the nuclei.

Viewing neutron and X-ray scattering together, the former a better probe of the atomic lattice structure, sensitive to isotope, the latter exclusive to high Z elements. X-ray difficult to distinguish elements with similar Z, while neutron scattering is more sensitive. As an side, plane waves of free electrons can also be used in scattering similar to how it works for plane waves of neutrons and X-rays.

9.2.3 Simple case studies

In this section we will look at some simple examples of scattering intensities using

$$I_{hkl} \propto |S_{hkl}|^2 \tag{248}$$

and

$$S_{hkl} = \sum_{u.c.} f_j e^{2\pi i(hx_j + ky_j + lz_j)} \tag{249}$$

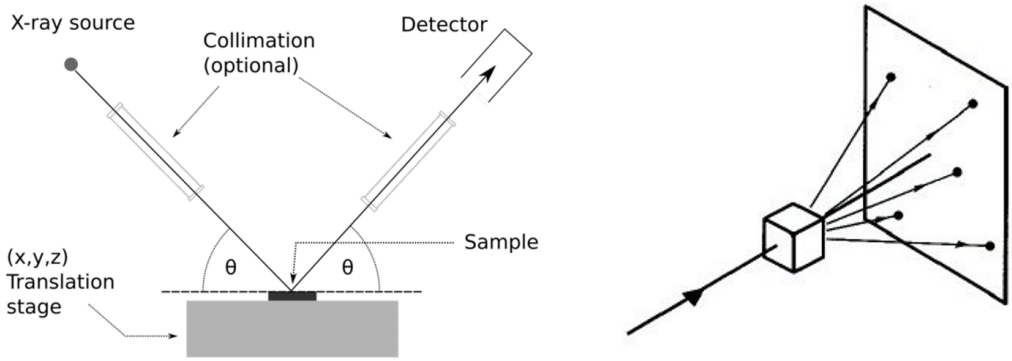

Figure 56: Caption

CsCl

The CsCl has a simple cubic Bravais lattice with two basis: Cs at [0,0,0] and Cl at [0.5,0.5,0.5]a. The corresponding structural factor is

$$S_{hkl} = f_{Cs} + f_{Cl}(-1)^{h+k+l} \tag{250}$$

One can see that the scattering from the two sublattices sometimes add up in a constructive manner and sometimes a destructive manner.

bcc Cs

Cs element itself prefers a bcc lattice. In the conventional unit cell, there are two atoms in the cell [0,0,0] and [0.5,0.5,0.5]a.

$$S_{hkl} = f_{Cs}[1 + e^{i2\pi(h,k,l)\cdot[1/2,1/2,1/2]}] = f_{Cs}[1 + (-1)^{h+k+l}] \tag{251}$$

At $h + k + l =$ odd, the two atoms in the conventional unit cell destructively interfere with each other and no scattering intensity can be obtained. This is called the extinction rule or systematic absence, whose root lies in the geometry of certain lattices.

fcc Cu

Cu crystallizes in a fcc lattice. Similarly for fcc lattice the four atoms in the conventional unit cells are [0,0,0]a, [0.5,0.5,0]a, [0,0.5,0.5]a, [0.5,0,0.5]a, which results in the following structural factor

$$S_{hkl} = f_{Cu}[1 + (-1)^{h+k} + (-1)^{h+l} + (-1)^{k+l}] \tag{252}$$

which will be non-zero unless h, k, l are all odd or all even.

ZnS

Here let's look at a more complex example of ZnS (cubic zincblende structure), which may be viewed as a fcc with a basis with Zn atom at [0,0,0] and S at [1/4,1/4,1/4]a. The structural factor is

$$S_{hkl} = [1 + (-1)^{h+k} + (-1)^{h+l} + (-1)^{k+l}][f_{Zn} + f_S e^{i\pi/2(h+k+l)}] \tag{253}$$

Generically, the overall structural factor will be that of the Bravais lattice times that of the basis.

9.3 Some scattering configurations

In this section we'd like to invoke some experimental configurations. In Fig. 56 the left panel illustrates a configuration where both X-ray source and detector can be viewed as points, and with collimator, the path of X-ray is well defined and this configuration can be used to map out $I(2\theta)$. The configuration on the right is called the Laue configuration, where the detection is done via a two-dimensional screen.

9.4 Asides

9.4.1 inelastic scattering

Scattering can take place between incident beam and outgoing beam having different energies. This is the inelastic scattering and it is a useful tool to study excitations in the system such as phonons. The conservation laws are

$$\boldsymbol{q} = \boldsymbol{k} - \boldsymbol{k}' + \boldsymbol{G}, E(\boldsymbol{q}) = \epsilon(\boldsymbol{k}) - \epsilon(\boldsymbol{k}') \tag{254}$$

9.4.2 scattering from liquids

Although liquids don't have a periodic structure, as the particles in liquids are strongly interacting with each other, there will be some incipient structure that can be detected by scattering. The peak position of the very broad scattering intensity would be on the order of $2\pi/d$, where d is the mean inter-particle distance. Similarly, scattering can be informative for amorphous structure as well.

9.4.3 Neutron diffraction and antiferromagnetism

Since neutron interacts with the dipole moments of electrons, it is the best tool to study the periodic structure of magnetic moments, especially the case of antiferromagnetism. Before neutron scattering was invented, antiferromagnetic orders are more or less "hidden orders" in solids. Fig. x illustrates the example of how neutron scattering reflects the antiferromagnetic order of MnF2.

10 Nearly free electrons in a periodic potential

As we get familiar with the notion of scattering of waves by the periodic structure, here we revisit the electronic eigenstates in solids from a very different starting point than the tight-binding model. The Hamiltonian of interest is

$$H = \frac{\hbar^2 \boldsymbol{k}^2}{2m} + V(\boldsymbol{r}) \tag{255}$$

where $V(\boldsymbol{r})$ is a periodic potential with $V(\boldsymbol{r}) = V(\boldsymbol{r} + \boldsymbol{R})$. If the second term of the Hamiltonian is viewed as a perturbation to the first term, it is convenient fo define the following matrix element

$$\langle \boldsymbol{k}'|V|\boldsymbol{k}\rangle = \frac{1}{V}\int d\boldsymbol{r} e^{i(\boldsymbol{k}-\boldsymbol{k}')\cdot\boldsymbol{r}} V(\boldsymbol{r}) \equiv V(\boldsymbol{k}' - \boldsymbol{k}) \tag{256}$$

which as we have worked out above is only non-zero when

$$\boldsymbol{k}' - \boldsymbol{k} = \boldsymbol{G} \tag{257}$$

In other words, any plane wave $\boldsymbol{k}$ can only be scattered to states with $\boldsymbol{k} + \boldsymbol{G}$.

Now one can examine how such scattering matrices modify the energy eigen states of the system. At a given state $\boldsymbol{k}$ to the first order, the perturbation modifies the energy via

$$\epsilon(\boldsymbol{k}) = \epsilon_0(\boldsymbol{k}) + \langle \boldsymbol{k}|V|\boldsymbol{k}\rangle \tag{258}$$

in the plane wave formulism $\langle \boldsymbol{k}|V|\boldsymbol{k}\rangle = V_0$, which shifts the energy of all $\boldsymbol{k}$ states by a constant. For simplicity we let $V_0 = 0$. The second order perturbation gives

$$\epsilon(\boldsymbol{k}) = \epsilon_0(\boldsymbol{k}) + \sum_{\boldsymbol{k}'=\boldsymbol{k}+\boldsymbol{G}} \frac{|\langle \boldsymbol{k}'|V|\boldsymbol{k}\rangle|^2}{\epsilon_0(\boldsymbol{k}) - \epsilon_0(\boldsymbol{k}')} \tag{259}$$

The form implies that when it is possible to satisfy $\epsilon_0(\boldsymbol{k}) = \epsilon_0(\boldsymbol{k}')$, special treatment (i.e.) degenerate perturbation is required. In particular, this would take place when $\boldsymbol{k} = -\boldsymbol{k}' = \dfrac{\boldsymbol{G}}{2}$. Recall our definition of the first Brillouin zone as the Wigner-Seitz cell of the reciprocal lattice, the above condition is satisfied at the Brillouin zone boundary.

Degenerate perturbation between $|\boldsymbol{k}\rangle$ and $|\boldsymbol{k}'\rangle$ can be performed by calculating the matrix elements:

$$\begin{aligned}
\langle \boldsymbol{k}|H|\boldsymbol{k}\rangle &= \epsilon_0(\boldsymbol{k}) \\
\langle \boldsymbol{k}'|H|\boldsymbol{k}'\rangle &= \epsilon_0(\boldsymbol{k}') = \epsilon_0(\boldsymbol{k} + \boldsymbol{G}) \\
\langle \boldsymbol{k}|H|\boldsymbol{k}'\rangle &= V_{\boldsymbol{k}-\boldsymbol{k}'} = V_{\boldsymbol{G}}^* \\
\langle \boldsymbol{k}'|H|\boldsymbol{k}\rangle &= V_{\boldsymbol{k}'-\boldsymbol{k}} = V_{\boldsymbol{G}}
\end{aligned} \tag{260}$$

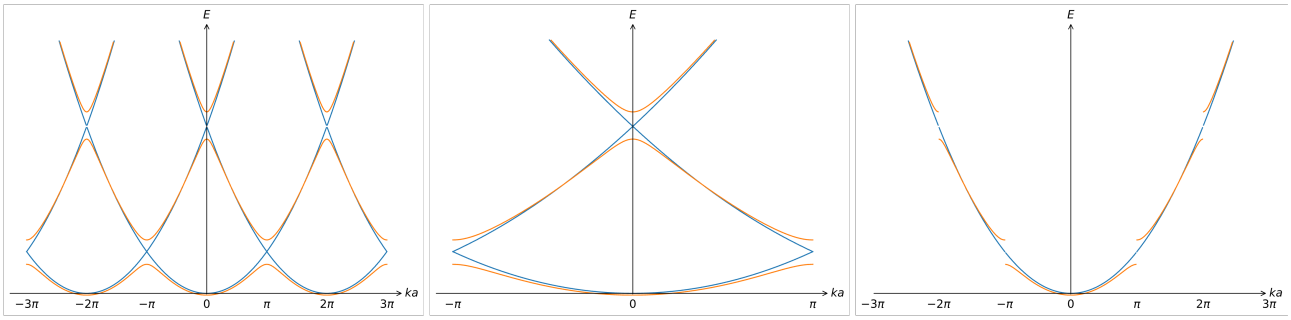

Figure 57: Nearly free electron model in repeated zone, reduced zone and extended zone schemes (reference: Open Solid State Note)

and the new eigenstates are the solution of the following matrix

$$\begin{pmatrix} \epsilon_0(\boldsymbol{k}) & V_{\boldsymbol{G}}^* \\ V_{\boldsymbol{G}} & \epsilon_0(\boldsymbol{k}+\boldsymbol{G}) \end{pmatrix} \tag{261}$$

10.1 At Brilluoin zone boundary

When $\boldsymbol{k} = -\boldsymbol{k}' = \boldsymbol{G}$, the solution becomes

$$E_\pm = \epsilon_0(\boldsymbol{k}) \pm |V_{\boldsymbol{G}}| \tag{262}$$

which corresponds to a gap-opening at the Brillouin zone boundary. The gap is proportional to the scattering potential. In the simplest one dimensional case with $V(x) = V_0\cos(2\pi x/a)(V_0 > 0)$, and for $k = \pi/a$, the eigen wave functions near the gap is

$$|\phi_\pm\rangle = \frac{1}{\sqrt{2}}(|k\rangle \pm |k'\rangle) \tag{263}$$

The linear superposition can be viewed as constructive and destructive interference, respectively.

10.2 Near the Brillouin zone boundary

Here we can expand the dispersion near the Brillouin zone boundary through the same perturbation scheme:

$$\begin{pmatrix} \epsilon_0(-\boldsymbol{G}/2+\boldsymbol{\delta}) & V_{\boldsymbol{G}}^* \\ V_{\boldsymbol{G}} & \epsilon_0(\boldsymbol{G}/2+\boldsymbol{\delta}) \end{pmatrix} \tag{264}$$

In 1D, near $k = \pm n\pi/a$, the matrix elements are

$$\begin{aligned} \epsilon_0(-\frac{n\pi}{a}+\delta) &= \frac{\hbar^2}{2m^*}(\frac{n^2\pi^2}{a^2} + \delta^2 - \frac{2n\pi\delta}{a}) \\ \epsilon_0(\frac{n\pi}{a}+\delta) &= \frac{\hbar^2}{2m^*}(\frac{n^2\pi^2}{a^2} + \delta^2 + \frac{2n\pi\delta}{a}) \end{aligned} \tag{265}$$

The eigenvalue equations will be

$$[E - \frac{\hbar^2}{2m^*}(\frac{n^2\pi^2}{a^2} + \delta^2 - \frac{2n\pi\delta}{a})][E - \frac{\hbar^2}{2m^*}(\frac{n^2\pi^2}{a^2} + \delta^2 + \frac{2n\pi\delta}{a})] = |V_G|^2 \tag{266}$$

which can be simplified to

$$[E - \frac{\hbar^2}{2m^*}(\frac{n^2\pi^2}{a^2} + \delta^2)]^2 = |V_G|^2 + (\frac{\hbar^2}{2m^*}\frac{2n\pi\delta}{a})^2 \tag{267}$$

The resulting eigenvalues are

$$E_\pm = \frac{\hbar^2}{2m^*}(\frac{n^2\pi^2}{a^2} + \delta^2) \pm \sqrt{|V_G|^2 + (\frac{\hbar^2}{m^*}\frac{n\pi\delta}{a})^2} \tag{268}$$

At small δ the eigenvalues are quaratic in δ near

$$\frac{\hbar^2}{2m^*}(\frac{n^2\pi^2}{a^2}) \pm |V_G| \tag{269}$$

10.3 Bloch theorem revisited

Here we verify that the eigenstates of the nearly free electron model satisfies the Bloch theorem. Since $\boldsymbol{k}$ is only connected to states of the form $\boldsymbol{k}+\boldsymbol{G}$, the eigenwave function $\Psi_{\boldsymbol{k}}$

$$\Psi_{\boldsymbol{k}} = \sum_{\boldsymbol{G}} u_{\boldsymbol{G},\boldsymbol{k}} e^{i(\boldsymbol{G}+\boldsymbol{k})\cdot\boldsymbol{r}} = e^{i\boldsymbol{k}\cdot\boldsymbol{r}}[\sum_{\boldsymbol{G}} u_{\boldsymbol{G},\boldsymbol{k}} e^{i\boldsymbol{G}\cdot\boldsymbol{r}}] \tag{270}$$

where $u_{\boldsymbol{G},\boldsymbol{k}}$ are coefficients. It is easy to verify that the second part in Eq. 270 is periodic with $\boldsymbol{R}$ because $e^{i\boldsymbol{G}\cdot\boldsymbol{R}} = 1$. In other words, even though the potential electrons feel from the atoms are significant, the electrons still behaves as a "modified" plane waves as if they don't feel the atoms at all–if the potential is periodic in space.

11 Primers on the Quantum Hall effect

In one of the assignments, you've worked out that Bloch electrons do oscillations in the presence of an electric field. In this chapter we will focus on the motion of electrons in a strong magnetic field. In contrast to the weak field limit where we've looked at the Hall effect linear in field, we are looking at magnetic fields that are sufficiently strong such that the cycltron motion is quantized.

11.1 Landau quantization for quadratic electrons

Consider a magnetic field with strength B along z, and its effect on itinerant electrons can be captured by the following vector potential following the Landau gauge

$$A_y = xB; A_x = A_z = 0 \tag{271}$$

the choice of gauge here satisfies $\nabla \times \boldsymbol{A} = \boldsymbol{B}$. The Hamiltonian of the electronic states under the Landau gauge becomes:

$$H = \frac{1}{2m^*}[\hbar^2 k_x^2 + (\hbar k_y + eBx)^2] + \frac{\hbar^2 k_z^2}{2m_z} \tag{272}$$

The Hamiltonian resembles a harmonic oscillator for x, but not quite exactly. Here we introduce a trick to separate the variables by letting the wave function taking the following form (plane wave-like along y, k being the momentum or the label of the translational symmetry along y)

$$\psi_k(x, y) = e^{iky} f_k(x) \tag{273}$$

The effective Hamitonian h_k in the (x, y) plane

$$h_k f_k(x) = \epsilon_k f_k(x) \tag{274}$$

becomes

$$h_k = \frac{\hbar^2 k_x^2}{2m^*} + \frac{1}{2m^*}(\hbar k + eBx)^2 = \frac{p_x^2}{2m^*} + \frac{1}{2}m^*\omega_c^2(x + kl^2)^2 \tag{275}$$

where

$$l^2 = \frac{\hbar}{eB}, \omega_c = \frac{eB}{m^*} \tag{276}$$

l is called the magnetic length, and ω_c the cyclotron frequency.

The quantized levels (Landau levels) of 275 are

$$\epsilon_{kn} = (n + \frac{1}{2})\hbar\omega_c \tag{277}$$

and these states are independent on k. k influences the origin X_l of the harmonic oscillator along the x direction with

$$X_l \equiv kl^2 \tag{278}$$

The the corresponding wave function is

$$\psi_{nk}(x, y) = e^{iky} H_n(x/l - kl) e^{-\frac{1}{2l^2}(x - kl^2)^2} \tag{279}$$

The degeneracy of each Landau level can be estimated from

$$N = \frac{L_x}{\delta k l^2} = \frac{L_x L_y q B}{2\pi\hbar} = \frac{\Phi}{\Phi_0} \tag{280}$$

where $\Phi_0 = h/e$ is the flux quanta. In other words, there's one state per flux quanta in the system in 2D. In 3D, the z direction momentum remains unaffected by the Landau quantization.

Fig. 1 sketches the oscillatory change of overall energy of the electrons depending on the relative position of the zero field Fermi energy E_F and the highest occupied Landau level at zero temperature: when the highest LL is aligned with E_F, the total energy of the system is higher than that at zero field; when LL is offset from E_F by half a LL, the total energy is identical from the zero field energy.

Fig. 2 illustrates how a three dimensional dispersion is modified under the formation of Landau levels in the xy plane: the free electron dispersion along the z direction gives rise to the $1/\sqrt{E - E_n}$ singularities in the density of states.

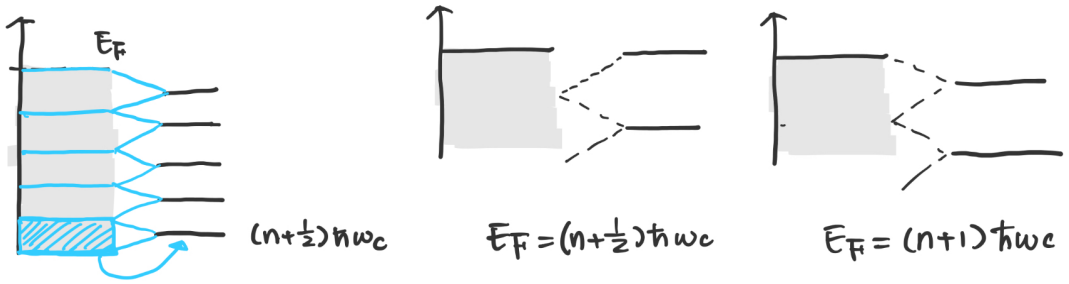

Figure 58: Sketch of the new electron distribution after the formation of Landau levels.

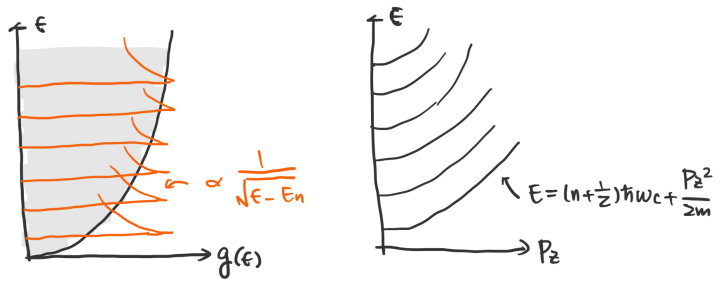

Figure 59: Density of states of a 3D system upon Landau quantization

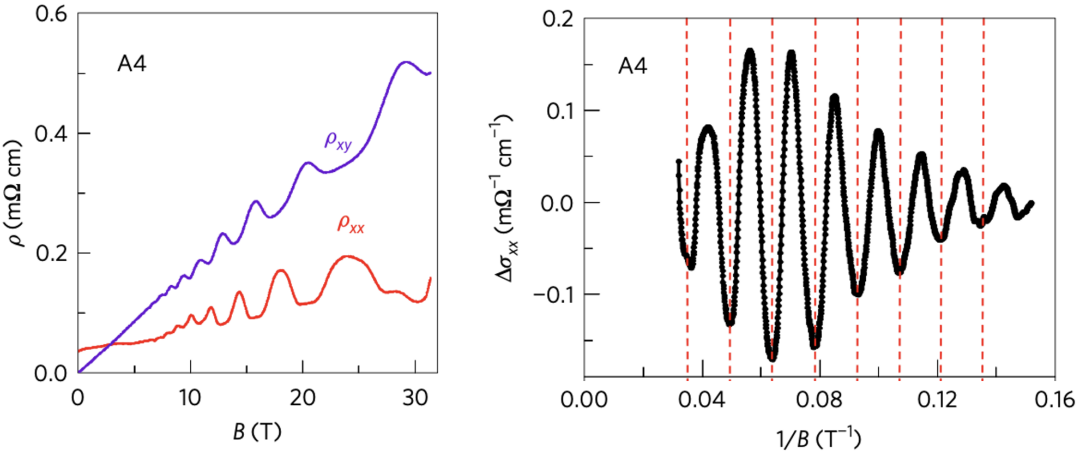

Figure 60: Quantum oscillation in SrMnSb2 (doi: 10.1038/nmat4953)

11.1.1 Onsager relation

Here we estimate the magnetic fields required for successive Landau levels to be aligned with the Fermi level E_F. Let's assume B_i to be the magnetic field for the i-th Landau level to be aligned with E_F:

$$E_F = (n+\frac{1}{2})\frac{\hbar e B_n}{m^*} = (n+1+\frac{1}{2})\frac{\hbar e B_{n+1}}{m^*} \tag{281}$$

which gives

$$\begin{aligned} \frac{1}{B_n} &= (n+\frac{1}{2})\frac{\hbar e}{m^* E_F} \\ \frac{1}{B_{n+1}} &= (n+1+\frac{1}{2})\frac{\hbar e}{m^* E_F} \end{aligned} \tag{282}$$

The periodicity of the energy oscillation is

$$\Delta(\frac{1}{B}) = \frac{\hbar e}{m^* E_F} = \frac{2\pi e}{\hbar A_k} \tag{283}$$

where A_k is the Fermi surface area perpendicular to the magnetic field. The above is the so-called Onsager relation, which states that quantum oscillations are periodic in $1/B$ and the periodicity can be used to extract the Fermi surface area of metallic systems (see Fig. 3).

11.2 Landau quantization for graphene

The low energy electron dispersion in graphene (resctricted to 2D) can be described by

$$H_{K,K'} = \hbar v_F(\pm\sigma_x k_x + \sigma_y k_y) \tag{284}$$

Under the magnetic field, let's use the following notation

$$\boldsymbol{\Pi} = \boldsymbol{p} + e\boldsymbol{A} \tag{285}$$

In the presence of a magnetic field Π_x and Π_y don't commute:

$$[\Pi_x, \Pi_y] = i\hbar e B = i\frac{\hbar^2}{l^2} \tag{286}$$

It is convenient to introduce the following ladder operators

$$a = \frac{l}{\sqrt{2}\hbar}(\Pi_x + i\Pi_y), a^\dagger = \frac{l}{\sqrt{2}\hbar}(\Pi_x - i\Pi_y), \tag{287}$$

Which gives

$$[a, a^\dagger] = 1 \tag{288}$$

And the Schrodinger equation under magnetic field becomes

$$H = \hbar\omega_c(a^\dagger a + 1/2) \tag{289}$$

The Dirac Hamiltonian under magnetic field is

$$H_K = v_F\boldsymbol{\sigma}\cdot\boldsymbol{\Pi} = v_F\begin{pmatrix} 0 & \Pi_x - i\Pi_y \\ \Pi_x + i\Pi_y & 0 \end{pmatrix} = \epsilon_D\begin{pmatrix} 0 & a^\dagger \\ a & 0 \end{pmatrix} \tag{290}$$

where $\epsilon_D = \sqrt{2}\hbar v_F/l$. To solve H_K we use the following trick to take the square of the Dirac Hamiltonian

$$H_K^2 = \epsilon_D^2\begin{pmatrix} a^\dagger a & 0 \\ 0 & a^\dagger a + 1 \end{pmatrix} \tag{291}$$

For $E = \pm\epsilon_D\sqrt{|n|}$, the corresponding eigenstate is of the form

$$\begin{pmatrix} \phi_n \\ \phi_{n-1} \end{pmatrix} \tag{292}$$

where ϕ_n is the n-th harmonic oscillator on a given sublattice. This implies that there is a zero energy state with eigenstate located on only one of the sublattices

$$\begin{pmatrix} 0 \\ \phi_0 \end{pmatrix} \tag{293}$$

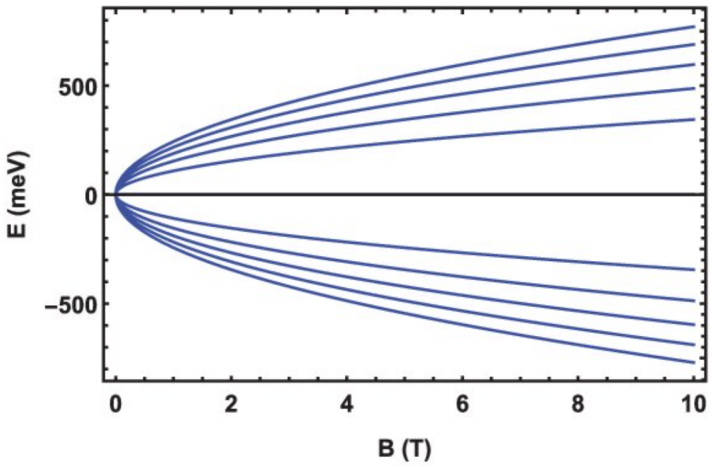

Figure 61: Landau levels of graphene

11.3 Quantum Hall effect

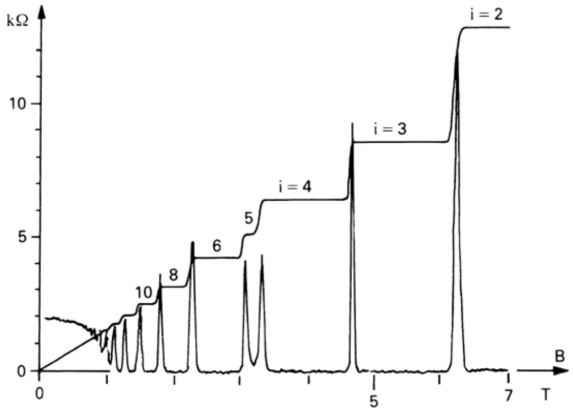

Figure 62: Quantum Hall effect with both ρ_{yx} and ρ_{xx} shown as a function of magnetic field.

A particularly intriguing collective phenomenon of electrons under a strong magnetic field is the quantum Hall effect as shown in Fig. 62. Thanks to the electrical nature of the experiments, the quantization nature of the Hall resistance plateaus are used for fundamental constants measurements.

In the density of state picture of 2D electrons (Fig. 63), when the Landau level is fully filled, the system resembles an insulator; experimentally it is observed that

$$\rho_{yx} = \frac{h}{e^2}\frac{1}{\nu}, \rho_{xx} = 0 \tag{294}$$

Here $h/e^2 = 25.8$ kΩ. This corresponds to the following conductivity tensor components, where ν is an integer filling factor

$$\nu = \frac{N}{\Phi/\Phi_0} \tag{295}$$

Recall that $\sigma = \rho^{-1}$

$$\sigma_{xy} = \nu\frac{e^2}{h}, \sigma_{xx} = 0 \tag{296}$$

That $\sigma_{xx} = 0$ is not surprising for an insulator, while the former is quite unusual. In this section we'd like to walk you through the physics of the quantized Hall conductance.

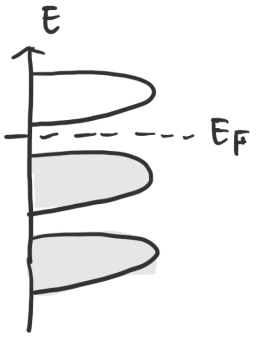

Figure 63: Density of state picture of LL of 2D electrons

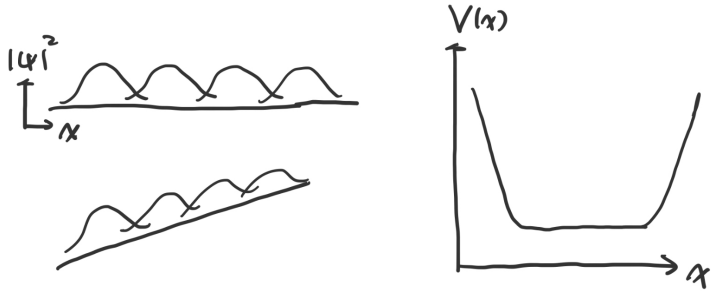

Figure 64: Schematic of the effects of an electric field and a confining potential for a sample with finite size along x

11.4 Drifting of Landau orbits in electric field

We begin by turning on an in-plane electric field to the Landau levels. We chose the electric field direction to be x, which aligns with the direction the Landau gauge is defined. The Hamiltonian becomes

$$H = \frac{p_x^2}{2m^*} + \frac{(p_y + eBx)^2}{2m^*} - eEx \tag{297}$$

Using the same form of wave function and absorbing the eEx term into x (which acts to shift the center of the wave function by $\frac{mE}{eB^2}$):

$$E_{n,k} = (n + \frac{1}{2})\hbar\omega_c - \frac{m}{2}\frac{E^2}{B^2} + \frac{\hbar k E}{B} \tag{298}$$

Which can be rewritten as

$$E_{n,k} = (n + \frac{1}{2})\hbar\omega_c - eE(\frac{mE}{eB^2} - kl^2) + \frac{m}{2}\frac{E^2}{B^2} \tag{299}$$

The second term may be viewed as the potential energy of the shifted drifting centers in the x direction. The meaning of the third term is more clear when we consider the group velocity along y of each state:

$$v_y = \frac{1}{\hbar}\frac{\partial E_{n,k}}{\partial k} = \frac{E}{B} \tag{300}$$

In other words, an electric field drives a transverse velocity in the Landau levels, and the final term in Eq. 299 can be viewed as the kinetic energy of this state under electric field. One may view this as an quantum mechanical version of the drift of electrons in the presence of both electric and magnetic fields.

Now let's consider instead a finite size sample in the x-direction. Instead of a uniform electric field, we consider the following confining potential shown in Fig. 64. Using results from Eq. 300, the group velocity

$$v_y = -\frac{1}{eB}\frac{dV(x)}{dx} \tag{301}$$

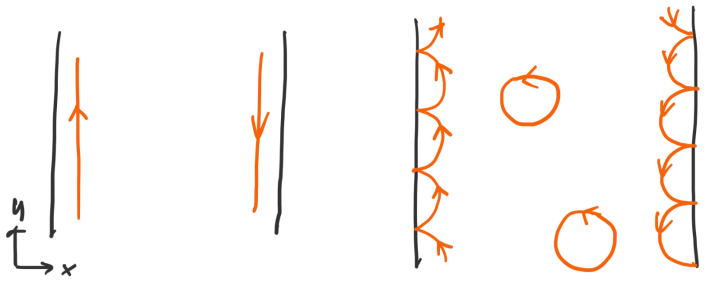

Figure 65: Schematic of edge currents of a fully filled Landau level and the corresponding semiclassical picture

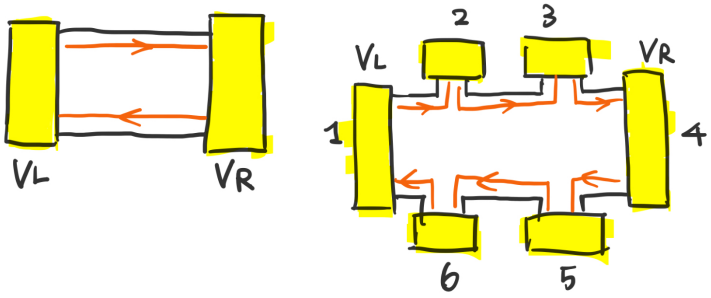

Figure 66: Schematic of two- and six-terminal configurations to probe the chiral edge modes of the quantum Hall effect

will have opposite sign near the two ends of the sample; while in the interior, if the sample is uniform, v_y=0. This suggests that in the ground state there are edge currents of opposite sign flowing in the sample. The semiclassical picture is the so-called skipping orbits of cicular cyclotron motion of electrons driven by the magnetic field.

Consider when the bulk of the sample has one fully occupied Landau level, and with edge currents at the two ends. Now let's work out the transport response of this situation.

11.5 Conductance in ballistic 1D channels

Now the edges can be considered as perfect 1D, chiral conducting channels. A robust result for 1D, unidirectional ballistic channels is that the conductance through the channel is quantized to be e^2/h, regardless of the details of the dispersion of the channel. Let's say we start from two electrodes with different electrochemical potential V:

$$J = ev\frac{dn}{d\epsilon}(Ve) \tag{302}$$

where

$$\frac{dn}{d\epsilon} = \frac{1}{2\pi}\frac{dk}{d\epsilon} \tag{303}$$

and recall that

$$v = \frac{1}{\hbar}\frac{d\epsilon}{dk} \tag{304}$$

The conductance

$$G = \frac{J}{V} = \frac{e^2}{h} \tag{305}$$

With this result we can set out and work out the conductance of a Hall bar with one chiral boundary mode.

In a multi-terminal experiment where the terminals are connected by 1D channels, the current through the i-th terminal can be given by the Landauer-Buttiker formula where T_{ij} is the transmission coefficient from terminal i to terminal j ($T_{ij} = 1$ for ballistic channels)

$$I_i = \frac{e^2}{h}\sum_j (T_{ji}V_j - T_{ij}V_i) \tag{306}$$

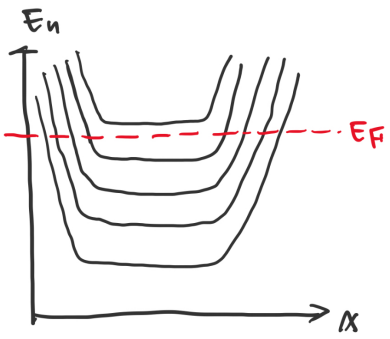

Figure 67: Schematic of multiple occupied Landau levels

The quantum Hall states in a two-terminal experiment,

$$I = \frac{e^2}{h}(V_R - V_L) \tag{307}$$

where the conductance is $G_{xx} = e^2/h$. In a six-terminal experiment, the following set of conditions can be written from the Landauer-Buttiker formula:

$$\begin{aligned} I_1 &= \frac{e^2}{h}(V_6 - V_1) = I \\ I_2 &= \frac{e^2}{h}(V_1 - V_2) = I_3 = \frac{e^2}{h}(V_2 - V_3) = 0 \\ I_4 &= \frac{e^2}{h}(V_3 - V_4) = I \\ I_5 &= \frac{e^2}{h}(V_4 - V_5) = I_6 = \frac{e^2}{h}(V_5 - V_6) = 0 \end{aligned} \tag{308}$$

Therefore

$$V_1 = V_2 = V_3, V_4 = V_5 = V_6 \tag{309}$$

while

$$\sigma_{xy} = \frac{V_1 - V_6}{I} = \frac{e^2}{h}, \sigma_{xx} = \frac{V_2 - V_3}{I} = 0 \tag{310}$$

When multiple Landau levels are occupied, ν chiral edge modes and therefore

$$\sigma_{xy} = \nu\frac{e^2}{h}, \sigma_{xx} = 0 \tag{311}$$

From this one can see that the quantization is directly related to the presence of edge modes when the bulk is insulating, and in this case the boundary modes originate from the wave function of the Landau levels themselves. This does not have to come from a physical magnetic field, but rather the topology of the electronic bands in the k-space.

12 Berry phase, Berry curvature and band topology

12.1 Berry phase, connection and curvature

Consider a Hamiltonian under adiabatic (slow) variation of its parameter $\boldsymbol{R}$ (here $\boldsymbol{R}$ is allowed to be a vector)

$$H(t) = H[\boldsymbol{R}(t)] \tag{312}$$

The eigenvalue at $\boldsymbol{R}(t)$ is ϵ_n

$$H(\boldsymbol{R})|n(\boldsymbol{R})\rangle = \epsilon_n(\boldsymbol{R})|n(\boldsymbol{R})\rangle \tag{313}$$

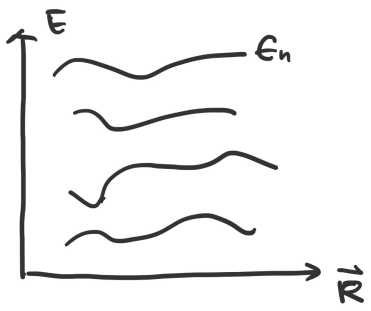

Figure 68: Schematic of evolution of eigenstates in parameter space.

In the scenario where the gaps in the system don't close during the slow evolution, the n-th eigenstate at time t will evolve into the n-th eigenstate at time t', up to a phase factor

$$|\psi_n(t)\rangle = C_n(t)|n[\boldsymbol{R}(t)]\rangle \tag{314}$$

For time-independent H

$$C_n(t) = \exp[-\frac{i}{\hbar}\epsilon_n t] \tag{315}$$

and for slowly time-varying t-dependent H, without losing generality

$$C_n(t) = e^{i\gamma_n(t)} \exp[-\frac{i}{\hbar}\int_0^t dt' \epsilon_n(t')] \tag{316}$$

Plugging this into the Schrodinger equation

$$i\hbar\frac{\partial}{\partial t}|\psi_n(t)\rangle = H[\boldsymbol{R}(t)]|\psi_n(t)\rangle \tag{317}$$

Taking an inner product with $\langle\psi_n(t)|$ we obtain

$$\frac{\partial}{\partial t}\gamma_n(t) = i\langle n(\boldsymbol{R})|\frac{\partial}{\partial t}|n(\boldsymbol{R})\rangle \tag{318}$$

Thus

$$\gamma_n(t) = i\int_0^t dt' \langle n(\boldsymbol{R})|\frac{\partial}{\partial t'}|n(\boldsymbol{R})\rangle = \int_C \boldsymbol{A}(\boldsymbol{R})\cdot d\boldsymbol{R} \tag{319}$$

Berry connection $\boldsymbol{A}(\boldsymbol{R})$ is defined as follows

$$\boldsymbol{A}(\boldsymbol{R}) = i\langle n(\boldsymbol{R})|\frac{\partial}{\partial \boldsymbol{R}}|n(\boldsymbol{R})\rangle \tag{320}$$

Two related concepts with Berry connection are Berry phase (defined with a closed loop)

$$\gamma_n = \oint \boldsymbol{A}^n(\boldsymbol{R})\cdot d\boldsymbol{R} \tag{321}$$

and Berry curvature

$$\boldsymbol{b}^n = \nabla_{\boldsymbol{R}} \times \boldsymbol{A}^n \tag{322}$$

The Berry phase is also related to the Berry curvature as a Berry flux in the parameter space

$$\gamma_n = \int_S \boldsymbol{b}^n \cdot d\boldsymbol{S} \tag{323}$$

From the above formulism it is clear that the set of Berry phase, connection etc. needs to be defined in a multi-dimensional space (at least two). If we label the two (orthorgonal) directions in the space to be μ and ν:

$$A_\mu = i\langle n|\frac{\partial n}{\partial \mu}\rangle, A_\nu = i\langle n|\frac{\partial n}{\partial \nu}\rangle \tag{324}$$

And the Berry curvature (sometimes labeled as Ω) can be written as

$$b_{\mu\nu} = \partial_\nu A_\mu - \partial_\mu A_\nu = i(\langle \frac{\partial n}{\partial \nu} | \frac{\partial n}{\partial \mu} \rangle - \langle \frac{\partial n}{\partial \mu} | \frac{\partial n}{\partial \nu} \rangle) \tag{325}$$

In the following we will encounter two different parameter space, the $\boldsymbol{k}$-space (here we restrict ourselves for being two dimensional) and the $\boldsymbol{d}$-space of a two band model.

The most well known application of the Berry phase is the Aharonov-Bohm effect, while we'd like to use it to describe the motion of electrons.

12.2 Berry curvature in a two-level system

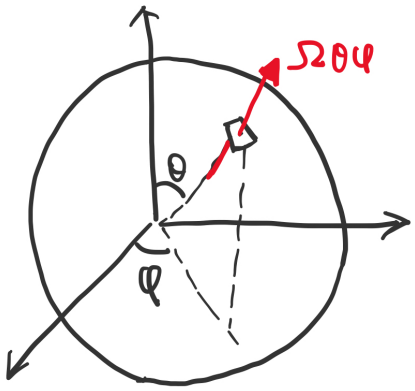

Figure 69: Schematic of $\Omega_{\theta\phi}$

The simplest case of non-zero Berry curvature can be introduced when we have a two band model. Any generic two-band model can be described by the following form of Hamiltonian

$$H = d_0 \boldsymbol{I} + \boldsymbol{d} \cdot \boldsymbol{\sigma} \tag{326}$$

where $\boldsymbol{\sigma}$ is the vector of the Pauli matrices $\{\sigma_x, \sigma_y, \sigma_z\}$, and $\boldsymbol{d}$ is a vector parameterizing the coefficients of the Pauli matrices. d_0 is the overall offset and will not affect our discussions.

The eigen value of H will be $\pm|d|$ while the eigenstates themselves will not depend on the magnitude of $|d|$. What's key here is rather the direction of d in the three-dimensional space. If this space is described by (r, θ, ϕ), only θ and ϕ directions give rise to finite Berry connection and curvatures. If $\boldsymbol{h} = h(\sin\theta\cos\phi, \sin\theta\sin\phi, \cos\theta)$, the two eigenstates will be

$$|-\rangle = \begin{pmatrix} \sin(\theta/2)e^{-i\phi} \\ -\cos(\theta/2) \end{pmatrix} \tag{327}$$

and

$$|+\rangle = \begin{pmatrix} \cos(\theta/2) \\ \sin(\theta/2)e^{i\phi} \end{pmatrix} \tag{328}$$

Here we focus on the ground state (assume there's always a gap in the system) wave function $|-\rangle$.

$$\begin{aligned} A_\theta &= i\langle -|\partial_\theta|-\rangle = 0 \\ A_\phi &= i\langle -|\partial_\phi|-\rangle = \sin^2\frac{\theta}{2} \end{aligned} \tag{329}$$

And accordingly the Berry curvature in the $\{\theta, \phi\}$ space is

$$\Omega_{\theta\phi} = \partial_\theta A_\phi - \partial_\phi A_\theta = \sin\frac{\theta}{2}\cos\frac{\theta}{2} = \frac{1}{2}\sin\theta \tag{330}$$

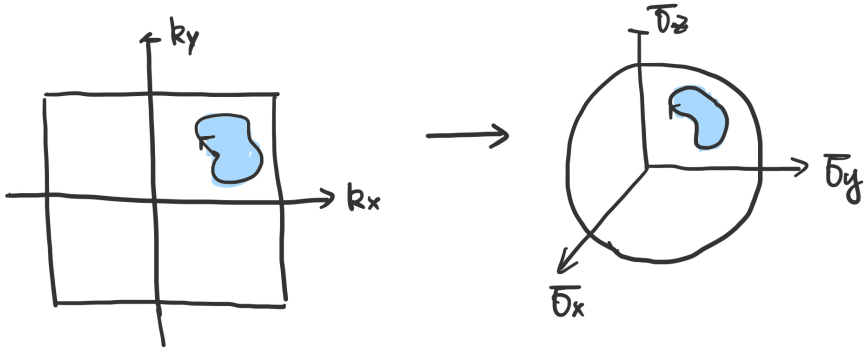

Figure 70: Mapping from Brillouin zone to the Bloch sphere.

One may think about this as the solid angle of a unit area on a unit length of the Bloch sphere (see Fig. 69). It should be perpendicular to the sphere as it has to be perpendicular to both $d\theta$ and $d\phi$.

$$\int_0^{\pi} d\theta \int_0^{2\pi} d\phi \Omega_{\theta\phi} = 2\pi \tag{331}$$

And the integration takes a very similar form with the Gauss's law for electric/magnetic charge (or magnetic monopole); where the integration of the field over a closed surface does not depend on the size of the sphere, but only depends on the charge it encloses.

Strictly speaking, in the above we've discussed non-zero Berry curvature in the $\{\theta, \phi\}$ space; at times we are more interested in this in the $\{k_x, k_y\}$ space. It is useful to think about the the mapping illustrated in Fig. 70, where the Berry flux closed by the two loops are identical (note that the two loops do not necessarily rotate in the same direction), while the Berry curvature may be different. In the $\{k_x, k_y\}$ space the Berry curvature is geometrically defined in the z-direction and can be expressed as

$$\Omega_z(k_x, k_y) = \frac{1}{2}\hat{d} \cdot (\frac{\partial \hat{d}}{\partial k_x} \times \frac{\partial \hat{d}}{\partial k_x}) \tag{332}$$

The integration of the Berry flux follows the following form

$$\int_{B.Z.} dk_x dk_y \Omega_z = 2\pi n \tag{333}$$

where n is the number of times the wave function wraps around the Bloch sphere.

12.3 Berry formulism for Bloch electrons

In this section we more systematically treat the Berry curvature of Bloch electrons in the $\{k_x, k_y\}$-space.

Starting from a very general form

$$H|n\rangle = \epsilon_n |n\rangle \tag{334}$$

And the Berry curvature in $\{k_x, k_y\}$-space is (Eq. 325)

$$b_z(k_x, k_y) = i(\langle \frac{\partial n}{\partial k_x} | \frac{\partial n}{\partial k_y} \rangle - \langle \frac{\partial n}{\partial k_y} | \frac{\partial n}{\partial k_x} \rangle) \tag{335}$$

Taking a partial derivative of Eq. 334 with respect to k_i:

$$\frac{\partial H}{\partial k_i}|n\rangle + H|\frac{\partial n}{\partial k_i}\rangle = \frac{\partial \epsilon_n}{\partial k_i}|n\rangle + \epsilon_n |\frac{\partial n}{\partial k_i}\rangle \tag{336}$$

Multiply by $\langle n'|$:

$$\langle n'|\frac{\partial H}{\partial k_i}|n\rangle = \langle n'|(\epsilon_n - \epsilon_{n'})|\frac{\partial n}{\partial k_i}\rangle \tag{337}$$

In other words

$$\langle n'|\frac{\partial n}{\partial k_i}\rangle = \frac{\langle n'|\frac{\partial H}{\partial k_i}|n\rangle}{\epsilon_n - \epsilon_{n'}} \tag{338}$$

Therefore

$$\begin{aligned} b_z(k_x, k_y) &= i\sum_{n'\neq n}(\langle\frac{\partial n}{\partial k_x}|n'\rangle\langle n'|\frac{\partial n}{\partial k_y}\rangle - \langle\frac{\partial n}{\partial k_y}|n'\rangle\langle n'|\frac{\partial n}{\partial k_x}\rangle) \\ &= i\sum_{n'\neq n}\frac{\langle n|\frac{\partial H}{\partial k_x}|n'\rangle\langle n'|\frac{\partial H}{\partial k_y}|n\rangle - \langle n|\frac{\partial H}{\partial k_y}|n'\rangle\langle n'|\frac{\partial H}{\partial k_x}|n\rangle}{(\epsilon_n - \epsilon_{n'})^2} \end{aligned} \tag{339}$$

One may note that H does not explicitly depend on k_x or k_y. It is convenient to perform the following unitary transformation

$$h(\boldsymbol{k}) = e^{-i\boldsymbol{k}\cdot\boldsymbol{r}}He^{i\boldsymbol{k}\cdot\boldsymbol{r}} \tag{340}$$

Recall that the Bloch wave function is $\psi_{n\boldsymbol{k}} = e^{ikr}u_{n\boldsymbol{k}}$ and

$$H|\psi_{n\boldsymbol{k}}\rangle = \epsilon_{n\boldsymbol{k}}|\psi_{n\boldsymbol{k}}\rangle \tag{341}$$

One can verify that

$$h(\boldsymbol{k})|u_{n\boldsymbol{k}}\rangle = \epsilon_{n\boldsymbol{k}}|u_{n\boldsymbol{k}}\rangle \tag{342}$$

suggesting that the conclusions from Eq. 65-70 can be directly applied to $h(\boldsymbol{k})$ and $u_{n\boldsymbol{k}}$. This is going to be a simplification, as one only needs to consider the wave function within each unit cell without the phase factor. In particular, recall the eigenwave function we've taken for tight-binding models is of the following form

$$\sum e^{ikna}|n\rangle \tag{343}$$

the simplification removes the phase factor from the formulism of Berry curvature of band electrons (one only needs to think about what happens within a unit cell). We've implicitly used this when talking about the Berry curvature associated with the Dirac electrons.

It is also not difficult to verify that the Berry curvature can be expressed as

$$b_z(k_x, k_y) = i(\langle\frac{\partial u_n}{\partial k_x}|\frac{\partial u_n}{\partial k_y}\rangle - \langle\frac{\partial u_n}{\partial k_y}|\frac{\partial u_n}{\partial k_x}\rangle) \tag{344}$$

It is clear from this that the Berry curvature of a one-band tight-binding model is zero everywhere in the k-space.

12.4 Anomalous velocity

Up to now we've looked at a case with non-zero Berry curvature, while we have not yet touched on the manifestation of the Berry curvature in experiments. One of the ways to see how Berry curvature contributes to the electronic transport is through considering the perturbation. Now let's connect this with the electronic motion itself. Without the Berry phase effect correction, given consider the following perturbation

$$H_1 = e\boldsymbol{E}\cdot\boldsymbol{r} \tag{345}$$

To the first order

$$|\delta\psi_{n\boldsymbol{k}}\rangle = e\boldsymbol{E}\cdot\sum\frac{|\psi_{n'\boldsymbol{k}'}\rangle\langle\psi_{n'\boldsymbol{k}'}|\boldsymbol{r}|\psi_{n\boldsymbol{k}}\rangle}{\epsilon_{n\boldsymbol{k}} - \epsilon_{n'\boldsymbol{k}'}} \tag{346}$$

This can be rewritten as

$$|\delta\psi_{n\boldsymbol{k}}\rangle = e\boldsymbol{E}\cdot\sum\frac{|\psi_{n'\boldsymbol{k}'}\rangle\langle\psi_{n'\boldsymbol{k}'}|[\boldsymbol{r}, H]|\psi_{n\boldsymbol{k}}\rangle}{(\epsilon_{n\boldsymbol{k}} - \epsilon_{n'\boldsymbol{k}'})^2} \tag{347}$$

As (Eherenfest theorem)

$$\begin{aligned} \boldsymbol{v} &= \frac{d\boldsymbol{r}}{dt} = \frac{1}{i\hbar}[\boldsymbol{r}, H] \\ [\boldsymbol{r}, H] &= i\hbar\boldsymbol{v} \end{aligned} \tag{348}$$

The perturbed wave function is

$$|\delta\psi_{n\boldsymbol{k}}\rangle = i\hbar e\boldsymbol{E}\cdot\sum\frac{|\psi_{n'\boldsymbol{k}'}\rangle\langle\psi_{n'\boldsymbol{k}'}|\boldsymbol{v}|\psi_{n\boldsymbol{k}}\rangle}{(\epsilon_{n\boldsymbol{k}} - \epsilon_{n'\boldsymbol{k}'})^2} \tag{349}$$

Here we decompose the Bloch function $\psi_{n\boldsymbol{k}}$ to its plane wave and periodic part $u_{n\boldsymbol{k}}$ and use the $h(\boldsymbol{k})$ defined above:

$$\langle\psi_{n'\boldsymbol{k}'}|\boldsymbol{v}|\psi_{n\boldsymbol{k}}\rangle = \langle u_{n'\boldsymbol{k}'}|\frac{1}{\hbar}\frac{\partial h(\boldsymbol{k})}{\partial \boldsymbol{k}}|u_{n\boldsymbol{k}}\rangle\delta_{\boldsymbol{k}\boldsymbol{k}'} \tag{350}$$

The perturbed periodic function is

$$|\delta u_{n\boldsymbol{k}}\rangle = ie\boldsymbol{E}\cdot\sum\frac{|u_{n'\boldsymbol{k}}\rangle\langle u_{n'\boldsymbol{k}'}|(\partial h(\boldsymbol{k})/\partial\boldsymbol{k})|u_{n\boldsymbol{k}}\rangle}{(\epsilon_{n\boldsymbol{k}}-\epsilon_{n'\boldsymbol{k}'})^2} \tag{351}$$

The velocity of the perturbed wave function is

$$\begin{aligned}\langle\boldsymbol{v}\rangle &= \langle u_{n\boldsymbol{k}}|\frac{1}{\hbar}\frac{\partial h(\boldsymbol{k})}{\partial\boldsymbol{k}}|u_{n\boldsymbol{k}}\rangle + \langle\delta u_{n\boldsymbol{k}}|\frac{1}{\hbar}\frac{\partial h(\boldsymbol{k})}{\partial\boldsymbol{k}}|u_{n\boldsymbol{k}}\rangle + \langle u_{n\boldsymbol{k}}|\frac{1}{\hbar}\frac{\partial h(\boldsymbol{k})}{\partial\boldsymbol{k}}|\delta u_{n\boldsymbol{k}}\rangle \\ &= \frac{1}{\hbar}\frac{\partial h(\boldsymbol{k})}{\partial\boldsymbol{k}} + \boldsymbol{v}_a\end{aligned} \tag{352}$$

$\boldsymbol{v}_a$ is the so-called anomalous velocity:

$$\begin{aligned}\boldsymbol{v}_a &= \frac{ie}{\hbar}\sum_{n'\neq n}\frac{\langle u_{n\boldsymbol{k}}|(\partial h(\boldsymbol{k})/\partial\boldsymbol{k})|u_{n'\boldsymbol{k}'}\rangle[\boldsymbol{E}\cdot\langle u_{n'\boldsymbol{k}'}|(\partial h(\boldsymbol{k})/\partial\boldsymbol{k})|u_{n\boldsymbol{k}}\rangle] - c.c.}{(\epsilon_{n\boldsymbol{k}}-\epsilon_{n'\boldsymbol{k}'})^2} \\ &= \frac{ie}{\hbar}\boldsymbol{E}\times[\sum_{n'\neq n}\frac{\langle u_{n\boldsymbol{k}}|(\partial h(\boldsymbol{k})/\partial\boldsymbol{k})|u_{n'\boldsymbol{k}}\rangle\times\langle u_{n'\boldsymbol{k}}|(\partial h(\boldsymbol{k})/\partial\boldsymbol{k})|u_{n\boldsymbol{k}}\rangle]}{(\epsilon_{n\boldsymbol{k}}-\epsilon_{n'\boldsymbol{k}'})^2}] \\ &= \frac{e}{\hbar}\boldsymbol{E}\times\boldsymbol{b}_n(\boldsymbol{k})\end{aligned} \tag{353}$$

suggesting that the Berry curvature induces a transverse motion of the electrons, similar to the Hall effect.

One may write the following set of semiclassical equation of motion of electrons

$$\begin{aligned}\dot{\boldsymbol{r}} &= \frac{1}{\hbar}\frac{\epsilon_n(\boldsymbol{k})}{\partial\boldsymbol{k}} - \dot{\boldsymbol{k}}\times\boldsymbol{\Omega}_n(\boldsymbol{k}) \\ \hbar\dot{\boldsymbol{k}} &= -e\boldsymbol{E} - e\dot{\boldsymbol{r}}\times\boldsymbol{B}(\boldsymbol{r})\end{aligned} \tag{354}$$

where the Berry curvature plays the role of the magnetic field in k-space.

12.5 Quantum anomalous Hall effect

For a filled band in 2D, the Hall conductivity

$$\sigma_{xy} = \frac{e^2}{h}\frac{1}{2\pi}\int b_z dk_x dk_y \tag{355}$$

where the Chern number

$$C = \frac{1}{2\pi}\int b_z dk_x dk_y \tag{356}$$

is quantized. $C = 0$ corresponds to a trivial insulator, and a non-zero Chern number corresponds to the number of times the wave function in the first BZ covers the Bloch sphere, and as no magnetic field is required here to generate a similarly quantized Hall conductance, this is termed the quanum anomalous Hall effect. Similar to the quantum Hall phase, this quantum anomalous Hall insulator phase has insulating interior and chiral edge modes.

12.6 Remarks

We have focused on the effects of Berry curvature on the anomalous transport in the Hall effect. Other Berry curvature/phase effects include the Landau quantization condition and thus quantum oscillation.